Politecnico di Milano

Facoltà di Ingegneria Civile, Ambientale e Territoriale

Polo Territoriale di Como

Master of Science in

Environmental and Land Planning Engineering

Improved dynamic emulation modelling by time series clustering: the case study of Marina Reservoir, Singapore

Supervisor:
Prof. Andrea Castelletti

Assistant supervisor:
Dr. Stefano Galelli

Master graduation thesis by:

Stefania Caietti Marin

Student Id. number: **745854**

Academic Year: **2011-2012**

Politecnico di Milano

Facoltà di Ingegneria Civile, Ambientale e Territoriale

Polo Territoriale di Como

Corso di Laurea Specialistica in

Ingegneria per l'Ambiente e il Territorio

Dynamic Emulation Modelling e Time Series Clustering: il caso di studio di Marina Reservoir, Singapore

Relatore:

Prof. Andrea Castelletti

Correlatore:

Dr. Stefano Galelli

Tesi di Laurea di:

Stefania Caietti Marin

Matricola: **745854**

Anno Accademico: **2011-2012**

"Fanciullino, tu sei savio: non vuoi ripetere il già detto, né trovare l'indicibile. Sai che nelle cose é il nuovo, per chi sa vederlo; e non t'indurrai a trovarlo, affatturando e sofisticando. Il nuovo non s'inventa: si scopre."

— Giovanni Pascoli

Acknowledgements

This master thesis was carried out under the supervision of Andrea Castelletti and the co-supervision of Stefano Galelli. I wish to thank them for the opportunity they gave me, and for being great advisors. Their ideas and support had a major influence on this work.
The case study described in this thesis was developed in collaboration with the Singapore-Delft Water Alliance (SDWA) at the National University of Singapore (Singapore), as part of the Multi-objective Multiple-Reservoir Management research program. I want to express gratitude to all SDWA staff, in particular to Vladan Babovic, who gave me the possibility of visiting SDWA and working there on the project activities.
I wish to thank Albert Goedbloed for his special advices and for his active help with the use of Matlab and I am grateful to Abhay, Ali, Samuel, Phil, Jingjie, and Javier for having been cooperative fellows and dear friends.

The first loving thanks goes to my family for having been close to me throughout my studies. A special thanks is for Donata because day by day she encourages me not to turn away from the truth, and to Serena for her unreserved support, especially during the most difficult moments.
Thanks also to Paola, Monia, Anna, Annina, Renée, and Maria, as with them I receive only affection and comprehension, even when I show the worst side of me.
I wish to thank Federica, who came into my life only by accident; she is a really precious person and I cannot forget what we shared in Singapore.
Thanks also to Trisha, Bokyung, Katja, Anna, Manhang, Hoi Yin, Przemyslaw, Andrew, David, Tae-Kyu, Karol, Baris, Maggie, Yevgeniy, Tommy, Stephanie, Pawel, and Konstantin as they made my staying in Asia delightful and amusing: with them I went through lots of new experiences and I saw magnificent and enchanting places that I will keep in mind for the rest of my life.

I also wish to thank Roberto for having been a constant presence during the preparation of the exams and the redaction of this thesis, and I am particularly grateful to all the students that passed me by during these years, as they made me reflect upon how I was in the past and they made me realize what I want to be in the future.
My final thanks is for Paolo, who is by my side in this special moment. Maybe I don't know what love means; but if it has to do with the encouragement helping the other to reach a goal, if it implies respect and freedom to express one's own nature every single day, then I can say I do love you.

Abstract

Dynamic Emulation Modelling (DEMo) is emerging as a viable solution to combine computationally intensive simulation models and dynamic optimization algorithms. A dynamic emulator is a low order surrogate of the simulation model identified over a sample data set generated by the original simulation model itself. When applied to large 3D models, any DEMo exercise does require a preprocessing of the exogenous drivers and state variables in order to reduce, by spatial aggregation, the high number of candidate variables to appear in the final emulator. This work describes a hybrid clustering-variable selection approach to automatically discover compact and relevant representations of high-dimensional data sets. Time series clustering (Liao, 2005) is adopted to identify spatial structures by objectively organizing data into homogenous groups, where the within-group-object similarity is minimized. In particular, the proposed approach relies on a hierachical agglomerative clustering method (Magni et al., 2008), which starts by placing each time-series in its own cluster, and then merges clusters into larger clusters, until a compact, yet informative, representation of the original variables can be processed with the Recursive Variable Selection - Iterative Input Selection algorithm (Castelletti et al., 2011), in order to single out the most relevant clusters. The approach is demonstrated on a real-world case study concerning the reduction of DELFT3D, a spatially distributed hydrodynamic model used to simulate salt intrusion dynamics in a tropical lake (Marina Reservoir, Singapore).

Sommario

Il Dynamic Emulation Modelling (DEMo) sta emergendo come possibile soluzione per un utilizzo combinato di algoritmi di ottimizzazione dinamica e di modelli di simulazione onerosi dal punto di vista computazionale. Un dinamic emulator é un modello semplificato e computazionalmente efficiente, di un modello di simulazione e può essere generato tramite simulazione a partire da un campione di dati prodotto dal modello originale. Se applicato a grandi modelli 3D, l'implementazione della procedura DEMo richiede un una preliminare trasformazione dei vettori degli ingressi esogeni e delle variabili di stato per ridurre, attraverso un'aggregazione spaziale, l'elevato numero di variabili candidate ad apparire nell'emulation model finale. Questo lavoro di tesi descrive un approccio combinato di techiche di clusterizzazione e di variable selection per scoprire in maniera automatica rappresentazioni compatte e rilevanti in data-set di grandi dimensioni. La clusterizzazione di serie temporali é qui adottata per identificare in modo oggettivo strutture spaziali nei dati e per organizzarli in gruppi omogenei, in cui il grado di similarità tra oggetti appartenenti ad uno stesso gruppo sia massimizzato. In particolare, l'approccio proposto si basa sull'utilizzo di un metodo di clusterizzazione gerarchico agglomerativo, che inizialmente pone ogni serie temporale in cluster differenti e successivamente li unisce in cluster di dimensioni sempre maggiori, fino a che una rappresentazione compatta, ma informativa, delle variabili originali puó essere processata con l'algoritmo di Recursive Variable Selection - Iterative Input Selection, al fine di individuare i cluster più rilevanti. L'approccio é dimostrato su un caso studio reale riguardante la riduzione di Delft3D, un modello idrodinamico spazialmente distribuito utilizzato per simulare la dinamica dell'intrusione salina in un lago tropicale (Marina Reservoir, Singapore).

Introduction

Advances in scientific computation and data collection techniques have increased the level of fundamental understanding that can be built into physically-based models, which are widely adopted to describe the dynamics of large environmental systems. These models, which are more and more realistic and complex, are often used also to support planning and management interventions. However, the practical application of a decision-making scheme in environmental problems can be particularly difficult as the physically-based models used to describe environmental systems are computationally intensive and thus ill-suited to support optimization-based decision-making, which normally requires hundreds or thousands of model evaluations.
A potentially effective approach to overcome these limitations is to perform a top-down reduction of the physically-based model by a simplified, computationally-efficient *emulation model* (Castelletti et al. (2012b) and references therein) constructed from and then used in place of the original physically-based model in highly resource-demanding tasks. The underlying idea is that not all the process details in the original model are equally important and relevant to the dynamic behaviours that result into an actual change in the values of the planning/management objectives of the decision-making problem, and thus affect the final decision.

Literature shows a variety of alternate emulation modelling approaches that explored different knowledge areas and engineering applications, including aeronautics, chemical engineering, robotics, electronics, and micro-engineering. Most of these methods tend to derive an emulator trying to exploit some peculiar features of the system under study, or are model-specific, in the sense that the type of emulator depends upon the type of physically-based model. Moreover, for decision-making problems (i.e. optimal control) the emulator must be *dynamic*, that is it must reproduce the trajectories over any specified horizon of the relevant variables. A shared theoretical vision is still missing and different techniques were independently developed in different domain of interest.

Castelletti et al. (2012a) re-organized the techniques adopted in environmental problems into a general framework to Dynamic Emulation Modelling (DEMo) and distinguished two categories of dynamic emulators: structure-driven and data-driven. The former are based on the idea of projecting the high-dimension equations of the physically-based models onto a lower-dimension space, where the model equations are solved for the substituted projected states. The latter are generally based on the identification of the emulator as an I/O relationship over a data set of input-output samples generated from the original physically-based model. The choice for one approach or the other depends on the level of complexity and non-linearities embedded into the original model.
Structure-driven dynamic emulators are well developed for linear, quadratic, and weakly non-linear models, while theory is still under development for non-linear models. This category of emulators is also naturally in the state-space form, which makes it directly and more effectively usable in any management problem. On the contrary, data-driven emulators can be easily applied to both linear and non-linear models, as they do not require any analytical assumption about the physically-based model structure. The resulting emulator, however, is in external form and, generally, must be converted into state-space form by solving a minimal realization problem, which can turn out particularly difficult in the non-linear case. Moreover, while literature shows some operational examples of emulators in external form interpretable in physical terms (see, for example, GAINS model (Amann, 2009) in the part related to climate change and air quality emulators), in the water resources sector both the original external form and the associated minimal realization typically lack of credibility by stakeholders and domain experts, apart from few particular cases (Young (1998); See et al. (2008); Babovic (2009)). Data-driven DEMo has been more extensively explored than its structure-driven twin in environmental modelling, where systems are typically complex and highly non-linear.
Lately, Castelletti et al. (2012) proposed a new data driven approach that preserves the internal representation of the original model and allows to get insight on the physical functioning of the emulator.

The purpose of my thesis is to enhance the status of these techniques, focusing on data-driven DEMo, and trying to combine the advantages of traditional data-

driven methods (i.e. fully automated, independent of domain experts and system knowledge, and suitable for non-linear processes), while preserving the state-space representation and the associated physical interpretability of structure-driven emulators.
Indeed, when applied to large 3D models, any DEMo exercise does require a pre-processing of the exogenous drivers, controls, and state variables in order to reduce, by spatial aggregation, the high number of variables candidate to appear in the final emulator. This operation can be performed by adopting different techniques: this work explores the potential of one of these, i.e. clustering, to automatically discover compact and relevant representations of high-dimensional data sets. Time series clustering is adopted to identify spatial structures by objectively organizing data into homogeneous groups, where the within-group-object similarity is maximized. In particular, the proposed approach relies on a hierarchical agglomerative clustering method, which starts by placing each time-series in its own cluster, and then merges clusters into larger clusters, until a compact, yet informative, representation of the original variables can be processed with a variable selection algorithm, in order to single out the most relevant clusters. The approach is demonstrated on a real-world case study concerning the reduction of Delft3D, a spatially distributed hydrodynamic model used to simulate hydrodynamic processes in a tropical reservoir (Marina Reservoir, Singapore).

The present work is organized as follows. *Chapter 1* describes the families of physically-based models and the corresponding decision-making problems on which they are employed, it introduces the different emulation modelling strategies and approaches, and it discusses the methods that have been used in the last years. As the selection of the most relevant variables appearing in the final emulator is commonly difficult, clustering techniques are introduced and described in *Chapter 2*. In particular, this chapter provides an overview of the clustering algorithms present in literature, it introduces the reader to time-series clustering, and it presents a critical analysis of the time-series clustering algorithms being developed so far, giving particular emphasis to the hierarchical agglomerative clustering method. Chapter 2 also presents some different similarity/distance measures and linkage methods, whose choice is the key point of any clustering study, and it distinguishes two categories of clustering evaluation criteria. The purpose of *Chapter 3* is then to introduce the case study to which the hybrid approach that couples DEMo procedure to clustering is applied. Water management issues in Singapore and Marina reservoir water system are here described in details, with particular emphasis on the management problem and to the modelling tools that constitute the basis for the emulator identification. *Chapter 4* describes the reduction of a 3D, physically-based model (Delft3D) describing the hydrodynamic conditions of Marina reservoir (Singapore). The scope of this application is to reduce the dimensionality of Delft3D, so that the resulting emulation model can be used to simulate salt intrusion dynamics in Marina Reservoir, and subsequently coupled with a real-time control of the system to account for both water quality and quantity targets. Concluding remarks are finally given in *Chapter 5*.

Contents

List of Figures

List of Tables

Chapter 1

Complexity reduction strategies for physically-based models[1]

1.1 Introduction

Advances in scientific knowledge and computational power have considerably enhanced the level of fundamental understanding that is built into the kind of physically-based models which are widely used in the modelling of large environmental systems. Nonetheless, the resulting increased complexity of the model structures poses strong limitations in terms of practical implementation and computational requirements, especially for those typical problems that require hundreds or thousands of model evaluations, as, for example, sensitivity analysis, scenario analysis and optimal control.

As a result, increasing attention is now being devoted to emulation modelling as a way of overcoming these limitations. An emulation model, or emulator, is a low-order approximation of the physically-based model that can be substituted for it in order to solve a high resource-demanding problem (for further details see Castelletti et al. (2012b)). Such a model can be derived by simplifying the physically-based model structure, or identified on the basis of the response data produced by simulating this large model with carefully selected input perturbations. Dynamic Emulation Modelling (DEMo) are a special type of model complexity reduction, in which the dynamic nature of the original physically-based model is preserved, with consequent advantages in a wide range of problems, such as optimal control. As the number

[1]This chapter is mostly taken from Castelletti et al. (2012b).

and forms of the problem that benefit from the identification and subsequent use of an emulator is very large and there are a variety of techniques available for this purpose, the analysis and classification of all these problems and the description of a unified design framework for the different strategies of complexity reduction and emulation is briefly described in the next sections.
In particular, this chapter is organized as follows: first, in Section 1.2, a review of all the elements required by any emulation modelling exercise is given: the system $\mathcal{E}$ being considered for emulation, the types of phisically-based model $\mathcal{M}$ available to describe it, and the variety of problems $\mathcal{P}$ that can take advantage of an emulator for their solution. In Section 1.3 the emulation modelling exercise is formulated and the difference between dynamic (DEMo) and non-dynamic emulators is discussed. In Section 1.4 a general procedure for DEMo is presented. Finally, Section 1.5 highlights the purpose of this work.

1.2 Framing the problem

1.2.1 The system $\mathcal{E}$

Let's consider a large environmental system $\mathcal{E}$, whose state $\mathcal{X}(t,s)$ varies in a time-space domain $\mathcal{T} \times \mathcal{S}$. The system is affected by a time-varying, often distributed in space, exogenous driver $\mathcal{W}(t,s)$.
The output $\mathcal{Y}(t)$ is generally, but not necessarily, lumped and is constituted by the variables that are relevant to the analyst: it usually comprises few variables but it can sometimes be distributed in space and coincide with the whole state.
Engineering applications are often related to the problem of controlling or managing the dynamics of $\mathcal{X}(t,s)$ and $\mathcal{Y}(t)$ through a sequence of decisions, periodically repeated over the whole system's life. In this case a control vector $\mathbf{u}_t$ is applied[2] to $\mathcal{E}$ at discrete time instants, according to a decision time-step. The system $\mathcal{E}$ can also be affected by a vector $\mathbf{v}$ of planning decisions that are normally not changed over the whole life of the system.

[2]We assume that system $\mathcal{E}$ is controllable. Operationally, the controllability of $\mathcal{E}$ must be verified before entering into the emulation modelling exercise.

1.2.2 The model $\mathcal{M}$

The scientific approach to environmental systems modelling normally exploits physical knowledge about the dynamic behaviour of the system $\mathcal{E}$ to build more or less sophisticated *process-based* models that reproduce the perceived reality as well as possible. These models can be separated into two, broad families: *physically-based* and *conceptual* models (Wheater et al., 1993).

Physically-Based models. The system $\mathcal{E}$ is described by a large, generally non-linear, dynamic model, normally defined in $\mathcal{T} \times \mathcal{S}$ by a set of partial differential equations (PDE). These equations describe the evolution of the system state $\mathcal{X}(t, s)$ and output $\mathcal{Y}(t)$ in response to external forcing $\mathcal{W}(t, s)$ (either deterministic or stochastic) and control $\mathbf{u}_t$.

Conceptual models.

a) Continuous-time. Although a PDE model could be used, the system $\mathcal{E}$ is normally described by a continuous-time, non-linear model, formulated as a system of ordinary differential equations, based on a conceptualization and simplification of the physical laws describing the system dynamics

$$\dot{\mathbf{X}}(t) = \mathbf{F}(t, \mathbf{X}(t), \mathbf{W}(t), \mathbf{u}(t), \mathbf{v}|\boldsymbol{\Theta}) \tag{1.1a}$$

$$\mathbf{Y}(t) = \mathbf{H}(t, \mathbf{X}(t), \mathbf{W}(t), \mathbf{u}(t), \mathbf{v}|\boldsymbol{\Theta}) \tag{1.1b}$$

where the information content of $\mathcal{X}(t, s)$ and $\mathcal{W}(t, s)$ is lumped into the vectors $\mathbf{X}(t)$ and $\mathbf{W}(t)$, and $\mathcal{Y}(t) = \mathbf{Y}(t)$, while $\mathbf{F}(\cdot)$ is a generally non-linear, time-variant, vector function that models the dynamics of $\mathbf{X}(t)$; $\mathbf{H}(\cdot)$ is a generally non-linear, possibly time-variant, output transformation function; and $\boldsymbol{\Theta}$ is the vector of the model parameters.

b) Discrete-time. The system $\mathcal{E}$ is described by a discrete-time, non-linear model, formulated as a system of finite-difference equations:

$$\mathbf{X}_{t+1} = \mathbf{F}_t(\mathbf{X}_t, \mathbf{W}_t, \mathbf{u}_t, \mathbf{v}|\boldsymbol{\Theta}) \tag{1.2a}$$

$$\mathbf{Y}_t = \mathbf{H}_t(\mathbf{X}_t, \mathbf{W}_t, \mathbf{u}_t, \mathbf{v}|\boldsymbol{\Theta}) \tag{1.2b}$$

where the information content of $\mathcal{X}(t, s)$, $\mathcal{W}(t, s)$ and $\mathcal{Y}(t)$ is now sampled, typically at a uniform sampling interval Δt, and transformed into the sampled data vectors $\mathbf{X}_t$, $\mathbf{W}_t$ and $\mathbf{Y}_t$.

The spatial aspects are normally defined by the state and exogenous driver vectors $\mathbf{X}_t$ and $\mathbf{W}_t$, which are defined at different spatial locations. In the presence of $\mathbf{u}_t$, the sampling time step is generally assumed equal to the decision time step, otherwise only the former exists and is related to the frequency of observations available or, when this is not limiting, based by the problem at hand.

The function $\mathbf{F}_t(\cdot)$ is a generally non-linear, time-variant, vector function that models the dynamics of $\mathbf{X}_t$; $\mathbf{H}_t(\cdot)$ is a generally non-linear, possibly time-variant, output transformation function, and $\mathbf{\Theta}$ is a vector of the model parameters.

When a physically-based (or a conceptual continuous-time) model is adopted, an explicit scheme is commonly used for its numerical solution. In practice, this requires the discretization of the time-space domain $\mathcal{T} \times \mathcal{S}$ (or simply the time domain $\mathcal{T}$) with an appropriate grid. In this way, the original continuous-time model is, *de facto*, transformed into a discrete-time model of the form (1.2). When the original model is physically-based, all the variables, apart from $\mathbf{u}_t$ and $\mathbf{v}$, which are not spatially distributed, have a dimensionality equal to their original dimensionality times the cardinality of the space discretization grid. When the original model is conceptual, the dimensionality of all the variables is unchanged.

In conclusion, whatever the process-based model adopted, a distinctive feature of the model $\mathcal{M}$ is the large dimensionality of the state, exogenous driver, and parameter vectors which, on one hand, is required for a detailed description of the processes in $\mathcal{E}$ but, on the other hand, makes it computationally too intensive for those problems that require hundreds or thousands of model runs.

1.2.3 The problem $\mathcal{P}$

Assume that we have a model $\mathcal{M}$ together with a certain defined problem $\mathcal{P}$. For this model, according to its complexity, a full and proper statistical estimation or 'calibration' of its parameters may not be feasible, so that this has been performed as well as possible. Depending on $\mathcal{P}$, our interest might be either in the trajectory of $\mathbf{Y}_t$, or in a functional $J(\cdot)$ of this trajectory. A review of the literature shows a variety of problems $\mathcal{P}$, whose names and tasks vary across different scientific disciplines. These problems are generally known and classified in the following categories.

Model diagnostics The selection and use of diagnostic measures are important elements in the modelling exercise, both within the model building itself (i.e. as a fundamental preliminary step prior to the practical application of the model) and in analysing the model-based results used to solve a problem $\mathcal{P}$. In the first case, diagnostic tools are used to test or validate hypotheses and parametrizations against available observations; or with respect to some desirable or plausible behaviour of model outputs of interest. In the second case, diagnostic tools can be used to assess the robustness of results (e.g. in control, planning problems) and make them more transparent to users, stakeholders and policy-makers. Diagnostic problems arising when evaluating the model $\mathcal{M}$ are summarized below.

- *Model structure identification.* The large physically-based model structure is usually specified by the modeller's choice of a specific model form and order that best represent the system under analysis. After the model structure is defined, however, the model should undergo a thorough identification, estimation (calibration) and validation analysis, before using it for practical applications. The relation between data and parameters $\mathbf{\Theta}$ must be considered: an increase in model complexity is indeed reflected on an increase in the number of parameter $\mathbf{\Theta}$ to be defined and calibrated. This can easily lead to over-parametrization and non-uniqueness (i.e. the presence of multiple models or parameter sets that have equally acceptable fits to observational data). To avoid this problem, statistical techniques can be used to assess the discrepancy between the data information content and the number of parameters to be calibrated.

- *Sensitivity analysis.* Uncertainty analysis aims at quantifying the uncertainty associated with the model output or a functional $J(\cdot)$ thereof, given some 'prior' uncertainty, usually based on expert judgement, or after parameter estimation (calibration) has been completed. Uncertainty quantification should be always accompanied by a sensitivity analysis (Saltelli et al., 2000, 2004, 2008). Performing an uncertainty and sensitivity analysis involves the use of Monte Carlo sampling and performing a large number of model evaluations by varying model parameters $\mathbf{\Theta}$. In the presence of large, complex models, this is simply not affordable and the use of emulators often represents the only possible solution to this kind of problem.

- *Data assimilation.* If some or all of the outputs $\mathbf{Y}_t$ of the system are being monitored on a regular basis, it is often possible to combine these measurements with the model $\mathbf{X}_t$ predictions to produce real-time estimates and forecasts of the state variables. Data assimilation, also known as state estimation, is largely adopted in weather forecasting, hydrology and oceanography (see Kalnay, 2002 and Bennett, 2002).

Optimal planning and management The vector $\mathbf{v}$ that maximizes $J(\cdot)$ has to be determined. Depending on the dimensionality of $\mathbf{v}$, the size of the associated feasibility domain, and the complexity of the functional and constraint shape, the algorithms available to solve optimal planning problems (basically, simulation-based optimization algorithms) are hardly usable with large process-based models. The topic has been widely explored in the environmental modelling literature; recent examples include air quality planning, water quality planning, water distribution networks, water supply system, etc. Instead, in optimal management problems, the purpose is to design the feedback control policy[3] p that maximizes the functional $J(\cdot)$.

Simulation The model $\mathcal{M}$ is the tool for analyzing the behaviour of the system $\mathcal{E}$ under different trajectories of the exogenous driver $\mathbf{W}_t$, the control variable $\mathbf{u}_t$ and alternatives of $\mathbf{u}^p$. Simulation analysis, often referred to as scenario analysis, what-if analysis or policy simulation, can be seen as an elementary and necessary step in almost all the above mentioned categories.

Real-world studies and applications often deal with more complicated problems that can be seen as a combination of the above mentioned problems. In all these cases the solution of (any) problem $\mathcal{P}$ is practically unfeasible due to the large computational requests. As the core of the difficulty stands in the dimensionality of model $\mathcal{M}$, the natural solution is to identify a reduced model that accurately emulates the output $\mathbf{Y}_t$, or the functional $J(\cdot)$, of model $\mathcal{M}$, but with a dimensionality such that problem $\mathcal{P}$ can be solved. The reduced model is named *emulation model* and it substitutes model $\mathcal{M}$ in problem $\mathcal{P}$: this replacement is possible because some processes described by the process-based model are more significant than others with respect to $\mathbf{Y}_t$ or $J(\cdot)$.

[3]A periodic sequence of control laws, which, given the current state $\mathbf{X}_t$ of the system $\mathcal{E}$ at each time instant t, suggests the optimal control to be adopted.

1.3 Complexity reduction

As said in the previous section, the *emulator* m, once identified, can be used in place of $\mathcal{M}$ in solving the problem $\mathcal{P}$. Depending on whether the purpose of the emulation modelling is to reproduce $\mathbf{Y}_t$ or $J(\cdot)$, the techniques available in the literature can be re-framed into two methodological approaches: *Dynamic Emulation modelling* (DEMo) and non-dynamic emulation modelling. The emulator neither modifies nor improves the conceptual features of the model $\mathcal{M}$; it simply makes it computationally more efficient in solving the problem $\mathcal{P}$. Hence, the consistency of an emulator is simply inherited from $\mathcal{M}$, which has to provide a meaningful and reliable representation of the system $\mathcal{E}$ for the range of inputs (exogenous drivers, control and planning variables) and parameters specified by the user.
This said, our purpose is to solve a *technical* problem: namely we cannot solve the problem $\mathcal{P}$ on $\mathcal{M}$ because of computational limitations and so we resort to m because we need to make it tractable. However, in the environmental context, where the stakeholder involvement often plays an important role (e.g. Castelletti and Soncini-Sessa, 2006, 2007; Voinov and Bousquet, 2010, and reference therein), these technical requirements have to be complemented by the fact that the emulator must also be *credible* from the user/analyst's point of view: : according to Aumann (2011), credibility will be taken to refer to a concept of adequacy when comparing a model, or simulation to a source system, with an intended use in mind. This concept needs to be distinguished from 'trust', which is taken to be a psychological state comprising the intention to accept vulnerability based upon positive expectations of the intentions or behaviour of another.

1.3.1 Dynamic Emulation modelling (DEMo)

According to Castelletti et al. (2012b), the purpose of any DEMo exercise is to provide a simplified description of the model $\mathcal{M}$ that preserves its dynamical nature. For this reason, the target of DEMo is to construct an approximation $\mathbf{y}_t$ of the model $\mathcal{M}$'s output $\mathbf{Y}_t$ (such that $\mathbf{y}_t \sim \mathbf{Y}_t$) by adopting a considerably smaller number of variables (states $\mathbf{x}_t$ and/or exogenous drivers $\mathbf{w}_t$) and, possibly, parameters $\mathbf{\Theta}$. The rationale behind this dimensionality reduction is that some of the processes described by the model $\mathcal{M}$ are more significant than others in affecting $\mathbf{Y}_t$, so that any simpler model that describes, as well as possible, only these processes and ignores the others can be considered as *operationally equivalent* to the model $\mathcal{M}$ with respect to the problem $\mathcal{P}$. Naturally, there is no attempt to reduce the dimensions of $\mathbf{u}_t$ and $\mathbf{v}$. Indeed, the controllability of the system $\mathcal{E}$ is assumed *a priori* . The identified dynamic emulator m is such that it's less computationally intensive than the model $\mathcal{M}$, its input-output behaviour approximates as well as possible the behaviour of $\mathcal{M}$, and it's credible to users in the sense discussed previously in this section; i.e. it reflects in a transparent and interpretable way the conceptual features of $\mathcal{M}$.

The emulator m can be either in an input-output or a state-space representation and one form may be more suitable than the other, depending upon the circumstances and the nature of the problem $\mathcal{P}$. One advantage of the input-output representation is that, in general, it requires less parameters than an equivalent state-space representation. On the other hand, in some problems, such as data assimilation and optimal management, the state-space representation can be more effective (Sadegh, 2001).

When an input-output representation is adopted, the emulator m is described entirely in the input-output space by a time-variant, generally non-linear transfer-function

$$\mathbf{y}_t = \mathbf{g}_t(\mathbf{y}_{t-1}, \dots, \mathbf{y}_{t-p}, \mathbf{w}_t, \dots, \mathbf{w}_{t-r}, \mathbf{u}_t, \dots, \mathbf{u}_{t-s}, \mathbf{v}|\boldsymbol{\theta}) \tag{1.3}$$

where $\boldsymbol{\theta}$ is a parameter vector and p, r and s are suitable time-lags. On the other hand, when a state-space representation is considered, the emulator m is described by the following, more complex, state transition and output transformation functions[4]

$$\mathbf{x}_{t+1} = \mathbf{f}_t(\mathbf{x}_t, \mathbf{w}_t, \mathbf{u}_t, \mathbf{v}|\boldsymbol{\theta}) \tag{1.4a}$$

$$\mathbf{y}_t = \mathbf{h}_t(\mathbf{x}_t, \mathbf{w}_t, \mathbf{u}_t, \mathbf{v}|\boldsymbol{\theta}) \tag{1.4b}$$

where $\mathbf{f}_t(\cdot)$ is a time-variant, generally non-linear vector function modelling the dynamics of $\mathbf{x}_t$, $\mathbf{h}_t(\cdot)$ is a a time-variant, generally non-linear, output transformation function, and $\boldsymbol{\theta}$ is a vector of parameters.

1.3.2 Non-dynamic emulation modelling

When the problem $\mathcal{P}$ concerns the optimal planning of the functional $J(\cdot)$ with respect to the vector $\mathbf{v}$, or the uncertainty and sensitivity analysis of $J(\cdot)$ with respect

[4]For convenience, it is assumed here that m is in a discrete-time form. However, often the emulator may well be better identified in continuous-time and then converted in discrete-time if required (Young and Ratto, 2009, 2011).

to the parameter $\mathbf{\Theta}$, the emulation modelling effort can be based on the identification of a static map between the planning variable $\mathbf{v}$ (and/or the parameters $\mathbf{\Theta}$) and the functional $J(\cdot)$.
Such non-dynamic emulation, first introduced as 'meta-modelling' by Blanning (1975), is based on the idea of identifying an emulator m that approximates the variation of the functional $J(\cdot)$ as well as possible. The terms *meta-model* (Blanning, 1975) or *response surface* (Box and Wilson, 1951; Kleijnen, 2008) are often used in place of emulator. When dealing with optimal planning $\mathcal{P}$ (see Section 1.2.3), non-dynamic emulation modelling is also known as *surrogate-based analysis and optimization* (Queipo et al., 2005).
The general theory of non-dynamic emulation modelling has been developed in the last two decades, especially in the fields of statistics and computer science (e.g. Sacks et al., 1989; Barton, 1998; Simpson et al., 2001; Chen et al., 2006, and references therein). In particular, research efforts have been concentrated on designing the simulation experiments to be conducted with the model $\mathcal{M}$ (the so-called Design Of Experiments (DOE)) and the development and testing of several emulator classes, e.g. polynomial regression models, kriging, radial basis functions, neural networks, Gaussian processes, adaptive regression splines, smoothing splines, ANOVA models and polynomial chaos expansion.
Non-dynamic emulation modelling has been used extensively in a wide variety of mechanical and aerospace engineering studies, but it has not been considered in the environmental field until more recently, with applications in the planning of agro-ecosystems, water distribution networks, groundwater resources, and surface water resources. In any case, non-dynamic emulation modelling can be considered as a simplified version of DEMo and, therefore, it is easily integrated within this wider concept and the subsequent discussion.

1.4 A general procedure for DEMo

The identification of a dynamic emulation model is made particularly difficult by the typically non-linear nature and large dimensionality of the model $\mathcal{M}$.
A number of different approaches, and corresponding techniques, have been developed as the basis for finding *ad-hoc* solutions to specific problems. However, all of these approaches can be re-conducted to the following general categories:

i) In the *structure-based* approach, the mathematical structure of the model $\mathcal{M}$ is 'manipulated', with the aim of deriving a simpler structure m. This approach is often adopted when the output $\mathbf{Y}_t$ of $\mathcal{M}$ is not defined, which is equivalent to saying that the output coincides with the state vector $\mathbf{X}_t$. Emulators identified using this approach are usually represented in a state-space form 1.4.

ii) the *data-based* approach identifies the emulator structure on the basis of a data-set $\mathcal{F}$ of state and output trajectories, obtained via simulation of the model $\mathcal{M}$ on a given horizon H under suitable input scenarios. The emulator structure can be either a black-box representation of some form; or a low order, conceptual, mechanistic model.

Whatever approach is adopted, the identification of an emulator can be structured as a six-step procedure (see Figure 1.1). The first step (Step 1 - *Design of experiments and simulation runs*) concerns the generation of the data-set $\mathcal{F}$. This is obviously required for the data-based approach, but it is also necessary in the structure-based one for the evaluation of the emulator in Step 6. The variables (exogenous drivers and states) that will be operated by the emulator are obtained by aggregating, in some appropriate way, the variables in the model $\mathcal{M}$ and/or selecting, among them, the most relevant ones. These two, not necessarily mutually exclusive operations, are the core of the complexity reduction process performed by DEMo and are considered in two separate steps (Step 2 - *Variable aggregation* and Step 3 - *Variable selection*). Variable selection generally follows the aggregation because it can be more effectively performed on a reduced number of variables. Once these steps are complete, the emulator is eventually identified in Step 4 (*Structure identification*). Finally, in Step 5 - *Evaluation and physical interpretation*, the emulator is validated and a physical interpretation is provided. Note that, in any real application, many recursions through this procedure may be required. The details in each step of the emulation modelling procedure are described in the next section.

1.4.1 Step 1 - Design of Experiments and simulation runs

The Design Of computer Experiments (DOE), also known as Design and Analysis of Computer Experiments (DACE), is used to design a sequence of simulation runs for the model $\mathcal{M}$ with the purpose of constructing the data-set $\mathcal{F}$ for the subsequent DEMo steps. This requires the specification of the input trajectories to the model $\mathcal{M}$ (i.e. the exogenous driver $\mathbf{W}_t$ and the control $\mathbf{u}_t$), as well as the values of the

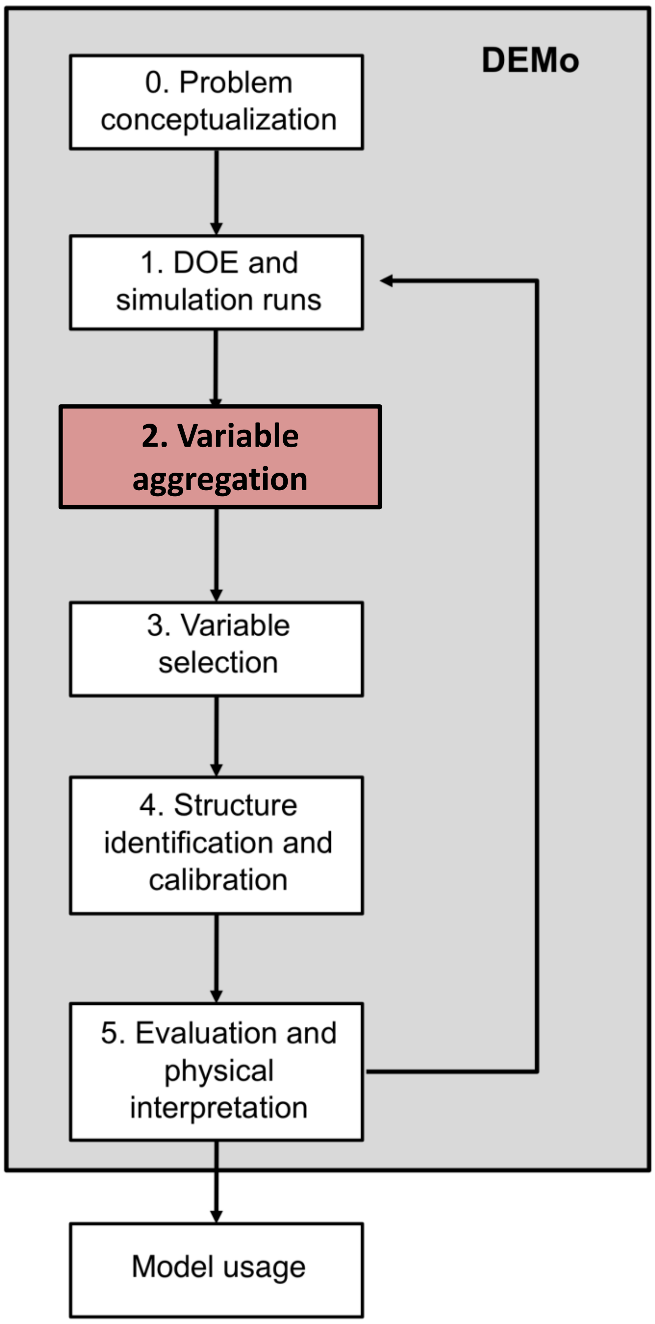
DEMo
0. Problem conceptualization
1. DOE and simulation runs
2. Variable aggregation
3. Variable selection
4. Structure identification and calibration
5. Evaluation and physical interpretation
Model usage

Figure 1.1: The DEMo procedure steps (see Castelletti et al., 2012b). Step 2, which is the one mainly explored in this work, is denoted in bold.

planning vector $\mathbf{v}$, that will drive the simulation runs, the parameters being set to their nominal value $\bar{\mathbf{\Theta}}$.
In principle, the data-set $\mathcal{F}$ should be sufficiently informative, reproducing all the possible system behaviours and features, excited and forced by the spectrum of external forces, controls and planning variables that may occur given the problem $\mathcal{P}$. This can be ensured by relying on the procedures used in the design of dynamic experiments, such as those discussed in Goodwin and Payne (1977). In other words the experiments have to be designed in such a way that all the dynamical modes of $\mathcal{M}$'s response that are of interest for $\mathcal{P}$ are activated.
However, according to the computational requirements for simulating $\mathcal{M}$ (i.e. the limit on the feasible number of simulation runs), a somewhat less formal experiment design may need be adopted (e.g. the historical observations available for the exogenous drivers and a well chosen periodic square wave input for the control, that allows the system to reach a steady state at each step). The accuracy requirements in the DOE also depends on the different approaches to the DEMo problem.

1.4.2 Step 2 - Variable aggregation

The purpose of this step is to aggregate the components of the state vector $\mathbf{X}_t$ (and of the exogenous driver vector $\mathbf{W}_t$) into lower dimensionality vectors. As common practice in environmental modelling, the model $\mathcal{M}$ is spatially-distributed: so the space discretization can lead to a strong increase in the dimensionality of the state and exogenous driver vectors.
The data generated via simulation in Step 1 (sometimes referred as *snapshots*) are used in an aggregation scheme to identify a mapping of the state $\mathbf{X}_t$ into a lower dimensional state $\tilde{\mathbf{X}}_t$, so that the majority of the variation in the $\mathbf{X}_t$ data is captured. The same is done with respect to $\mathbf{W}_t$, thus obtaining a reduced exogenous driver vector $\tilde{\mathbf{W}}_t$. The most simple and 'natural' aggregation scheme is based on the expert knowledge of the system (see Galelli et al., 2010; Castelletti et al., 2010b). This is particularly the case when $\mathcal{M}$ is spatially-distributed.
Alternatively, formal and analytical aggregation techniques can be employed. Such techniques are commonly referred to as *feature extraction* techniques (Guyon et al., 2006). The technique that has been adopted most often, up to now, is Principal Component Analysis (Jollife, 1986) (also known as proper orthogonal decomposition (Willcox and Peraire, 2002) or Karhunen Loève Transform (Zhang and Michaelis, 2003)), which performs a linear mapping of the data produced by the model $\mathcal{M}$ to a

lower dimensional space in such a way that the variance of the data in the lower dimensional representation is maximized, local linear embedding (Lee and Verleysen, 2007) and clustering (Jain et al., 1999a). The literature also presents a variety of non-linear feature extraction techniques (for a review, see Lee and Verleysen, 2007). Eventually, the data-set $\mathcal{F}$ is transformed into a lower-dimension data-set $\tilde{\mathbf{F}}$ of tuples $\tilde{\mathbf{X}}_t$, $\tilde{\mathbf{W}}_t$, $\mathbf{u}_t$, $\tilde{\mathbf{X}}_{t+1}$ and $\mathbf{Y}_t$. The step is useful when the dimensionality of the state vector $\mathbf{X}_t$ and of exogenous drivers vector $\mathbf{W}_t$ is considerable (thousands of components), as in spatially distributed models. On the other hand, when they are not too large (say a few dozens of components), this step can be avoided.
Variable aggregation is the step on which this thesis is focused on. The pre-processing of the exogenous drivers, controls and, state variables (to reduce the high number of variables appearing in the final emulator) can in fact be performed by adopting all the different above-mentioned techniques: the purpose of this work is to explore the potential of one of these methods, i.e. clustering, to automatically discover compact and relevant representations of high-dimensional data sets.

1.4.3 Step 3 - Variable selection

Based on the information content of $\tilde{\mathbf{F}}$, model $\mathcal{M}$ is further simplified by selecting the components of $\tilde{\mathbf{X}}_t$ and $\tilde{\mathbf{W}}_t$ that will constitute the emulator's state $\mathbf{x}_t$ and exogenous driver $\mathbf{w}_t$ vectors. Generally, this operation relies on some automated technique, since $\tilde{\mathbf{X}}_t$ and $\tilde{\mathbf{W}}_t$ are often too large to be handled by a human operator. Next subsection describes one of these automated techniques, i.e. Recursive Variable Selection (RVS) algorithm.

Recursive Variable Selection (RVS)

Recursive Variable Selection (RVS) algorithm (Castelletti et al., 2012b) is a selection algorithm that is able to automatically identify the most relevant variables among the components of $\tilde{\mathbf{X}}_t$ and $\tilde{\mathbf{W}}_t$ for building an emulator able to accurately reproduce the output values of the phisically-based model $\mathcal{M}$, but with a reduced dimensionality so that the original problem $\mathcal{P}$ is practically solvable.
In principle, the goal is a *lossless* complexity reduction (Givan et al., 2003): this is achieved through an automatic, data-driven method that recursively defines a sequence of variable selection problems, in which the accuracy of the results is tuned to the desired emulator parsimoniousness.

The RVS algorithm Castelletti et al. (2011) propose proceeds iteratively in three steps over each component of $\mathbf{Y}_t$. *i*) Given the information content of the dataset $\tilde{\mathcal{F}}$, the most relevant variables in explaining the given component are selected, with some appropriate Input Selection (IS) algorithm, among the components of the vectors $\tilde{\mathbf{X}}_t$, $\tilde{\mathbf{W}}_t$ and $\mathbf{u}_t$. This gives the arguments of the output transformation function (eq. (1.4b)) associated to the considered output. *ii*) For each state variable selected in the previous step, a new run of the IS algorithm is performed to select the variables relevant to describe its dynamics. This gives the arguments of the corresponding component of the vector state transition function (eq. (1.4a)) associated to the considered state variable. *iii*) If the second step leads to the selection of further variables from the vector $\tilde{\mathbf{X}}_t$ (i.e. state variables not yet included in $\mathbf{x}_t$), it is recursively repeated, until all the selected state variables are given a dynamic description. Once the RVS algorithm is over, the arguments of eqs. (1.4a) and (1.4b) are known. A detailed description of the RVS algorithm is reported in Castelletti et al. (2012a) and the meta-code is available in Appendix A (see Algorithm 1).
Each invocation of the RVS algorithm requires to run an IS algorithm that selects the most relevant input variables to explain a specified output variable. Algorithms suitable for this task must account for both significance and redundancy: in other words, they must be able to select only the most relevant input variables, while trying to avoid the inclusion of redundant ones, which would unnecessarily add to the emulator complexity. Literature reports a variety of input variable selection methods (for an overview see Peng et al. (2005); Bowden et al. (2005); Hejazi and Cai (2009) and May et al. (2008a,b)); the following subsection presents the one used in this thesis, the *Iterative Input Selection* algorithm (Castelletti et al., 2012a).

Iterative Input Selection (IIS)

As previously said, the ideal selection algorithm should account for non-linear dependencies and redundancy between variables, as real-world optimal management problems are usually characterized by non-linear dynamic models with multiple coupled variables. Moreover, it must be computationally efficient, since the number of candidate variables is generally large, particularly when the original process-based model is spatially distributed. To fulfil these requirements, Castelletti et al. developed the Iterative Input Selection (IIS) algorithm (see Algorithm 2 in Appendix A), a model-free, forward-selection algorithm, which has been firstly experimented in a traditional hydrological input selection problem (Castelletti et al., 2010a).

Given the output variable to be explained and the set of candidate variables, the IIS algorithm first exploits an Input Ranking (IR) algorithm that provides the best performing input according to a global ranking based on a statistical measure of significance (preferably accounting for non-linear dependencies, as proposed byWehenkel (1998)). To account for variable redundancy, only the most significant variable is then added to the set of selected variables. The reason behind this choice is that, once an input variable is selected, all the inputs that are highly correlated with it may become useless and the ranking needs to be re-evaluated. So, the algorithm proceeds first as follows: first it estimates, with an appropriate model building (MB) algorithm[5], an underlying model $\hat{m}(\cdot)$ to explain the output; then it repeats the ranking process using the residuals of model $\hat{m}(\cdot)$ as new output variable.
The algorithm iterates these operations until the best variable returned by the ranking algorithm is not in the already selected ones or the accuracy of $\hat{m}(\cdot)$ does not significantly improve. The accuracy can be computed with a suitable distance metric between the output and the model $\hat{m}(\cdot)$ prediction, or more sophisticated metrics accounting for both accuracy and parsimoniousness (e.g. the Akaike information criterion, Bayesian information criterion or Young identification criterion). In this thesis the accuracy of the model is expressed through the parameter R^2: in particular the algorithm stops when the value of R^2 increases less than a small constant ϵ).
The choice of a suitable model building algorithm (MB) and ranking procedure (IR) is thus fundamental to let the IIS algorithm be capable of dealing with non-linearities, redundancy and high-dimension data-sets. Among the many alternative model classes, in this thesis *Extremely randomized trees* (or Extra-Trees, a tree-based method proposed by Geurts and Ernst (2006) that can provide all these desirable features) are used. As a consequence, also the choice of which ranking algorithm (Jong et al., 2004) to use has fallen on a method based on Extra-Trees, since their particular structure can be exploited too to infer the relative importance of the input variables.

[5]Depending on whether a parametric or a non-parametric model structure is adopted for the underlying model, the model building (MB) algorithm can be either a traditional parameter estimate algorithm or the building algorithm of the regressor.

1.4.4 Step 4 - Structure identification

The outcome of the variable selection (Step 3) are the variables characterizing the emulator, as well as the nature of the relationship between these variables and the output $\mathbf{y}_t$. This information can be exploited in this step of the DEMo procedure:in particular, this step is generally performed in two stages. The first stage is 'structure identification', and the second is 'parameter estimation': first the structure of the function $\mathbf{g}_t(\cdot)$ (or $\mathbf{f}_t(\cdot)$ and $\mathbf{h}_t(\cdot)$) is identified (e.g. using model structure identification criteria. Some insight on candidate model structures might come from the variable selection process (see Castelletti et al., 2010b)), then the value of $\boldsymbol{\theta}$ that characterizes the best model structure is estimated (optimally in some sense, if this is possible, but otherwise to yield statistically consistent estimates). In general, the emulator structure is only obtained tentatively in the first step, which serves as a 'screening' step for the variables to be finally included in the emulator. The class of functional relationships underlying the variable selection process (Step 3) is usually the first option for the structure identification (e.g. when correlation analysis is employed, a linear model is the most coherent choice) but, usually, the exploration of a wider class of models is more effective (Guyon and Elisseeff, 2003).
In any case, whatever approach is used, this step is concluded with a parameter estimation performed over the data-set $\tilde{\mathcal{F}}$ that provides the actual values for the $\boldsymbol{\theta}$ parameters. If the performance measures are satisfactory, one can proceed with the following step; otherwise, one of the previous step must be re-considered.

1.4.5 Step 5 - Evaluation and physical interpretation

As introduced in Section 1.3, the emulator must be evaluated from two different points of view (see, e.g., Castelletti et al., 2010f): *i*) it must reproduce as well as possible the input-output behaviour of the model $\mathcal{M}$; *ii*) it must be credible. With respect to point *i*), the emulator is validated against that part of the data-set $\tilde{\mathcal{F}}$ that has not been used for the model identification (the validation data-set). As for point *ii*), the credibility of the emulator is directly related to its physical interpretability. This latter property is inherent when the emulator structure is obtained with the techniques proposed for the structure-based approach in Section 1.4.3; or with the data-based approach, when it can be satisfactorily interpreted in a physically meaningful manner. Generally, the identification of an emulator in state-space representation makes it easier to maintain a physically meaningful relationship between the emulator and the original model variables.

1.4.6 Step 6 - Model usage

Once the emulator has been successfully validated against the data, it is ready to be employed by the user in the resolution of the problem $\mathcal{P}$. However, during the identification of the emulation model more than one run of the entire procedure can arise. In fact, if the performance of the model is not considered sufficient for the future use of the model itself, it's possible to design different simulation runs in order to evaluate other reduction approaches.

1.5 Purpose of this work

In this thesis the attention is focused on Step 2 of emulation modelling procedure (i.e. Variable Aggregation). As said, when applied to large 3D models, any DEMo technique does require a pre-processing of the exogenous drivers, controls and state variables to reduce the high number of variables appearing in the final emulator: at the moment this operation is hard to perform, and it is usually based on the expert knowledge of the system. Moreover, at the moment emulation modelling techniques are available only for linear and weakly non-linear models, while theory is still under development for non-linear models, and, apart from particular cases, the final emulator lacks of credibility by stakeholders and domain experts, as it is often hard to preserve the physical interpretability of the system.
The purpose of the research here presented is thus to propose a formal procedural approach to improve Variable Aggregation so that the final emulator embodies the following important properties: *i*) be fully automated, independent of domain experts and system knowledge, and suitable for non-linear processes; *ii*) have high potential in terms of complexity reduction, thus allowing for the management of large-scale environmental systems; *iii*) provide a physical interpretation of the reduced model structure, thus enhancing the credibility of the model to stakeholders and decision-makers. Among the different existing techniques, this work explores the potential of clustering as lumping method, to automatically discover compact and relevant representations of high-dimensional data sets. In particular, agglomerative hierarchical clustering is the selected technique.

Chapter 2

Clustering of data time series

In Chapter 1 Dynamic Emulation Modelling techniques are introduced as effective solution to overcome the limitations that arise when dealing with complex physically-based models in high-resources demanding problems. As anticipated, the purpose of this thesis is to enhance the status of these techniques, focusing on data-driven DEMo, in such a way that the derived emulator is fully automated, independent of domain experts and system knowledge, and suitable for non-linear processes. Moreover, the state-space representation and the associated physical interpretability of the system should be preserved.
Chapter 2 is focused on Step 2 of the DEMo procedure, variable aggregation: cluster analysis is introduced as aggregation technique to reduce the number of variables appearing in the final emulation model, while preserving the above-mentioned important properties. The novel aspect is that the aggregation procedures is here applied to data time series.
The chapter is organized as follows: Section 2.1 describes the basics of clustering methods and introduces the reader to time series clustering. Section 2.2 shows the main time series clustering algorithms. The key points of any clustering algorithm are the similarity/distance measures between objects when forming the clusters, and the linkages methods, to determine when two clusters are sufficiently similar to be linked together: the former are described in Section 2.3, the latter in Section 2.4. Finally, clustering results evaluation criteria are in Section 2.5.

2.1 Basics of clustering

The term cluster analysis (first used by Tryon, 1939) encompasses a number of different algorithms and methods for grouping objects of similar kind into respective categories: it is an exploratory data analysis tool that aims at identifying structures in an unlabelled data set by objectively organizing data into homogeneous groups where the within-group-object similarity is minimized and the between-group-object dissimilarity is maximized (see Nayak and Dash, 2012).

Clustering is necessary when no labelled data are available regardless of whether the data are binary, categorical, numerical, interval, ordinal, relational, textual, spatial, temporal, spatio-temporal, image, multimedia, or mixtures of the above data types. Clustering main task is explorative data mining, and a common technique for statistical data analysis used in many fields, including machine learning, pattern recognition, image analysis, information retrieval, and bioinformatics. Basic texts for cluster analysis include those by Anderberg (1973), Hartigan (1975), Everitt (1980), Aldenderfer and Blachfield (1984), Romesburg (1984), Jain and Dubes (1988) and Kaufman and Rousseeuw (1990).

Cluster analysis itself is not one specific algorithm, but the general task to be solved. It can be achieved by various algorithms that differ significantly in their notion of what constitutes a cluster and how to efficiently identify it. The appropriate clustering algorithm and parameter settings (including values such as the distance function to use, a density threshold or the number of expected clusters) depend on the individual data set and intended use of the results (Jain et al., 1999b). Cluster analysis as such is not an automatic task, but an iterative process of knowledge discovery that involves trial and error. Anderberg (Anderberg, 1973) states that there should be at least the following elements in a cluster analysis study before the final results can be attained: *i*) choice of a clustering approach; *ii*) choice of a similarity/dissimilarity measure; *iii*) choice of a linkage method; *iv*) choice of an evaluation criteria. These are the most significant steps of a general clustering process, and a detailed description of each element is given in the following sections. The reader is referred to Liao (2005) for further details.

2.1.1 Clustering algorithms

To date, most, if not all, clustering programs developed as an independent program or as part of a large suite of data analysis or data mining software work only with static data set. Han and Kamber (2001) classify clustering methods for static data into five major categories: partitioning methods, hierarchical methods, density-based methods, grid-based methods, and model-based methods. A brief description of each category of methods follows.

Partitioning methods Given a set of n unlabelled data tuples, a partitioning method constructs k partitions of the set, where each partition represents a cluster containing at least one object and $k \leq n$. The partition is crisp if each object belongs to exactly one cluster, or fuzzy if one object is allowed to be in more than one cluster to a different degree. Two renowned heuristic methods for crisp partitions are the *k-means* algorithm (MacQueen, 1967), where each cluster is represented by the mean value of the objects in the cluster and the *k-medoids* algorithm (Kaufman and Rousseeuw, 1990), where each cluster is represented by the most centrally located object in the cluster. The fuzzy duals are the *fuzzy c-means* algorithm (Bezdek, 1987) and the *fuzzy c-medoids* algorithm (Krishnapuram et al., 2001).

Hierarchical methods A hierarchical clustering method works by grouping data objects into a tree of clusters. There are generally two types of hierarchical clustering methods: agglomerative and divisive. Agglomerative methods start by placing each object in its own cluster and then merge clusters into larger and larger clusters, until all objects are in a single cluster or until certain termination conditions, such as the desired number of clusters, are satisfied. Divisive methods do just the opposite. A pure hierarchical clustering method suffers from its inability to perform adjustment once a merge or split decision has been executed. For improving the clustering quality of hierarchical methods, there is a trend to integrate hierarchical clustering with other clustering techniques (e.g., BIRCH (Zhang et al., 1996), CURE (Guha et al., 1998), and Chameleon (Karypis et al., 1999)).

Density-based methods The general idea of density-based methods such as DB-SCAN (Ester et al., 1996) is to continue growing a cluster as long as the density (number of objects or data points) in the neighbourhood exceeds some threshold. Rather than producing a clustering explicitly, OPTICS (Ankerst et al., 1999) computes an augmented cluster ordering for automatic and interactive cluster analysis. The ordering contains information that is equivalent to density-based clustering obtained from a wide range of parameter settings, thus overcoming the difficulty of selecting parameter values.

Grid-based methods Grid-based methods quantize the object space into a finite number of cells that form a grid structure on which all of the operations for clustering are performed. A typical example of the grid-based approach is STING (Wang et al., 1997), which uses several levels of rectangular cells corresponding to different levels of resolution. Statistical information regarding the attributes in each cell are pre-computed and stored. A query process usually starts at a relatively high level of the hierarchical structure. For each cell in the current layer, the confidence interval is computed reflecting the cell's relevance to the given query. Irrelevant cells are removed from further consideration. The query process continues to the next lower level for the relevant cells until the bottom layer is reached.

Model-based methods Model-based methods assume a model for each of the clusters and attempt to best fit the data to the assumed model. There are two major approaches of model-based methods: statistical approach, e.g. AutoClass (Cheeseman and Stutz, 1996), which uses Bayesian statistical analysis to estimate the number of clusters, and neural network approach, e.g. ART (Carpenter and Grossberg, 1987) and self-organizing maps (Kohonen, 1990).

2.2 Time series clustering

Unlike static data, the time series of a variable comprise values changing with time. Time series data are of interest because of their pervasiveness in various areas ranging from science, engineering, business, finance, economic, health care, to government. Formally, a time series data is defined as a sequence of pairs

$$T = [(p_1, t_1), (p_2, t_2), \ldots, (p_i, t_i), \ldots, (p_n, t_n)] \tag{2.1}$$

where $t_1 < t_2 < \ldots < t_i < \ldots < t_n$, each p_i is a data point in a d-dimensional data space, and each t_i is the time stamp at which p_i occurs. If the sampling rates of two time series are the same, one can omit the time stamps and consider them as sequences of d-dimensional data points. In reality, however, sampling rates of time series may be different. Furthermore, some data points of time series may be affected by noise or even completely missing, which poses additional challenges to

the processing of such data.
Given a set of unlabelled time series, it is often desirable to determine groups of similar time series. These unlabelled time series could be monitoring data collected during different periods from a particular process or from more than one process. Works devoting to the cluster analysis of time series are relatively scant compared with those focusing on static data. However, there seems to be a trend of increased activity (Košmelj and Batagelj (1990); Shaw and King (1992); Van Wijk and Van Selow (1999); Beran and Mazzola (1999); Xiong and Yeung (2002)).
Just like static data clustering, time series clustering requires a clustering algorithm or procedure to form clusters given a set of unlabelled data objects, and the choice of the clustering algorithm depends both on the type of data available and on the particular purpose and application. As far as time series data are concerned, distinctions can be made as to whether the data are discrete-valued or real-valued, uniformly or non-uniformly sampled, univariate or multivariate, and whether data series are of equal or unequal length. Non-uniformly sampled data must be converted into uniformed data before clustering operations can be performed. This can be achieved by a wide range of methods, from simple down sampling based on the roughest sampling interval to a sophisticated modelling and estimation approach.

Various algorithms have been developed to cluster different types of time series data. Putting their differences aside, it is far to say that in spirit they all try to modify the existing algorithms for clustering static data in such a way that time series data can be handled or to convert time series data into the form of static data so that the existing algorithms for clustering static data can be directly used. The former approach usually works directly with raw time series data, thus called raw-data-based approach, and the major modification lies in replacing the distance/similarity measure for static data with an appropriate one for time series. The latter approach first converts a raw time series data either into a feature vector of lower dimension or a number of model parameters, and then applies a conventional clustering algorithm to the extracted feature vectors or model parameters, thus called feature- and model-based approach, respectively. Generally speaking, three of the five major categories of clustering methods for static data, specifically *partitioning methods*, *hierarchical methods*, and *model-based methods*, have been utilized directly or modified for time series clustering. A brief review of the some general-purpose algorithms commonly employed in most clustering studies on time series is presented below.

Relocation clustering belongs to partitioning methods, which seek to divide a data set into some number of disjoint clusters such that related compounds will all be in the same cluster, with compounds unrelated to that cluster being distributed among the other clusters in the set. Relocation involves the movement of compounds between clusters in such a way as to increase the homogeneity of the individual clusters, the degree of inter-cluster similarity as measured by some similarity or distance function. The relocation clustering procedure has the following four steps:

Step 1 The initial set of clusters is obtained by randomly assigning integers in the range 1 to c, where c is the desired number of clusters, to each of the compounds in a data set. Denote by C the initial clustering, having the prescribed c number of clusters.

Step 2 For each time point compute the dissimilarity matrix and store all resultant matrices computed for all time points for the calculation of trajectory similarity.

Step 3 Each of the structures is matched against the mean vector of each of the clusters and assigned to that cluster which results in the smallest (or largest) value for the chosen dissimilarity (or similarity) measure, and then the mean vectors of the new clusters are computed.
The relocation is repeated for some fixed number of iterations, or until no further relocation of compounds takes place: this will correspond to a local, but not necessarily global, minimum in the clustering criterion.

Step 4 Find a clustering $\tilde{C}$, such that $\tilde{C}$ is better than C in terms of one similarity measure (see Section 2.3). If no such clustering exists, then stop; else replace C by $\tilde{C}$ and repeat *step 3*.

This procedure works only with time series with equal length because the distance between two time series at some cross sections (time points where one series does not have value) is ill defined.

To partitioning methods belongs also the *k-means* method (interchangeably called *c-means* in this study), which was first developed more than three decades ago. The main idea behind it is the minimization of an objective function, which is normally chosen to be the total distance between all patterns (i.e. the time series) from their respective cluster centers. Its solution relies on an iterative scheme, which starts with arbitrarily chosen initial cluster memberships or centers. The distribution of objects among clusters and the updating of cluster centers are the two main steps of the c-means algorithm.

The algorithm alternates between these two steps until the value of the objective function cannot be reduced anymore. Given n time series $\{x_k|k = 1, \cdots, n\}$, c-means determine c cluster centers $\{v_i|i = 1, \cdots, c\}$), by minimizing the objective function given as

$$\min J_1(U, V) = \sum_{i=1}^{c}\sum_{k=1}^{n} \mu_{ik} \parallel x_k - v_i \parallel^2 \tag{2.2}$$

s.t. (1) $\mu_{ik} \epsilon \{0, 1\} \forall i, k$ is the membership matrix; (2) $\sum_{i=1}^{c} \mu_{ik} = 1, \forall k$ $\|\cdot\|$ in the above equation is normally the Euclidean distance measure (other distance measures could also be used); (3) U and V are respectively the membership matrix and the vector of the cluster centers at a fixed iteration.

The iterative solution procedure generally has the following steps:

(1) Choose c $(2 \leq c \leq n)$ and ε (a small number for stopping the iterative procedure). Set the counter $l = 0$ and the initial cluster centers, $V^{(0)}$, arbitrarily.

(2) Distribute $x_k, \forall k$ to determine $U^{(l)}$ such that J_1 is minimized. This is achieved normally by reassigning x_k to a new cluster that is closest to it.

(3) Revise the cluster centers $V^{(l)}$.

(4) Stop if the change in V is smaller than ε; otherwise, increment l and repeat Step 2 and Step 3.

Dunn (1973) first extended the c-means algorithm to allow for fuzzy partition, rather than hard partition, by using the objective function given in the equation below:

$$\min J_2(U, V) = \sum_{i=1}^{c}\sum_{k=1}^{n} (\mu_{ik})^2 \parallel x_k - v_i \parallel^2 \tag{2.3}$$

Note that $U = [\mu_{ik}]$ in this and the following equations denotes the matrix of a fuzzy c-partition. The fuzzy c-partition constraints are (1) $\mu_{ik} \epsilon [0, 1] \forall i, k$, (2) $\sum_{i=1}^{c} \mu_{ik} = 1, \forall k$, and (3) $0 < \sum_{k=1}^{n} \mu_{ik} < n, \forall i$.

In other words, each x_k could belong to more than one cluster with each membership taking a fractional value between 0 and 1. Bezdek (1987) generalized $J_2(U, V)$ to an

infinite number of objective functions, i.e., $J_m(U, V)$, where $1 \leq m \leq \infty$.
The new objective function subject to the same fuzzy c-partition constraints is

$$\min J_m(U, V) = \sum_{i=1}^{c} \sum_{k=1}^{n} (\mu_{ik})^m \parallel x_k - v_i \parallel^2 \tag{2.4}$$

By differentiating the objective function with respect to v_i (for fixed U) and to μ_{ik} (for fixed V) subject to the 3 conditions as in (2.3), one obtains the following two equations:

$$v_i = \frac{\sum_{k=1}^{n} (\mu_{ik})^m x_k}{\sum_{k=1}^{n} (\mu_{ik})^m}, i = 1, \ldots, c \tag{2.5}$$

$$\mu_{ik} = \frac{(1/ \parallel x_k - v_i \parallel^2)^{1/(m-1)}}{\sum_{j=1}^{c} (1/ \parallel x_k - v_j \parallel^2)^{1/(m-1)}}, i = 1, \ldots, c; k = 1, \ldots, n; \tag{2.6}$$

To solve the fuzzy c-means model, an iterative alternative optimization procedure is required. To run the procedure the number c of clusters, and the weighting coefficient m must be specified. The fuzzy c-means algorithm has the following steps:

(1) Choose c ($2 \leq c \leq n$), m ($1 \leq m \leq \infty$) and ε (a small number for stopping the iterative procedure). Set the counter $l = 0$ and initialize the membership matrix $U^{(l)}$.

(2) Calculate the cluster center $v_i^{(l)}$, by using Equation (2.5).

(3) Update the membership matrix $U^{(l+1)}$ by using Equation (2.6). if $x_k \neq v_i^{(l)}$. Otherwise, set $\mu_{ik} = 1(0)$ if $j = (\neq) i$.

(4) Compute $\mathit{\Delta} = \|U^{(l+1)} - U^{(l)}\|$. If $\mathit{\Delta} > \varepsilon$, increment l and go to step 2. If $\mathit{\Delta} \leq \varepsilon$, stop.

This group of algorithms works better with time series of equal length because the concept of cluster centers becomes unclear when the same cluster contains time series of unequal length.

The most widely used hierarchical method is *agglomerative hierarchical clustering*, which works by grouping time series data into a tree of clusters. It starts by placing each object in its own cluster and then it calculates the proximity matrix[1]. Afterwards, it merges these atomic clusters into larger and larger clusters according to

[1]i.e. the square matrix in which the entry in cell *(j, k)* is some measure of the similarity (or distance) between the items to which row j and column k correspond.

the distances between the clusters themselves, until all the objects are in a single cluster or until certain termination conditions are satisfied. At each clustering step, all possible mergers of two clusters are tried. The closest clusters are merged together, according to the selected linkage method (see Section 2.4). This approach is expressed more formally as follows.

```
Algorithm Basic agglomerative hierarchical clustering algorithm
1. Compute the proximity matrix.
2. Repeat
        3. Merge the closest two clusters.
        4. Update the proximity matrix to reflect the proximity
        between the new cluster and the original clusters.
        5. until: only one cluster remains.
```

A part from its intrinsic simplicity, the hierarchical agglomerative cluster algorithm provides a number of advantages:

i) the algorithm works directly on raw time series data, and does not require any conversion of the data into lower-dimension vectors, thus preserving the initial data integrity;

ii) time series are grouped into a tree of clusters that shows the relative distance between clusters;

iii) unlike other algorithms (e.g. k-means, Hartigan and Wong (1979)), the number of clusters has not to be specified a-priori and this leaves a certain degree of freedom for the final choice.

Self-organizing maps (SOM) belong to the category of model-based methods, and they were developed by Kohonen (1990) as a class of neural networks with neurons arranged in a low dimensional structure and trained by an iterative, unsupervised, or self-organizing procedure.
This particular type of neural network is trained to produce a low-dimensional (typically two-dimensional), discretized representation of the input space of the training samples, called a map. Self-organizing maps are different from other artificial neural networks in the sense that they use a neighbourhood function to preserve the

topological properties of the input space. The training process is initialized by assigning small random values to the weight vectors w of the neurons in the network. Each training-iteration consists of three steps: *i*) the presentation of a randomly chosen input vector *x(t)* from the input space; *ii*) the evaluation of the network; *iii*) the update of the weight vector *w(t)*. After the presentation of a pattern, the Euclidean distance between the input pattern and the weight vector is computed for all neurons in the network. The neuron with the smallest distance is marked as t. Depending upon whether a neuron is within a certain spatial neighbourhood around t, its weight is updated according to the following updating rule:

$$w(t+1) = w(t) + \alpha(t)[x(t) - w(t)] \tag{2.7}$$

Since the neighbouring neurons are updated at each step, there is a tendency that neighbouring neurons in the network represent neighbouring locations in the feature space. In other words, the topology of the data in the input space is preserved during the mapping. Like the group of k-means and fuzzy c-means algorithms, SOM does not work well with time series of unequal length due to the difficulty involved in defining the dimension of weight vectors.

2.3 Similarity/Distance measures

Almost without exception each of the clustering algorithms/procedures reviewed in the previous section requires a measure to compute the distance or similarity between two time series being compared. Depending upon whether the data are discrete-valued or real-valued and whether time series are of equal or unequal length, a particular measure might be more appropriate than another.

One possible classification of the different similarity measures present in literature is according to the method the distance between two time series being compared is calculated with (see Ding et al. (2008)). There are, in fact, some distance measures that compare the i^{th} point of one time series to the i^{th} point of another time series: these are the *lock-step measures* (e.g., euclidean distance, root mean square distance, Mikowski distance, Manhattan distance (Yi and Faloutsos, 2000), DISSIM (Frentzos et al., 2007), and so on). Besides being relatively straightforward and intuitive, lock-step distance measures have several other advantages. The complexity of evaluating these measures is linear, and they are easy to implement and indexable with any access method and, in addition, are parameter-free. Moreover, they are surprisingly competitive compared to other more complex approaches, especially if the size of the training set/database is relatively large. However, since the mapping between the points of two time series is fixed, these distance measures are very sensitive to noise and misalignments in time, and are unable to handle local time shifting, i.e., similar segments that are out of phase. This negative aspect, however, do not always invalidate the results, thus making this category of distance measures really competitive.

Elastic measures, on the contrary, are distance measures that allow comparison of one-to-many or one-to-none points (e.g., Dynamic time warping distance, Longest Common SubSequence distance (Vlachos et al., 2002), Edit Sequence on Real Sequence distance (Chen and Ozsu, 2005), and so on). This category of distance measures comes from the need to handle time warping in similarity computation, in order to allow a time series to be stretched or compressed to provide a better match with another time series. It has been shown that the cost for computing this kind of distance measures on large data sets is almost linear (see Keogh and Ratanamahatana (2005)). The main disadvantage is that some parameters have to be introduced, such as threshold parameters or a constant reference point, for computing the distance between the time series.

Finally, a further approach regards *pattern-based measures* (Chen et al., 2007), which find out matching segments within the time series, thus allowing comparison of many-to-many points. The algorithm identifies the different patterns by permitting shifting and scaling in both the temporal and amplitude dimensions. The problem of computing similarity value between time series is then transformed to the one of finding the most similar set of matching patterns. One disadvantage of this approach is that, as for elastic distance measures, it requires tuning a number of parameters, such as the temporal scale factor, amplitude scale factor, pattern length, and sliding step size.

In the following subsections, a brief review of the most common above-mentioned similarity measures for each category is presented. Particular emphasis is given to Euclidean distance as it is the selected distance measure implemented in this thesis.

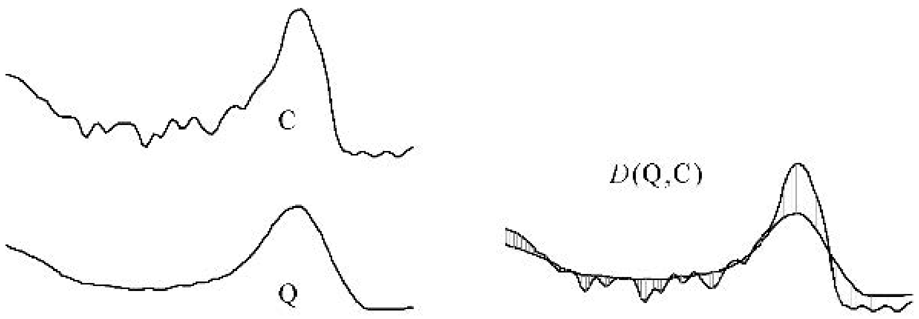

Figure 2.1: The intuition behind the Euclidean distance metric (from Ratanamahatana et al. (2010)).

2.3.1 Euclidean distance, root mean square distance and Mikowski distance

One of the simplest similarity measures for time series is the Euclidean distance measure (see Figure 2.1). Let x_i and v_j each be a n-dimensional vector. The Euclidean distance is computed as

$$d_E = \sqrt{\sum_{k=1}^{n}(x_{ik} - v_{jk})^2}. \tag{2.8}$$

The root mean square distance (or average geometric distance) is simply

$$d_{rms} = d_E/n \tag{2.9}$$

where n is the number of elements of the vectors x_i and v_j. Mikowski distance is a generalisation of Euclidean distance, and it is defined as

$$d_M = \sqrt{\sum_{k=1}^{P}(x_{ik} - v_{jk})^q}. \tag{2.10}$$

In the above equation, q is a positive integer. A normalized version can be defined if the measured values are normalized via division by the maximum value in the sequence. It is interesting to notice that Euclidean (and squared Euclidean) distances are usually computed from raw data, and not from standardized data. Such a measure is simple to understand and easy to compute, which has ensured that the Euclidean distance is the most widely used distance measure for similarity search (Agrawal et al. (1993), Chan and Fu (1999), Faloutsos et al. (1994)). However,

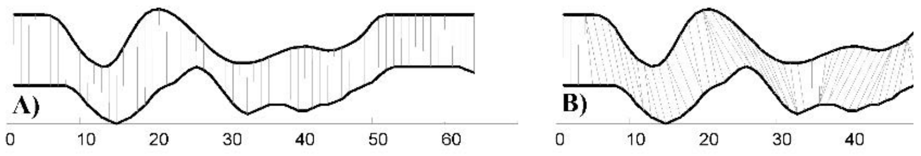

Figure 2.2: Two time series requiring a warping measure. Note that while the sequences have an overall similar shape, they are not aligned in the time axis (from Ratanamahatana et al. (2010)).

one major disadvantage is that it is very brittle; it does not allow for a situation where two sequences are alike, but one has been 'stretched' or 'compressed' along one direction in the space. This problem can be dealt easily with offset translation and amplitude scaling, which requires normalizing the sequences before applying the distance operator.

2.3.2 Dynamic time warping distance

In some time series domains, a very simple distance measure such as the Euclidean distance will suffice. However, it is often the case that the two sequences have approximately the same overall component shapes, but these shapes do not line up in X-axis. Figure 2.2 shows this with a simple example. In order to find the similarity between such sequences or as a preprocessing step before averaging them, the time axis of one (or both) sequences must be warped to achieve a better alignment.
Dynamic Time Warping (DTW) is a technique for effectively achieving this warping. Euclidean distance, which assumes the i^{th} point on one sequence is aligned with i^{th} point on the other (A), will produce a pessimistic dissimilarity measure. A non linear alignment (B) allows a more sophisticated distance measure to be calculated. In Berndt and Clifford (1996), the authors introduce the technique of dynamic time warping to the Data Mining community. Dynamic time warping is an extensively used technique in speech recognition, and allows acceleration-deceleration of signals along the time dimension. The basic idea is described below. Consider two time series of possibly different lengths, $C = \{c_1, \ldots, c_m\}$ and $Q = \{q_1, \ldots, q_n\}$. When computing the similarity of the two time series using Dynamic Time Warping, it is permitted to extend each sequence by repeating elements.
A straightforward algorithm for computing the Dynamic Time Warping distance between two sequences uses a bottom-up dynamic programming approach: although this technique is impressive in its ability to discover the optimal of an exponential

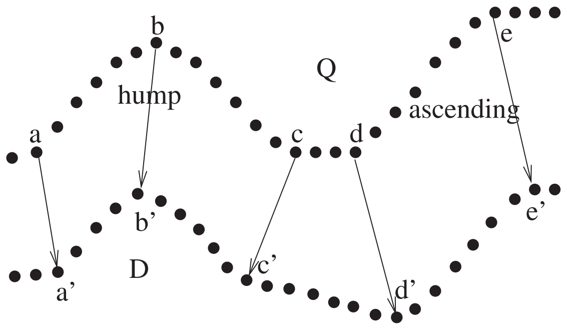

Figure 2.3: Illustration of shifting and scaling in temporal and amplitude dimensions of two time series, handled by pattern-based similarity measures (from Chen et al. (2007)).

number alignments, a basic implementation runs for a long time, proportional to the length of the time series. If a warping window w is specified, then the running time reduces considerably: anyway the computational requirements of this algorithm are still high for most large scale application. In Ratanamahatana and Keogh (2004), the authors introduce a novel framework based on a learned warping window constraint to further improve the classification accuracy, as well as to speed up the DTW calculation.

2.3.3 Spatial Assembling distance (SpADe)

As anticipated, Euclidean distance has been shown to be ineffective in measuring distances of time series in which shifting and scaling usually exist. Consequently, warping distances (such as the above-mentioned Dynamic Time Warping and Longest Common Subsequence distance), have been proposed to handle warps in temporal dimension. However, they are inadequate in handling shifting and scaling in amplitude dimension. Moreover, they have been designed mainly for full sequence matching, whereas in on-line monitoring applications, there is typically no knowledge on the positions and lengths of possible matching subsequences.
Pattern-based similarity measures, such as Spatial Assembling Distance (SpADe), have thus been introduced to handle shifting and scaling in both temporal and amplitude dimensions of time series. Figure 2.3 shows cases of warps (shifting and scaling) existing between query pattern Q and data sequence D. Note that D is similar to Q at semantic level, as there is a hump followed by an ascending trend in both of them. The first warp is time shifting, i.e., the lag of ascending trend to

the hump in Q (measured as $d - c$) is different from that (measured as $d' - c'$) in D. The second is amplitude shifting, e.g., the values of data items between d and e in Q are larger than those of the corresponding items between d' and e' in D. The third is scaling, the extensions of humps in Q and D are different in both temporal dimension (from $c - a$ and $c' - a'$) and amplitude dimension (from $Q(b) - Q(a)$ and $D(b') - D(a')$). The main disadvantage of such an approach is that it is computational intensive, and incurs redundant computational overhead. As a subsequence matching problem, pattern detection on streaming time series is naturally expensive. The reader is referred to Chen et al. (2007) for further details.

2.4 Linkage methods

Once the distance between the time series is performed, the following operation of each clustering algorithm is the computation of the proximity between two clusters, in order to build bigger and bigger clusters until only one cluster remains or a termination condition is satisfied (or, viceversa, to divide one big clusters in smaller clusters). Some definition of cluster proximity will be described in the following sections.

2.4.1 Single

For the single linkage method (Hartigan, 1981), the proximity of two clusters is defined as the minimum of the distance between any two points in the two different clusters. Using graph terminology, starting with all points as singleton clusters and adding links between points one at a time, shortest links first, then these single links combine into clusters. Mathematically:

$$d(C_i, C_j) = \min_{x \in C_i, y \in C_j} d(x, y). \tag{2.11}$$

where x and y are two generic points belonging respectively to cluster C_i and C_j, and d is the mathematical operator that computes the distance between these points. The single linkage technique is good at handling non-elliptical shapes, but it is sensitive to noise and outliers. By imposing no constraints on the shape of clusters, it sacrifices performance in the recovery of compact clusters in return for the ability to detect elongated and irregular clusters. Also, single linkage tends to chop off the tails of distributions before separating the main clusters (Jardine and Sibson, 1971).

2.4.2 Complete

For the complete linkage method (first introduced in Sorensen, 1948), the proximity of two clusters is defined as the maximum (minimum of the similarity) between any two points in the two different clusters. Using graph terminology, starting with all points as singleton clusters and adding links between points one at a time, shortest links first, then a group of points is not a cluster until all the points in it are completely linked, i.e., form a clique. Mathematically:

$$d(C_i, C_j) = \max_{x \in C_i, y \in C_j} d(x, y). \tag{2.12}$$

where x and y are two generic points belonging respectively to cluster C_i and C_j, and d is the mathematical operator that computes the distance between these points. Complete link is less susceptible to noise and outliers, but it can break large clusters and it favours globular shapes. Unfortunately, it is strongly biased toward producing compact clusters with roughly equal diameters, and it can be severely distorted by moderate outliers.

2.4.3 Average

For the average linkage method (first introduced in Sokal and Michener, 1958), the proximity of two clusters is defined as the average pairwise proximity among all pairs of points in the different clusters. This is an intermediate approach between the single and complete link approaches. Thus, for group average, the cluster proximity $d(C_i, C_j)$ of clusters C_i and C_j, which are of size m_i and m_j, respectively, is expressed by the following equation:

$$d(C_i, C_j) = \frac{\sum\limits_{x \in C_i, y \in C_j} d(x, y)}{m_i \cdot m_j}. \tag{2.13}$$

Average linkage tends to join clusters with small variances, and it is slightly biased toward producing clusters with the same variance. Because it considers all members in the cluster rather than lust a single point, however, average linkage tends to be less influenced by extreme values than other methods.

2.4.4 Centroid

Centroid methods (first introduced in Sokal and Michener, 1958) calculate the proximity between two clusters by calculating the distance between the centroids of clusters. If $\hat{x}$ and $\hat{y}$ are the centroids of clusters C_i and C_j, the proximity between two clusters can be calculated as follows:

$$d(C_i, C_j) = \|\hat{x} - \hat{y}\|^2. \tag{2.14}$$

These techniques have a peculiar characteristic, i.e. the possibility of inversions. Specifically, two clusters that are merged may be more similar (less distant) than the pair of clusters that were merged in a previous step, while for other methods the distance between merged clusters monotonically increases (or is, at worst, non-increasing) proceeding from singleton clusters to one all-inclusive cluster. Furthermore, as the centroid method compares cluster means, outliers affect it less than other methods, even if it may not perform as well as Ward's method or average linkage method (Milligan, 1980): in fact, the larger of two unequally sized groups merged using centroid linkage tends to dominate the merged cluster.

2.4.5 Ward's method

For Ward's method, the proximity between two clusters is defined as the increase in the squared error that results when two clusters are merged. Thus, this method uses the same objective function as k-means clustering. While it may seem that this feature makes Ward's method somewhat distinct from other techniques, it can be shown mathematically that Ward's method is very similar to the group average method when the proximity between two points is taken to be the square of the distance between them. If n_i and n_j are the numbers of data belonging to clusters C_i and C_j, Ward's proximity between the clusters can be expressed as follows:

$$d(C_i, C_j) = \frac{\|\hat{x} - \hat{y}\|^2}{\left(\dfrac{1}{n_i} + \dfrac{1}{n_j}\right)}. \tag{2.15}$$

Ward's method considers the union of every possible pair of clusters and combines the two clusters whose combination results in the smallest increase in ESS (Total Error Sum of Squared deviations from the cluster centroid). It joins clusters to maximize the likelihood at each level of the hierarchy under some assumptions: multivariate normal mixture, equal spherical covariance matrices and equal sampling probabilities (Lorr, 1983).

2.5 Clustering results evaluation criteria

The last step of any clustering exercise is the evaluation of the resulting partition of the original data set. Because of its very nature, cluster evaluation is not a well-developed or commonly used part of cluster analysis. Nonetheless, cluster evaluation, or cluster validation as it is more traditionally called, is important, and this section will review some of the most common and easily applied approaches. A key motivation is that almost every clustering algorithm will find clusters in a data set, even if that data has no natural cluster structure. Being able to distinguish whether there is no-random structure in the data is just one important aspect of cluster validation. The following is a list of several important issues for cluster validation:

1. Determining the clustering tendency of a data set, i.e. distinguishing whether non-random structure actually exists in the data;
2. Determining the correct number of clusters;
3. Evaluating how well the results of a cluster analysis fit the data;
4. Comparing the results of a cluster analysis to externally known results, such as externally provided class labels;
5. Comparing different sets of clusters to determine which is better.

Item 1, 2, and 3 do not make use of any external information (they are unsupervised techniques), while item 4 requires external information. Item 5 can be performed in either a supervised or an unsupervised manner.

The evaluation measures, or indices, that are applied to judge various aspects of cluster validity are traditionally classified into the following two types. The first is based on *external criteria*: this implies that the results of a clustering algorithm are evaluated based on a pre-specified structure, which is imposed on a dataset, i.e. external information that is not contained in the dataset. The second approach is based on *internal criteria*: the results of a clustering algorithm are in this case evaluated using information that involves the vectors of the datasets themselves. This class of measures is often divided into two groups: measures of cluster cohesion (compactness, tightness), which determine how closely related the objects in a cluster are, and measures of cluster separation (isolation), which determine how distinct or well-separated a cluster is from other clusters. Sometimes also a third

approach of clustering validity is introduced: this particular approach is based on *relative criteria*, which consists of evaluating the results (clustering structure) by comparing them with other clustering schemes. Thus, relative measures are not actually a separate type of cluster evaluation measure, but are instead a specific use of such measures.
Considering only the first two types of cluster validation to determine the correct number of groups from a data-set, one option is to use external validation indices for which a priori knowledge of dataset information is required, but they can hardly be adopted for real problems (usually, real problems do not have prior information of the dataset in question). The other option is to use internal validity indices which do not require a priori information from data-set. For further details, the reader is referred to Rendon et al. (2011) and references therein.
In recent times, many indices have been proposed in the literature to measure the fitness of the partitions produced by clustering algorithm: next sections provide an overview of some of these indices, with particular emphasis on Davies-Bouldin and Dunn indices, because they are the most widely used in lots of clustering studies, and the ones used in this thesis.

2.5.1 External validity indices

In the case of external evaluation, clustering results are judged based on data that was not used for clustering, such as known class labels and external benchmarks. Such benchmarks consist of a set of pre-classified items, and these sets are often created by human (experts). These types of evaluation methods measure how close the clustering is to the predetermined benchmark classes. However, it has recently been discussed whether this is adequate for real data, or only on synthetic data sets with a factual ground truth, since classes can contain internal structure, the attributes present may not allow separation of clusters or the classes may contain anomalies. Additionally, from a knowledge discovery point of view, the reproduction of known knowledge may not necessarily be the intended result.
The two most used external validity indices are below described in details.

The *Rand Index* (Rand, 1971) computes how similar the clusters returned by one clustering algorithm are to a benchmark classification. This index can be view as a measure of the percentage of correct decisions made by the algorithm. It can be computed in the following way.

Given a set S of n elements and two partition of S to compare, $X = \{X_1, \ldots, X_r\}$, a partition of S into r subsets, and $Y = \{Y_1, \ldots, Y_s\}$, a partition of S into s subsets. X is the benchmark classification to which the partition Y has be compared. The Rand index is defined as follows:

$$R = \frac{a + b}{a + b + c + d} \tag{2.16}$$

where a is the number of pairs of elements in S that are in the same set in X and in the same set in Y, b is the number of pairs of elements in S that are in different sets in X and in different sets in Y, c is the number of pairs of elements in S that are in the same set in X and in different sets in Y, d is the number of pairs of elements in S that are in different sets in X and in the same set in Y.
Intuitively, $a + b$ can be considered as the number of agreements between X and Y, and $c + d$ as the number of disagreements between X and Y. The Rand index has a value between 0 and 1, with 0 indicating that the two data clusters do not agree on any pair of points and 1 indicating that the data clusters are exactly the same. It is very easy to implement, so it is often used to have a first impression of how good a partition is, compared to other partitions of the same pairs of elements.

Also *Jaccard index* (Jaccard, 1908) is a statistic index that can compute how similar the clusters returned by one clustering algorithm are to a benchmark classification. The mathematical definition is similar to the one of Rand Index.
Given a set S of n elements and two partition of S to compare, $X = \{X_1, \ldots, X_r\}$, a partition of S into r subsets, and $Y = \{Y_1, \ldots, Y_s\}$, a partition of S into s subsets, X is the benchmark classification to which the partition Y has be compared. The Jaccard index is defined as follows:

$$R = \frac{a}{a + c + d} \tag{2.17}$$

where a is the number of pairs of elements in S that are in the same set in X and in the same set in Y, c is the number of pairs of elements in S that are in the same set in X and in different sets in Y, d is the number of pairs of elements in S that are in different sets in X and in the same set in Y. The Jaccard index has a value between 0 and 1, with 0 indicating that the two data clusters do not agree on any pair of points and 1 indicating that the data clusters are exactly the same. In its computation this index does not consider the elements that are in different sets in X and in different sets in Y.

2.5.2 Internal validity indices

When a clustering result is evaluated based on the data that was clustered itself, this is called internal evaluation. These methods usually assign the best score to the algorithm that produces clusters with high similarity within a cluster and low similarity between clusters. One drawback of using internal criteria in cluster evaluation is that high scores on an internal measure do not necessarily result in effective information retrieval applications. Among the different internal validity indices and criteria available in literature, the most commonly adopted are the Davies-Bouldin index (DBI) and Dunn index (DI) (Davies and Bouldin (1979); Dunn (1973)), which favor cluster configurations with small within-cluster variance and large between-clusters variance, thus resulting in compact and well separated clusters.

The *Dunn index* aims at identifying sets of clusters that are compact, with a small variance between members of the cluster, and well separated, where the means of different clusters are sufficiently far apart, as compared to the within cluster variance. For a given assignment of clusters, a higher Dunn index indicates better clustering. One of the drawbacks of using this, is the computational cost as the number of clusters and dimensionality of the data increase. DI is defined as follows:

$$DI = \min_{i \neq j, j \subset \{1,\dots,k\}} \left\{ \min_{1 \leq j \leq k \wedge i \neq j} \left\{ \frac{inter(C_i, C_j)}{\max_{1 \leq z \leq k} intra(C_z)} \right. \right. \tag{2.18}$$

where $inter(C_i, C_j)$ is the inter-cluster distance between cluster i and cluster j, $\max_{1 \leq z \leq k} intra(C_z)$ is the maximum value of intra-cluster distances and k is the number of clusters.
This formulation has a peculiar problem: if one of the clusters is badly formed, where the others are tightly packed, since the formula contains a 'max' term instead of an average term, the Dunn index for that set of clusters will be uncharacteristically low. This is thus some sort of a worst case indicator, and has to be used keeping that in mind.

The *Davies-Bouldin index* is really similar to Dunn index. It uses an internal evaluation scheme, where the validation of how well the clustering has been done is made using quantities and features inherent to the dataset. This has a drawback that a good value reported by this method does not imply the best information retrieval.
In order to get a good clustering results, data should be divided in compact groups

that show low degree of similarity (this condition can be mathematically expressed by a high value of $S(C_i, C_j)$, i.e. the distance between centroids of cluster i and the centroid of cluster j). DBI is defined as follows:

$$DBI = \frac{1}{n} \sum_{i=1}^{n} \max_{i \neq j} \left\{ \frac{S_n(C_i) + S_n(C_j)}{S(C_i, C_j)} \right\} \tag{2.19}$$

where $S_n(C_x)$ is the average distance of each element of a cluster with respect to the centroid of cluster C_x (and $1 \leq x \leq k$) to which they belong, $S(C_i, C_j)$ is the distance between centroids of cluster i and the centroid of cluster j and k is the number of clusters. Hence the ratio is small if the clusters are compact and far from each other. The index is symmetric and non-negative. Due to the way it is defined, as a function of the ratio of the within cluster scatter, to the between cluster separation, a lower value will mean that the clustering is better.

Davies-Bouldin index and Dunn index are the indices used in this work to evaluate the performance of obtained clustering. This choice is mainly due to the fact that the optimal configuration (i.e. the optimal number of clusters) for the system under consideration is not known, so that only internal validity measures can be used. As already stressed, these indices have the main drawback that good values reported by these methods do not imply the best information retrieval: to overcome this limitation the most reasonable solution is a multi-assessment, employing more than one internal validity measure. Both Davies-Bouldin index and Dunn index are thus employed in this work, and the choice of the optimal number of clusters is made according to the values of both indices: in particular the optimal number of clusters is the one that maximizes the Dunn index and minimizes the Davies-Bouldin index.

Chapter 3

The Marina Reservoir case study

The purpose of this chapter is to introduce the case study to which the hybrid approach that couples DEMo procedure to clustering techniques is applied. In particular in Section 3.1 and 3.2 the reader is introduced to water management issues in Singapore and to a general description of Marina Reservoir water system. Then, Section 3.3 describes the management problem of the reservoir, while Sections 3.4 and 3.5 give an overview of Marina Reservoir developed modelling tools that constitutes the basis for the identification of an emulator.

3.1 Water management issues in Singapore

Lying almost on the equator, the Republic of Singapore, the second-smallest country in Asia, consists of Singapore Island and 63 smaller adjacent islets. It's situated in the Indian Ocean off the southern tip of the Malay Peninsula, and has an area of 693 km^2. Singapore's position at the eastern end of the Strait of Malacca, which separates western Malaysia and the Indonesian island of Sumatra, has given it economic and strategic importance out of proportion to its small size. The climate is tropical, with heavy rainfall and high humidity. The range of temperature is slight: the average annual maximum is 31 ℃, and the average minimum 24 ℃. The annual rainfall of 2500 mm is distributed fairly evenly throughout the year, mainly from December to February. Singapore is facing a serious shortage of water resources. Its current water demand is about 1.4 million cubic meters daily. Water resource management becomes, therefore, a strategically important issue for national economic development and public and social life.
From the 1980s to 1990s Singapore made tremendous efforts in a legal and manage-

ment system for the environment (including water), in conducting pollution control, river cleaning and setting up industrial estates according to land planning, and in building up a world class urban sanitation system including water and sewerage networks and treatment plants covering the whole island. From the later 1990s until the present the government has set sustainable water supply as the main target of water strategy, and for this a series of initiatives and actions have been taken, and the country has achieved remarkable progress in water resource management. To achieve this, several ambitious programs are being undertaken. Among this, the 4 national taps strategy (see Board, 2005 and Bank, 2006) is by far the most important. The taps are organized as follows:

TAP 1. Catchment Management Watershed conservation is vitally important to ensure water quality in the reservoirs, especially considering that most of the catchments are located in urban areas. Because of close coordination between land use planning and water catchment activities, water catchment accounted for about 50% of the land area of Singapore. After the creation of Marina barrage, the increase in the supply of water was about 10 % of current water needs, and the effective catchment area in Singapore increased to two thirds of the total land area.

TAP 2. Imported water Singapore imports its entitlement of water from the neighbouring Johor state of Malaysia, under long-term agreements signed in 1961 and 1962, when Singapore was still a self-governing British colony. Under these agreements, Singapore can transfer water from Johor for a price of less than 1 cent per 1,000 gallons until the years 2011 and 2061 respectively. The water from Johor is imported through three large pipelines across the 2-km course way that separates the two countries. Singapore would like to ensure its long-term water security by having a treaty which will provide it with the stipulated quantity of water well beyond the year 2061. In contrast, the main Malaysian demand has been for a much higher price of water, which has varied from 15 to 20 times the present price. That's why the target of Singapore government is increasing the portions of the first, third and fourth Taps.

TAP 3. NEWater program The PUB started to test the production of NEWater (treated waste-water) in 1998. The treated waste-water becomes a new water resource, which closes the water loop. The NEWater application in Singapore is the largest in non-potable waste-water reuse in the world, and marks a milestone in the development of water reuse. The target was to supply 250,000 m^3/day of NEWater for direct non-potable use, or 15% of the Singapore water supply, by the year 2011. To launch such a potentially controversial product due to the nature of its source, and make it acceptable by Singaporeans in such a short span of time requires a careful plan, and a well-timed and properly coordinated public communications strategy.

TAP 4. Desalinated water The first desalination plant using reverse osmosis (RO) technology and with a capacity 136,380 m^3/day was commissioned in September 2005. This seawater plant is one of the first and largest of such facilities in the region.

3.2 Marina Reservoir water system

Among these taps, the maximization of water yields from local catchments is potentially one of the most important sources, and with the inclusion of Marina Reservoir the Singapore's effective catchment area is now increased to about 50% of the total available area. Marina Reservoir, which was created in late 2008 with the construction of a 350 m wide barrage across Marina Channel, represents one of the largest fresh water bodies in Singapore. Besides this strategic water supply role, the reservoir has two further functions: floods control and lifestyle attraction. Indeed, the Marina Bay area coincides with most of Singapore's Central Region and it has been the site around which an ambitious urban development project took place.
The reservoir has a surface area of 2.45 km^2 and an active storage of about 3.2 hm^3. Five main tributaries (Singapore, Geylang and Kallang river and Bukit Timah and Stamford Canal) discharge water into the reservoir draining a catchment of approximately 100 km^2, about 1/7 of Singapore total surface area, that produces a mean annual inflow of about 150 hm^3 with a typical tropical pattern.
The catchment mainly consists of urbanized land and it is characterized by the presence of three further reservoirs, only managed for drinking water supply and whose discharge to Marina Reservoir is rare and negligible. The weather conditions are mainly driven by the monsoon seasons, but with no distinct wet or dry periods, as rainfall events can occur during every month of the year (Selvalingam et al., 1987). The North-East monsoon occurring from November to February/March is the wettest season with strong rainfalls coming from the South China Sea, while

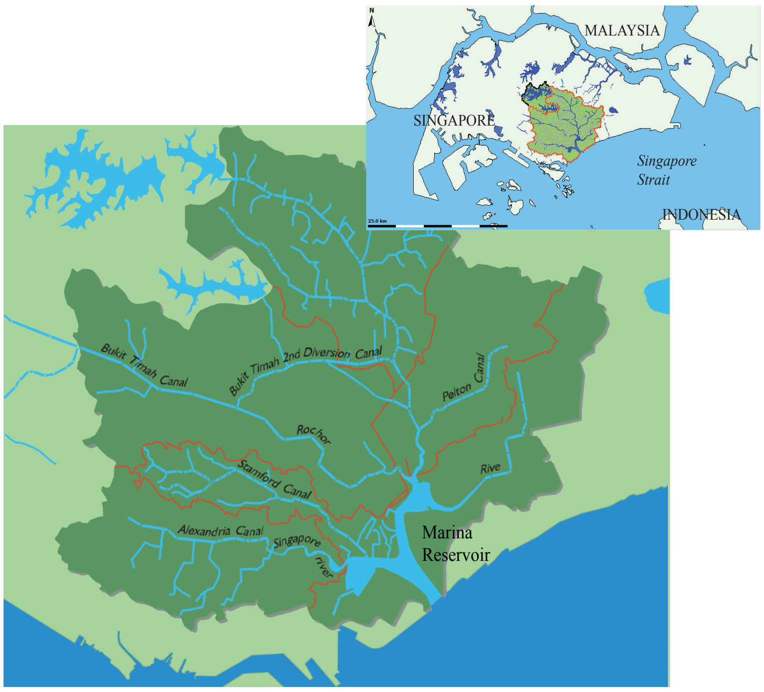

(a) Marina Reservoir and its catchment

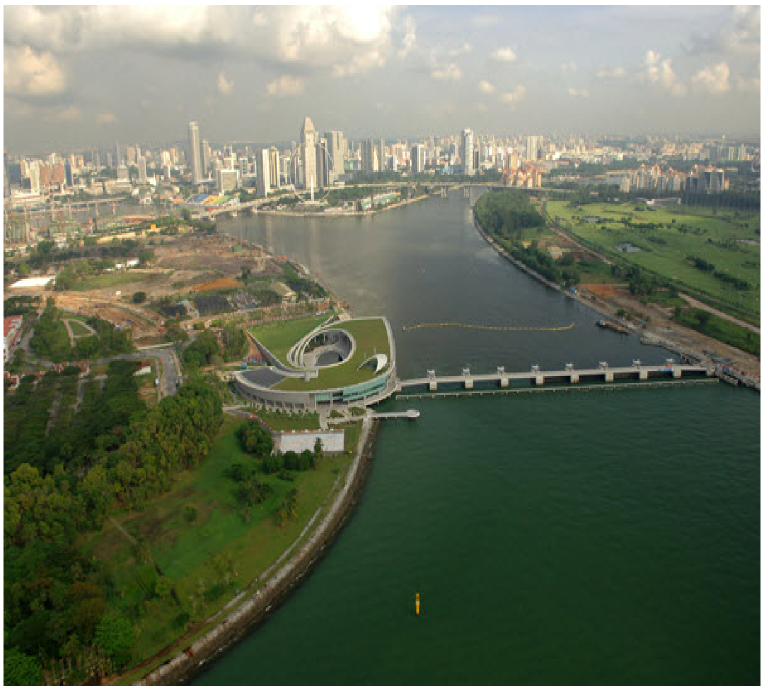

(b) Overview of the Barrage and the visitor center where pumps are located

Figure 3.1: The Marina Reservoir water system.

the South-West monsoon from June to September is less intense. During the inter-monsoon seasons Sumatra squall lines, coming from the westward Indonesian Sumatra Island, usually shower Singapore on early mornings. Moreover, added to this large scale pattern, convection enhanced by the warm water pool surrounding the island, the high relative humidity of the atmosphere and the hot spots of heat especially spread in the urban areas, bring heavy rainfall events associated with strong and relatively-fast thunderstorms of about 2-3 hours.

The drainage system consists of concrete lined canals, thus making the concentration time of the catchment extremely short (about two hours). Rainfall tends to come in high intensity events and discharges occur in high peaks over short periods, typically a few hours. Base flow is low and the upstream canals are mostly dry. In the downstream parts of the drainage system the bottom level of the canals is often lower than the reservoir level, with stagnant water being present during draught periods (Liew et al., 2001). Its peculiar location makes water quality control a relevant issue: the inflow is characterized by short bursts of high flow with sediment and nutrient rich water followed by dry periods with almost no flow, and because of its location in the tropics temperature and light intensity are high (as shown in Antenucci et al., 2012 and Smits and J.V., 2007b). This typically leads to eutrophic in-reservoir water conditions.

However, satisfying this operational target is not straightforward, mainly because of the extremely short concentration time of the catchment that causes high peaks of discharge over a period of few hours (Janssen and Ogink, 2007). Moreover, the relatively recent formation of the impoundments from a former estuary and the presence of salinity intrusion make salinity control another important objective.

3.3 Motivation

The efficient management of Marina Reservoir calls for the adoption of novel tools, capable of accounting for the aforementioned water quantity and quality targets in a fast-varying hydro-meteorological system. In particular, this management problem requires a research activity in both a modelling and control domain: in fact the physically-based models traditionally adopted to describe the ecological conditions of water reservoirs cannot be employed for optimal decision-making purposes, since their computational requirements does not allow for their integration with optimization framework.

This problem can be addressed by resorting to emulation techniques (see Chapter 1), which allow identifying a simple and computationally efficient copy of the original model to be used for optimization purposes.
As far as the control domain is concerned, one possible solution is adopting a real-time control approach that can exploit the availability of hydrological information (e.g. precipitation and runoff forecasts) thus enhancing the efficiency of the management system. The proposed management system to be developed is thus a combination of emulators with real-time control techniques.
In the context of Marina Reservoir it must be understood that an operational management system is already in place (Twigt and Burger, 2010): the barrage is equipped with 9 surface gates, 7 pumps (to discharge water when the sea level is higher than the reservoir one, with an installed capacity of 280 m^3/s) and 2 bottom pipes, which can release water at deeper levels, thus allowing for the mechanical control of the temperature profile and the salinity concentration. This tools are not sufficient because also water quality objectives have to be taken into account in the real-time control of the water system.
Actually, there is a model available for the water system but this is computationally too intensive to be used for real time control. An effective approach to overcome this limitation is to perform a top-down reduction of the physically-based mode describing the hydro-dynamics of Marina Reservoir by identifying a simplified, computationally efficient emulator, constructed from, and then used in place of the original process-based model in highly resource-demanding tasks, like the optimal management of the reservoir.
Next section gives an overview of Marina Reservoir developed modelling tools that constitute the basis for the identification of the above-mentioned emulator.

3.4 Description of the models available

For Marina Reservoir, an extensive modelling framework is available for simulation and forecasting (Twigt and Burger, 2010). These models are also integrated into the operational management system. Different components of the water system are modelled by different modules that can either run independently or coupled from each other. The modules are:

- rainfall-runoff and 1D flow module that calculates the runoff from the different sub-catchments and the water flow through the drainage system;

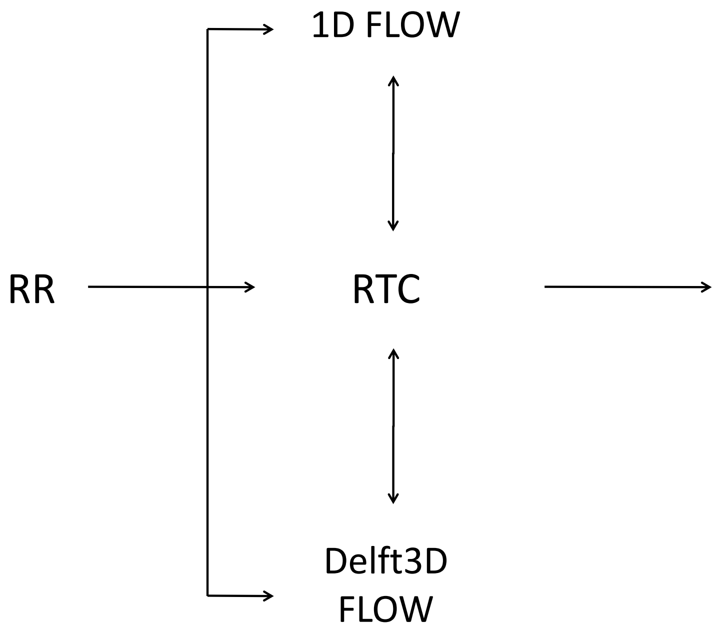

Figure 3.2: Flow diagram of simulation model.

- 3D flow that calculates the hydrodynamics of Marina reservoir;
- real-time control module that applies the control of structures in the model depending on the simulation results.

All the different modules are integrated in a 1D-3D coupled model, whose architecture is shown in Figure 3.2, where RR and RTC stand for rainfall-runoff module and real-time control module. Its operation is as follows: the rainfall runoff module runs independently first. This provides boundary conditions for the 1D and 3D flow modules. These two modules run together with the RTC module. The 1D flow and 3D flow coordinates discharge and water level at their combined boundary. The RTC module sets the states of controllable structures (gates and pumps of the marina barrage) depending on the state in the system. Currently there is a fixed set of operating rules that is implemented by this module. There is also an emission module that calculate the loads of constituents at the rainfall runoff boundary after which the 1D and 3D water quality modules calculates the transport of and the processes associated with the constituents. As these modules are not used in this work, the reader is referred to Smits and J.V. (2007a) and Smits and J.V. (2007b) for further details.

All the models are built using the commercial software packages Sobek (Deltares, 2010) and Delft3D (Deltares, 2010) that are developed by Deltares. In the following paragraph a short overview of the modelling concepts is given for each module. For a more detailed description the reader is referred to the available documentation about the model development and the user guides of the Sobek and Delft3D software packages.

3.4.1 Rainfall-runoff and 1D flow module

The hydrology is described in the rainfall-runoff module Sobek RR and the hydraulics is described in a combined application of the Channel Flow and Sewer Flow modules Sobek CF/SF (see Zijl and Twigt, 2007 for further details). The input for the model consisted of a MIKE11 model of the catchment as provided by PUB (Public Utilities Board).

Since it is not possible to include all small drains in the schematization of the model, the catchment has been divided into 196 sub-catchments for which a general schematization is applied. In each of these sub-catchments the rainfall-runoff process and the drainage to the main channels is described using the following two network elements: manholes and pipes. The manhole stores the total runoff (or acts as a collection point for the runoff) and the pipe conveys the stored runoff to the main channel.

The Sobek schematization has been extended with artificial manholes used in the rainfall-runoff module, and pipes connecting the manholes to the channel flow system. Various adjustments to the schematization have been made. Rainfall stations of PUB and NEA are assigned to rainfall-runoff manhole nodes to get the rainfall data. The assignment is based on Thiessen polygons. For this hourly rainfall data is used. Evaporation is set to a constant value of 3.23 mm/day (Singapore mean daily evaporation).

The calculation was not done at every cross-section, but with a 1D discretization of the Saint-Venant equations. Sobek uses a staggered grid discretization (with a resolution of 100 m) in which the water level is calculated in nodes and the discharge between nodes. This choice makes the model much faster (reduces computation times by a factor of four). The rainfall-runoff module and channel flow module are run sequentially. The results of the Sobek model are used as input to the Delft3D model.

3.4.2 3D flow module

The 3D hydrodynamic models (see Zijl and Twigt, 2007 for further details) used to calculate the flow condition in Marina Reservoir have been developed as applications of Delft3D. At the core of Delft3D is the FLOW module (Deltares, 2010) for the simulation of water flow in three dimensions. The three-dimensional hydrodynamic model equations that form the basis of FLOW are written in a generalised orthogonal coordinate system. Depending on the size and complexity of the problem and model domain, a choice between a rectangular model grid, a curvilinear or a curvilinear spherical model grid in the horizontal can be made. The non-linear equations are discretized using a finite difference discretization and are solved by an efficient, stable and accurate ADI-type solution technique. For complex geometries such as Marina Bay, a curvilinear grid allows for maximal boundary fitting, that is to say best grid representation of the curved contours of shores.
The horizontal model grid of the 3D Marina Reservoir model covers the Marina Bay basin, Kallang basin and Marina Channel. Furthermore it extends up to 2 km upstream into Kallang River, Rochor Channel, Geylang River, Singapore River and Stamford Canal. This is done because stratification can be expected in those areas. The areas of the Marina Bay basin, Kallang basin and Marina Channel have a grid size of 25 m by 25 m. Further upstream larger grid cells have been used, with grid sizes (in the direction along the river) of more than 100 m. By varying the grid sizes, computational time is saved, while correctly representing relevant local spatial scales. Figure 3.3 shows Delft3D bathymetry. By shutting off Marina Bay from the tide coming from Singapore Straits, Marina Reservoir can be characterised as weekly-dynamic system presumably with temporary stratified areas. Therefore, the z-layer approach for the vertical schematization is used. This implies that strictly horizontal computational layers are defined, with a user-defined thickness.
In the 3D Marina Reservoir model a maximum of 12 computational layers (in the deepest parts) is used. The layer thickness varies over the vertical. The thinnest layer can be found at the water surface, gradually increasing towards the bottom. The vertical schematization has been decided after a number of sensitivity tests. With Delft3D it is possible to make an on-line coupling with a Sobek model. This can be useful when a model is required that covers extensive river branches as well as basins or estuaries where 3D effects (e.g. stratification) play a significant role. There are 33 boundaries at which the 3D model connects with the 1D network: 30 inflow points (29 surface flow and one groundwater flow), weirs, pumps and pipes. Both

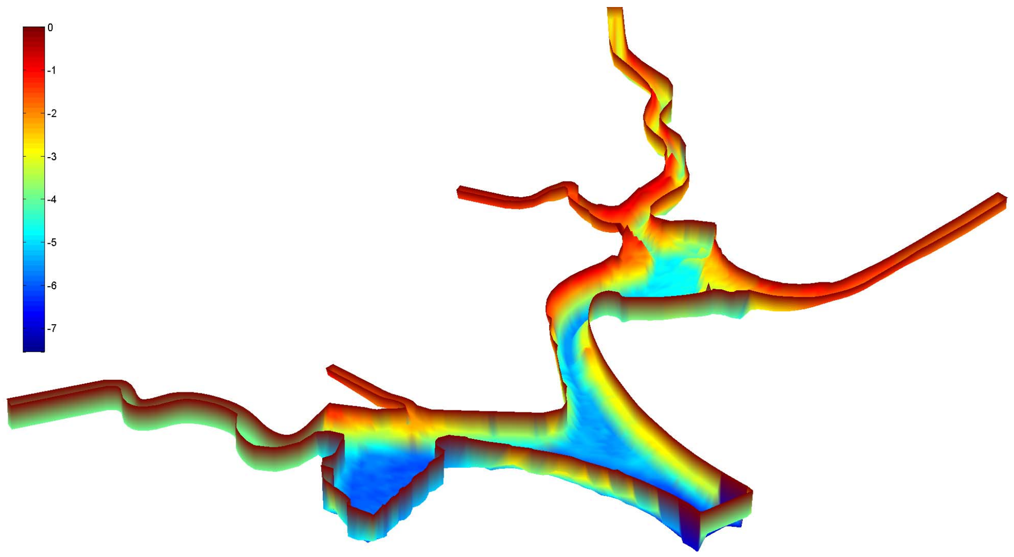

Figure 3.3: Delft3D bathymetry.

systems simulate time dependent processes for which a time stepping procedure is applied. In the coupled 1D-3D hydrodynamic model quantities are exchanged at each time step. As an explicit coupling is applied, every time step Sobek sends discharge values to Delft3D and Delft3D sends water level data to Sobek.
Consequently, there is a time step restriction. The exchange of data is done every time step of the 1D model, that corresponds with each half time step of the 3D model because of the specific alternate direction implicit method that is used to solve the 3D equations.

3.4.3 Operating rules of barrage

The barrage consists of 9 gates, 2 bottom pipes and seven pumps. The maximum allowed reservoir water level is 1.1 m. However, the goal of the operation rules for the weirs (gates), pipes and pumps at the barrier is to keep the water level in Marina Reservoir between -0.2 (-0.3) and +0.3 m (i.e. levels between 99.8 m and 100.3 m in Singapore Datum) as often as possible.
The pipes and weirs are used to discharge water during low tide periods, when the sea water level is at least 20 cm below the reservoir water level.
All weirs are opened when the water level is greater than 1.0 m and outside water level is at least 20 cm lower. All pumps are switched on during high tide periods when the reservoir water level greater than 0.7 m. However, gates, pipes and pumps

are operated according to fixed operating rules, that are briefly described in (Smits and J.V., 2007a).

3.5 DEMo problem conceptualization

As anticipated, the efficient management of Marina Reservoir should be capable of accounting for water quantity and quality targets: this calls for the adoption of novel tools in a fast-varying hydro-meteorological system. Delft3D cannot be employed for optimal decision-making purposes, since its computational requirements does not allow for its integration with optimization framework.
This problem can be solved by means of the emulation techniques, which allow identifying a simple and computationally efficient surrogate of Delft3D to be used for the optimization purposes introduced in Section 3.3. Before applying any DEMo technique to Delft3D, a pre-processing of the exogenous drivers, controls, and state variables to reduce the high number of variables appearing in the final emulator is required.
This operation can be either performed in different ways: with the purpose of preserving the physical interpretation of the aggregated state variables, while developing an automatic and system-independent tool, Chapter 4 of this thesis explores the potential of cluster techniques to discover compact and relevant representations of high-dimensional data sets produced via simulation of Delft3D.
The identified clusters are then processed with a Recursive Variable Selection algorithm, in order to single out the most relevant clusters of some specific state variable that are relevant to the emulator's output, which, in this case, is the salinity concentration in a point close to the barrage. The rationale behind this choice is that in this point the salinity concentration trajectories assume the highest values with respect to all the other areas within the reservoir. These high values are in fact not consistent with the high daily demand of fresh water, coupled with the serious shortage of water that Singapore is nowadays facing. The presence of the desalination plant from 2005 is not sufficient to ensure the necessary water supply, and an optimal management of the reservoir should take into account a reduction of the salinity concentration of the water sent to the plant itself. Moreover a lower level of salinity would guarantee better in-reservoir water quality conditions for aquatic animals and plants.

Chapter 4

DEMo by hierarchical clustering

The scope of this emulation modelling exercise is to reduce the dimensionality of Delft3D so that the emulation model can be used to design, via the resolution of a management problem, the optimal control policy for the gates, pipes and pumps being employed to reduce the water quantity and quality problems affecting the reservoir. In particular, this work concerns the management of salinity concentration in the reservoir itself. The chapter is organized as follows: Section 4.1 describes the Design of computer experiments and simulation runs phases, while Section 4.2 is mainly concerned with variable aggregation, which is the core of this work. In Section 4.3 variable selection is performed and in Section 4.4 the emulation model is identified. Section 4.5 finally shows a comparison of hierarchical clustering results with the results of another simpler aggregation method applied to the same dataset, in order to stress the potential of a completely automatic aggregation procedure with respect to an expert-skills based one.

4.1 DOE and simulation runs

The final scope of DOE is to explore, via simulation of the physically-based model, the largest possible area within the $\mathcal{L}_{\mathbf{Y}_t} \times \mathcal{L}_{\mathbf{W}_t} \times \mathcal{L}_{\mathbf{u}_t}$ and $\mathcal{L}_{\mathbf{X}_t} \times \mathcal{L}_{\mathbf{W}_t} \times \mathcal{L}_{\mathbf{u}_t}$ spaces (where, in particular, $\mathcal{L}_{\mathbf{W}_t}$ is the space of drivers, $\mathcal{L}_{\mathbf{u}_t}$ is the space of controls, $\mathcal{L}_{\mathbf{Y}_t}$ is the space of the output to be explained, and $\mathcal{L}_{\mathbf{X}_t}$ is the space of the states). To this purpose, for each simulation run, it is necessary to specify a trajectory over the whole simulation horizon H for all the physically-based model input variables, namely the exogenous driver $\mathbf{W}_t$ and the control $\mathbf{u}_t$.
To calculate the flow conditions in Marina Reservoir the 3D model Delft3D was

Variable	Description	Units
I_t	surface inflow	m^3/s
GI_t	groundwater inflow	m^3/s
CC_t	fraction of cloud coverage	%
RH_t	relative humidity	%
AT_t	air temperature	°C
WS_t	wind speed	m/s
WD_t	wind direction	deg

Table 4.1: Components of exogenous driver vector $\mathbf{W}_t$.

Variable	Description	Units
u_t^1	release from gates	m^3/s
u_t^2	release from pipes	m^3/s
u_t^3	release from pumps	m^3/s

Table 4.2: Components of control vector $\mathbf{u}_t$.

adopted. The Delft3D exogenous driver $\mathbf{W}_t$ includes 7 components accounting for the main hydro-meteorological processes (i.e. surface inflow, groundwater inflow, fraction of cloud coverage, relative humidity, air temperature, wind speed, and wind direction), while the control vector $\mathbf{u}_t$ has three components, i.e. the release from gates, pipes and pumps (see Tables 4.1 and 4.2).

The model has 7 state variables (salinity concentration, temperature, salinity and temperature transport[1], u-direction velocity, v-direction velocity, and w-direction velocity) for each computational cell, hence considering a total of 111 observation points and 12 computational layers, the state vector $\mathbf{X}_t$ (see Table 4.3) has a total of nearly 10^4 variables. Also water level in each observation point is examined. The real-to-run time ratio associated to this set-up is of about 1:100. With the purpose of generating the data-set of samples $\mathcal{F}$, a set of trajectories for the model inputs $\mathbf{W}_t$ and $\mathbf{u}_t$ is designed.

[1]Dimensionless coefficients. Notice that the transport of matter (salinity in this case) and heat is modelled by an advection-diffusion equation in the three coordinate directions.

Variable	Description	Units
sal_t^i	salinity	ppt
$temp_t^i$	temperature	°C
ST_t^i	salinity transport	%
TT_t^i	temperature transport	%
UV_t^i	u-velocity	m/s
VV_t^i	v-velocity	m/s
WV_t^i	w-velocity	m/s

Table 4.3: Summary of Delft3D state variables $\mathbf{X}_t$ notation (computed for each i cell of the spatial domain).

As for the exogenous driver $\mathbf{W}_t$, the time-series of observational data over the period April 2009 - April 2010 is available, while, concerning $\mathbf{u}_t$, 10 different management scenarios are generated, for a total of 10 simulation scenarios.

- **Scenario 1** In this simulation pipes are always used when it's possible;
- **Scenario 2** In this simulation pipes are not used;
- **Scenario 3** In this simulation pumps are not used;
- **Scenario 4** In this simulation only gates are used;
- **Scenario 5-10** The difference among the simulations stands in the way in which the controls are managed or simply in the decision of employing all or only some control devices.

The target of the emulation modelling exercise is to reduce as much as possible the number of state variables involved in the physically-based model concerning salinity concentration in the reservoir. Thus, the output $\mathbf{Y}_t$ is the salinity concentration [ppt] in the deepest point of the reservoir, located few hundred meters from the barrage, where the effect of salinity is stronger (see Figure 4.1 for its localization in the bathymetry); the output is therefore characterized by a dimensionality equal to 1, with an hourly time-step.
All the simulations are run with 30 sec simulation time-step, and an average vertical resolution of about 0.5 m. The data are sampled with an hourly time-step, and finally stored in a data-set $\mathcal{F}$ of $\sim 8 \cdot 10^4$ tuples.

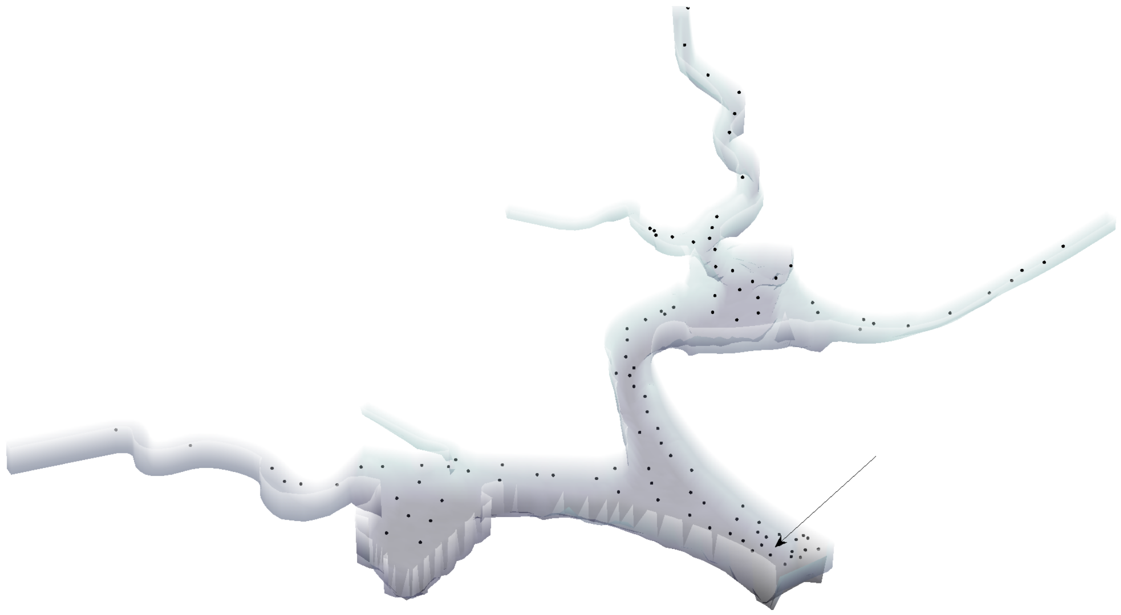

Figure 4.1: Localization of the point used in the elaborations.

4.2 Variable aggregation by time-series clustering

The spatially-distributed nature of Delft3D model leads to a large dimensionality of the state and exogenous driver vectors. By processing the data in $\mathcal{F}$ with a suitable aggregation scheme, $\mathbf{X}_t$ and $\mathbf{W}_t$ are transformed in two lower-dimension vectors $\tilde{\mathbf{X}}_\mathbf{t}$ and $\tilde{\mathbf{W}}_\mathbf{t}$, so that the majority of the variation in the original vectors is captured. The aggregation scheme can be done in different ways: with the purpose of preserving the physical interpretation of the aggregated state variables, while developing an automatic and system-independent tool, this section explores the potential of clustering techniques to discover compact and relevant representations of high-dimensional data sets. The rationale behind this choice is that clustering, by organizing data into homogeneous groups with minimized within-group-object similarity and maximized between-group-object dissimilarity (Liao, 2005), can be effective in providing a compact, yet informative, representation of the data produced with the Delft3D, thus enhancing the final emulator accuracy and reducing the computational and analytical effort of the DEMo process. Unlike static problems, the data here considered are a set of time-series with a spatial distribution. This implies the adoption of time-series clustering techniques that aims at determining groups of similar time-series.

The *hierarchical agglomerative cluster algorithm* (Magni et al., 2008) is the selected method: it works by organizing the data (the time-series) into a tree of clusters. In the present configuration, the distance between each cluster is measured as *Euclidean distance*, while clusters are merged according to the *Ward's minimum variance method* (at each clustering step, the merge that minimizes the increase in the sum-of-squares variance is chosen). The Ward's method minimizes the total within-cluster variance, and thus goes in the desired direction of creating compact and informative clusters, which can then be processed with the RVS-IIS algorithm.
Eventually, the choice of the optimal number p of clusters for each state variable is chosen according to the *Davies-Bouldin* (DBI) and *Dunn* (DI) index (Davies and Bouldin, 1979; Dunn, 1973), which favour cluster configurations with small within-cluster variance and large between-clusters variance, thus resulting in compact and well separated clusters.
Next sections examine in detail the selected clustering algorithm and show the primary positive aspects of the chosen distance measure, linkage method, and clustering evaluation criteria.

Hierarchical clustering

In this work, *hierarchical clustering* method is adopted. Hierarchical clustering techniques (Magni et al., 2008) are the second important category of clustering methods. As with K-means, these approaches are relatively old compared to many clustering algorithms, but they still enjoy widespread use: in particular, agglomerative hierarchical clustering techniques are by far the most common. Hierarchical clustering algorithm applied on time-series data works by organizing the time-series into a tree of clusters. At the first iteration the algorithm places each time-series in its own cluster and then starts to merge these small clusters, until a single cluster is obtained or an a-priori defined stopping condition is satisfied (e.g. the minimum number of clusters). In order to perform hierarchical clustering, TimeClust software package is used (see Figure 4.2).

Euclidean distance

Agglomerative clustering methods uses the dissimilarities (similarities) or distances between objects when forming the clusters. Similarities are a set of rules that serve as

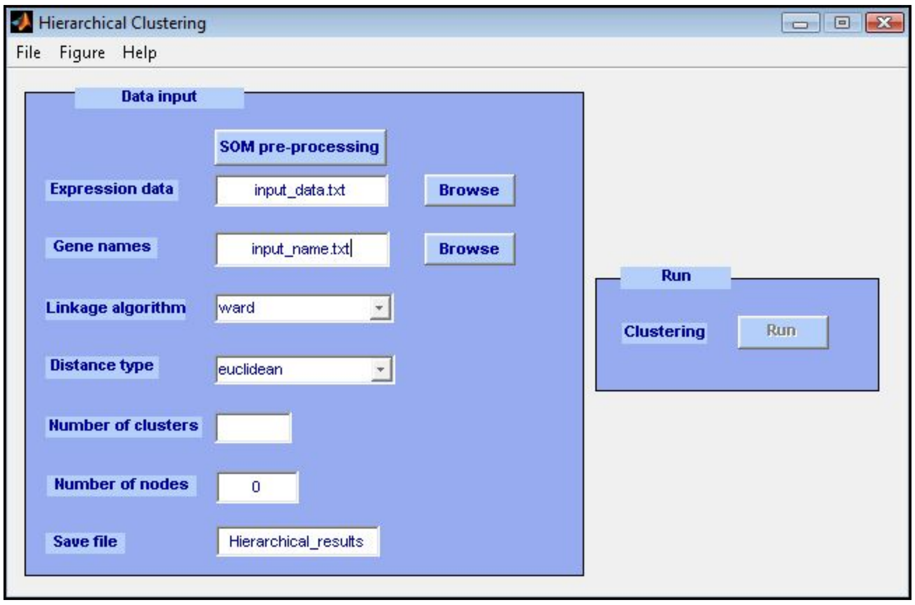

Expression data	input_data.txt
Gene names	input_name.txt
Linkage algorithm	ward
Distance type	euclidean
Number of clusters	
Number of nodes	0
Save file	Hierarchical_results

Figure 4.2: Time Clust input screen example.

criteria for grouping or separating items. These distances (similarities) can be based on a single dimension or multiple dimensions, with each dimension representing a rule or condition for grouping objects. In the present configuration, the distance between each cluster is measured as *Euclidean distance*, that is computed as shown in equation 2.8. One reason is that the centroid or the ward algorithms should be used only with the euclidean distance; moreover, this distance measure is not affected by the presence of outliers.

Ward linkage method

At the first step, when each object represents its own cluster, the distances between the objects are defined by the chosen distance measure. However a linkage or amalgamation rule to determine when two clusters are sufficiently similar to be linked together is needed. There are numerous linkage rules such as these that have been proposed in Section 2.4: in this thesis, clusters are merged according to the *Ward's method* (at each clustering step, the merge that minimizes the increase in the sum-of-squares variance is chosen). The Ward's method considers the union of every possible pair of clusters and combines the two clusters whose combination results in the smallest increase in ESS (Total Error Sum of Squared deviations from the cluster centroid), and thus goes in the desired direction of creating compact and informative clusters.

Dunn index and Davies-Bouldin index

Dunn index and Davies-Bouldin index are the indexes chosen to decide how many clusters actually exists in the data: the simplest way to do it is to plot them against the number of clusters they are calculated over. The number p for which DB (DI) value is the lowest (highest) is a good measure of the number of clusters the data could be ideally classified into. This approach allows indeed to analyse a-posteriori the clustering results and to choose the number of clusters p (for each sub-set) that best satisfies the DBI and DI indexes.

4.2.1 Clustering results

The algorithm of hierarchical clustering is thus applied to time series data: notice that the clustering algorithm is not directly applied to the complete set of state variables in $\mathcal{F}$, but to 7 sub-sets, each containing the temporal and spatial realizations for temperature and salinity concentration *temp* and *sal*, temperature and salinity transport TT and ST, and the horizontal and vertical velocities UV, VV and WV. The rationale behind the choice of keeping the state variable separated one from the other is due to the purpose of preserving a sort of physical interpretability of the aggregated time-series, as the knowledge of the system behaviour was not sufficient to intuitively understand the reasons why many state variables could result in the same cluster (e.g., how to legitimate the simultaneous presence in the same cluster of temperature and horizontal velocities?).
Because of the computational requirements of the algorithm, this clustering exercise is solved for each of the 10 simulation run of the original model Delft3D: also in this case the idea is to keep each simulation separated from the others to preserve their own distinctive traits in the clustering results. This gives a total of 70 clustering problems (one for each state variable for each simulation).
These problems are solved without specifying a-priori the desired minimum number of clusters (i.e. no stopping condition), which means that the algorithm is run until a full tree of clusters is obtained.

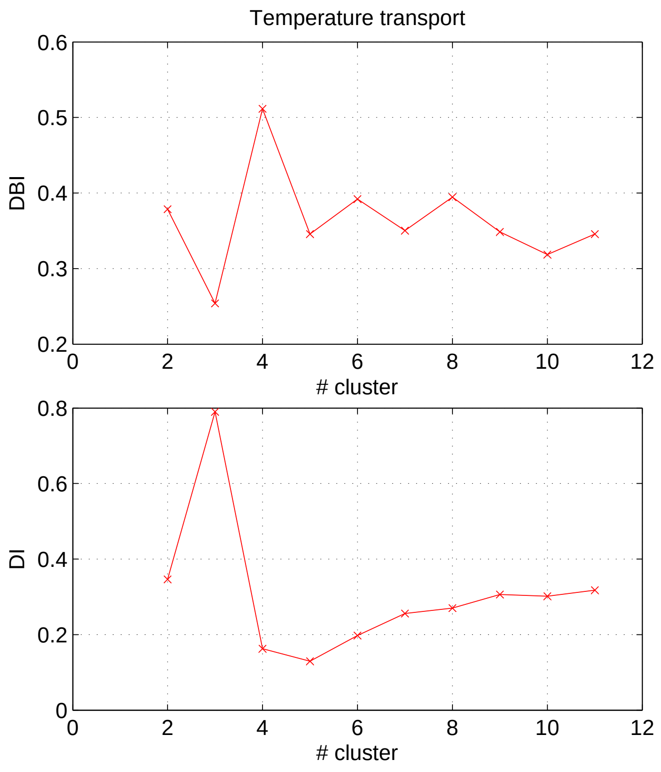

Figure 4.3: Average value (over the 10 simulation runs) of the DBI and DI indexes for the temperature transport TT.

Figure 4.3 reports the average value (over the 10 simulation runs) of the DBI and DI indexes as a function of p for the temperature transport TT. Results show that the best number p^* of clusters that minimizes the DBI and maximizes the DI index is 3, while the introduction of a larger number of clusters does not improve the clustering results any further. The plots of the DBI and DI indexes as a function of p for the other state variables are reported in Appendix A.

This analysis is performed for a maximum value of p equal to 11 corresponding to the number of layers (a part from the surface layer) in the original model. This value provides an empirical upper bound to p, since the data could be for example aggregated by considering the spatial average of each sub-set in the original model vertical layers (see Section 4.5.1).

The final results obtained for the remaining sub-sets are reported in Table 4.4, where

Table 4.4: Selected number of clusters for the different sub-sets composing the vector $\mathbf{X}_t$. The symbols are explained in Table 4.3.

State Variable	sal	$temp$	ST	TT	UV	VV	WV	h
Number of clusters	6	6	4	3	4	6	8	10

the results obtained for the water level h are also shown. The time series algorithm found a total of 8 different clusterings, each one identifying a set of homogeneous areas of a particular variable. These areas can vary from sub-set to sub-set, so, for example, the salinity concentration sal can be grouped into 6 different areas, while the vertical velocity WV into 8.
In the following sections a more detailed description of clustering results for each state variable is given.

Salinity

The number of homogeneous areas identified for salinity is 6. As Figure 4.4 shows, Cluster 1 and Cluster 2 contain the points closer to the barrage. Points in the middle of Marina channel and in correspondence of the upper part of the reservoir (i.e. near Kallang River and Geylang River) are in Cluster 4, Cluster 5 and Cluster 6. Table B.1 shows the number of points per layer belonging to each cluster. Cluster 1, Cluster 4, and Cluster 5 contain points in the deepest layers (i.e. from Layer 1 to Layer 5), while points in Layers 6 and 7 are in Cluster 3. Cluster 6 is the biggest and contains all the points belonging to the upper layers. The number of points per cluster is not homogeneous: Cluster 2 and Cluster 4, for example, are made up of only 2 and 4 points, while Cluster 6 contain more than 300 points.

Salinity transport

The number of homogeneous areas identified for salinity transport is 4. As Figure 4.5 shows, Cluster 4 contain points belonging to all the areas of the reservoir, except the upper part. Points in correspondence of the upper part of the reservoir (i.e. near Kallang River and Geylang River) are in fact in Cluster 1, Cluster 2 and Cluster 3. Considering how clusters are composed from the point of view of the depth (see Table B.2) it is possible to notice that Cluster 1 and Cluster 2 mainly contain points of Layers 7-11, while Cluster 3 contains points belonging only to Layer 10 and 11.

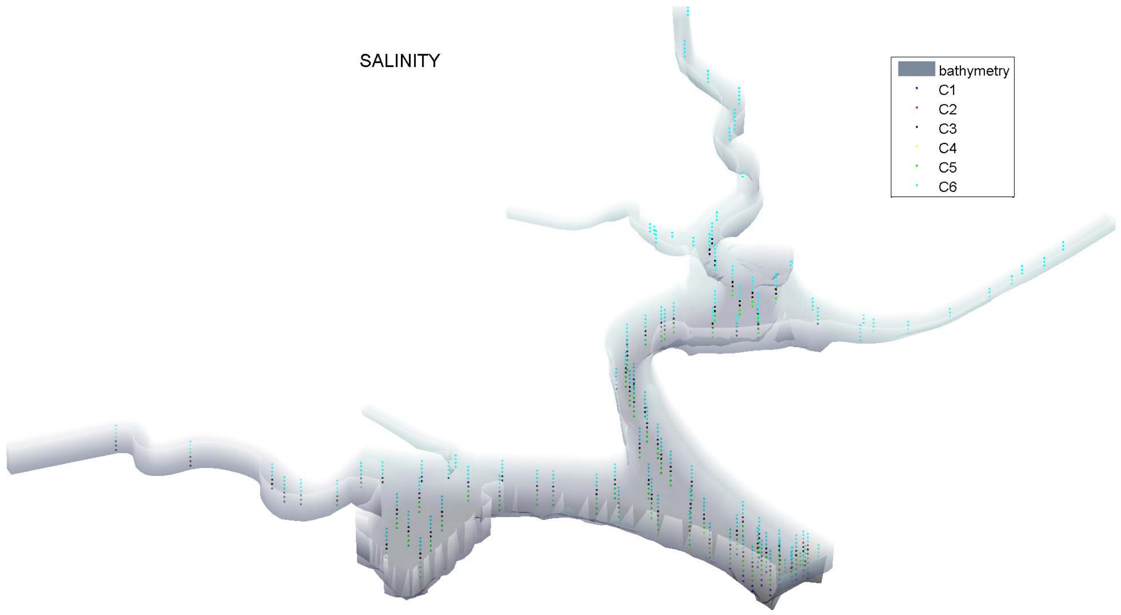

Figure 4.4: The 6 clusters identified for the salinity concentration.

Salinity						
	Cluster 1	Cluster 2	Cluster 3	Cluster 4	Cluster 5	Cluster 6
Layer 1	8	0	0	0	0	0
Layer 2	14	0	0	4	4	0
Layer 3	0	0	0	0	48	0
Layer 4	0	0	0	0	59	0
Layer 5	0	0	5	0	66	0
Layer 6	0	0	79	0	0	1
Layer 7	0	0	81	0	0	4
Layer 8	0	2	0	0	0	96
Layer 9	0	0	0	0	0	108
Layer 10	0	0	0	0	0	111
Layer 11	0	0	0	0	0	111

Table 4.5: Number of points per layer per cluster for salinity (*sal*).

Cluster 4 is the biggest and contains all the points belonging to all the layers. The number of points per cluster is not homogeneous: Cluster 3 is made up of only 2 points, while Cluster 4 contain more than 500 points.

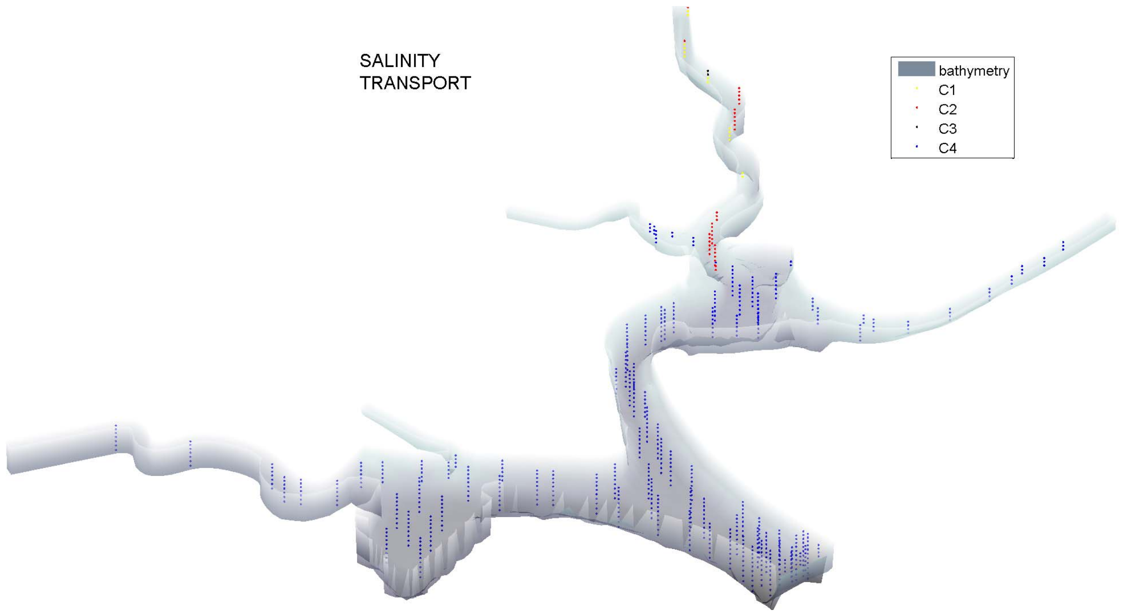

Figure 4.5: The 4 clusters identified for the salinity transport.

Temperature

The number of homogeneous areas identified for temperature is 6. As Figure 4.6 shows, Cluster 1 contains points belonging to the area near the inlet of Bukit Timah canal, while Cluster 2 is made up of points located near the inlet of Stamford Canal. Cluster 6 contains points belonging to Marina Channel and the ones next to the barrage, and Cluster 5 the points near Geylang River and the ones near the inlet of Stanford Canal. Table B.3 shows that Cluster 1, Cluster 2, and Cluster 3 contain points in the middle layers (i.e. from Layer 5 to Layer 7), while points in Layers 2, 3, and 4 are in Cluster 5. Cluster 6 is the biggest and contains points belonging to all the layers, including the ones in Layer 1. Cluster 2 and Cluster 6 are the biggest compared to all the others that contain less than 100 points.

Temperature transport

The number of homogeneous areas identified for temperature transport is 3. As Figure 4.7 shows, Cluster 1 and Cluster 2 contain points belonging to the upper part of the reservoir (i.e. Kallang River). All the other points are in Cluster 3. Considering how clusters are composed from the point of view of the depth (see Table B.4), Cluster 1 and Cluster 2 mainly contain points of the middle and upper

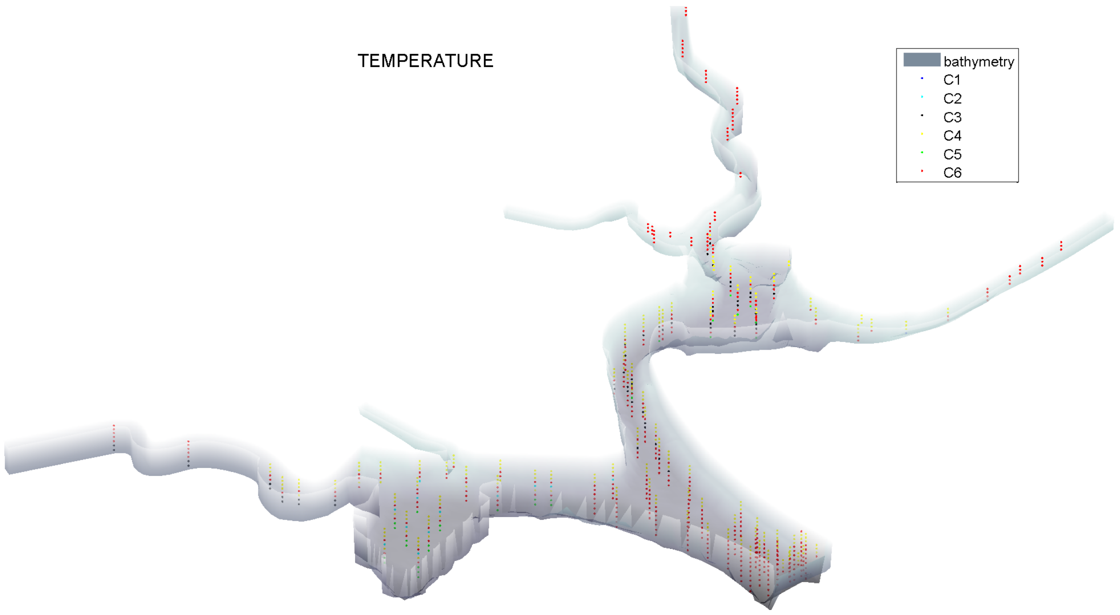

Figure 4.6: The 6 clusters identified for the temperature.

Layers (i.e. from 6 to 11), while Cluster 3 contains points belonging only to all the layers. Cluster 1 and Cluster 2 are really small and contain respectively 1 and 5 points.

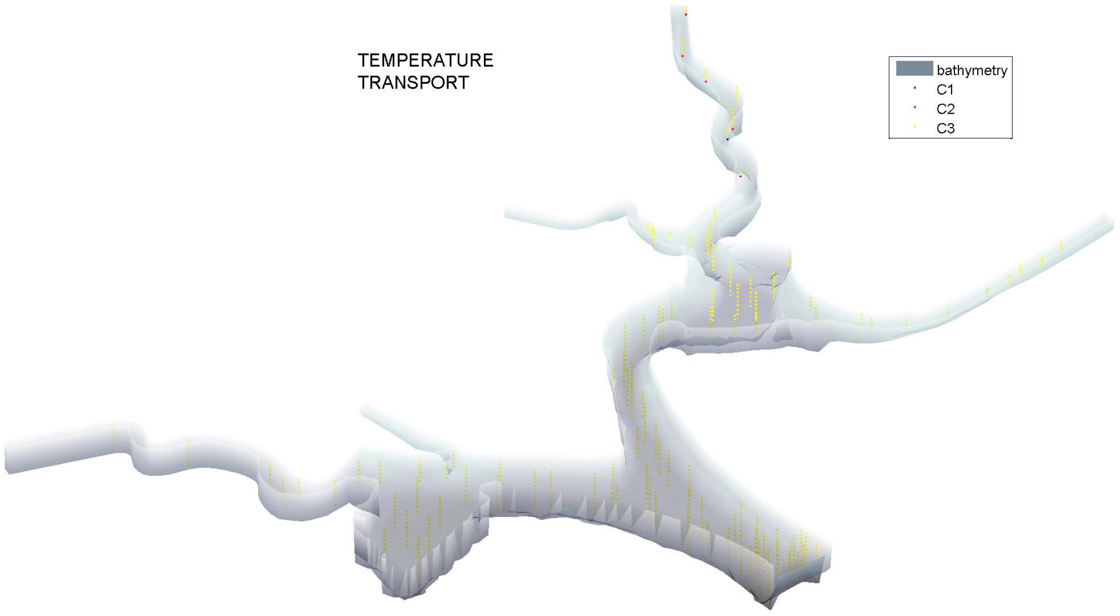

Figure 4.7: The 3 clusters identified for the temperature transport.

U-velocity

The number of homogeneous areas identified for u-velocity is 4. As Figure 4.8 shows, Cluster 1 contains points belonging to the area near Singapore river and its inlet, while Cluster 2 is made up of points located near the barrage and some in the area of Kallang river. Cluster 3 and Cluster 4 contain points belonging to Marina Channel, near Geylang River and near the inlet of Stanford Canal. Table B.5 shows the number of points per layer belonging to each cluster. Cluster 1 contains points of the middle and upper layers (i.e. from Layer 5 to Layer 11), while points in Cluster 2 are part in Layer 2 and part in Layer 8. Cluster 3 is one of the biggest and contains points belonging to all the layers, except Layers 9 and 10. Cluster 4, instead, doesn't contain points belonging to Layer 1.

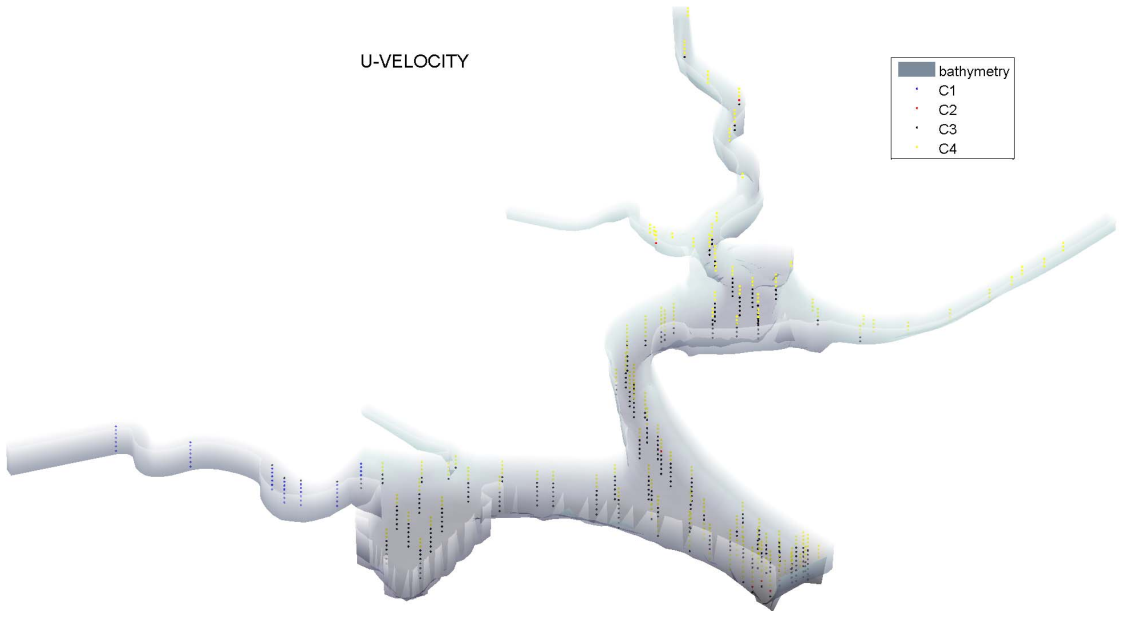

Figure 4.8: The 4 clusters identified for the u-velocity.

V-velocity

The number of homogeneous areas identified for v-velocity is 6. As Figure 4.9 shows, Cluster 1, Cluster 2, and Cluster 5 contain points belonging to the area near the inlet of Bukit Timah canal, Kallang river, and, Geylang river, while Cluster 3 is made up of points located near the barrage. Cluster 6 contains points belonging to Marina channel and near the inlet of Stamford canal, while Cluster 4 is made up of points located on Kallang river. Table B.6, instead, shows that Cluster 1 and Cluster 5 contain points of Layer 10 and 11, while Cluster 2 and Cluster 4 contain points of the middle and upper layers (i.e. from Layer 4 to Layer 9-10); points of the lower layers are in Cluster 3. Cluster 6 is the biggest and contains points belonging to all the layers.

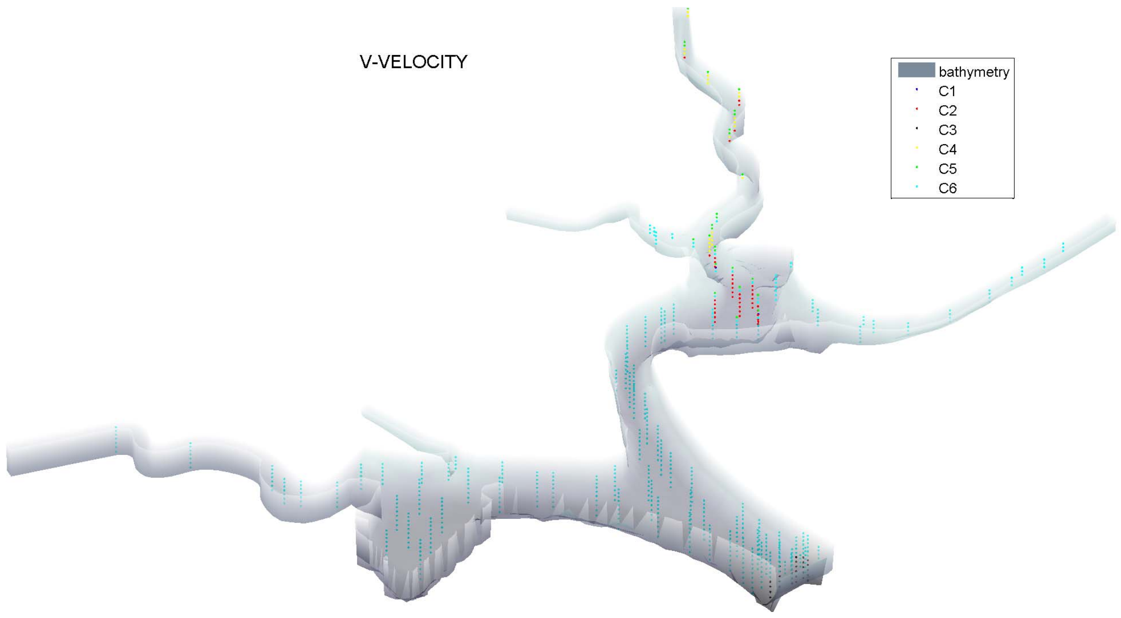

Figure 4.9: The 6 clusters identified for the v-velocity.

W-velocity

The number of homogeneous areas identified for w-velocity is 8. As Figure 4.10 shows, Cluster 1, Cluster 2, Cluster 3, Cluster 4, Cluster 7 and Cluster 8 contain the points closer to the barrage and in Marina channel. Points near the inlet of Stamford canal and Singapore river are in Cluster 6. This latter contains also points of other areas, like the ones near the inlet of Geylang river, Kallang river and Bukit Timah canal. Some of these points are also in Cluster 5. Looking at Table B.7 it is possible to notice that Cluster 3 and Cluster 4 contain points in the deepest layers (i.e. Layer 1 and 2), while Cluster 5, Cluster 7 and Cluster 8 contain points of the medium and upper layers (i.e. from Layer 5 to Layer 11). Cluster 2 is made up of points belonging only to Layer 10 and 11. Cluster 6 is the biggest and contains points of all the layers.

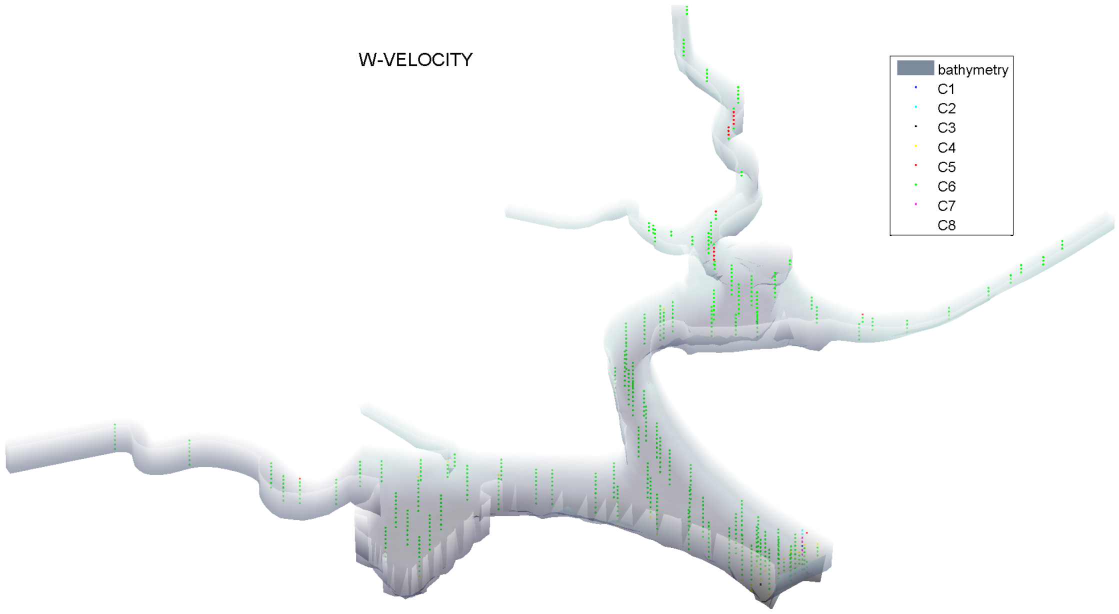

Figure 4.10: The 8 clusters identified for the w-velocity.

Water level

The number of homogeneous areas identified for water level is 10. As Figure 4.11 and Table B.4 show, Cluster 1 and Cluster 2 contain points close to Singapore river, while Cluster 5 is made up of points belonging to Marina channel and the ones closer to the barrage. Cluster 8 and Cluster 9 contain points near the inlet of Stamford canal and Cluster 4, Cluster 6, and Cluster 7 the ones near the upper part of the reservoir (i.e. the inlet of Kallang river, Bukit Timah canal and Geylang river). In this case there is no difference along the depth, as the water level is calculated as mean value in each observation point.
As a result of this pre-processing phase, the vectors to be considered in the next variable selection are $\tilde{\mathbf{X}}_{\mathbf{t}}$, $\tilde{\mathbf{W}}_{\mathbf{t}}$, and $\mathbf{u}_t$, with dimensionality $\mathcal{M}_x$, n_w, and n_u respectively equal to 47 (for details see Table 4.4), 7 and 3.
To these vectors, two more variables were eventually added, i.e. the variable t, which accounts for the system daily periodicity by taking value in the range [1, 365], and the variable H, which accounts for the system hourly periodicity by taking value in the range [1, 24]. This gives a total of 59 candidate variables.

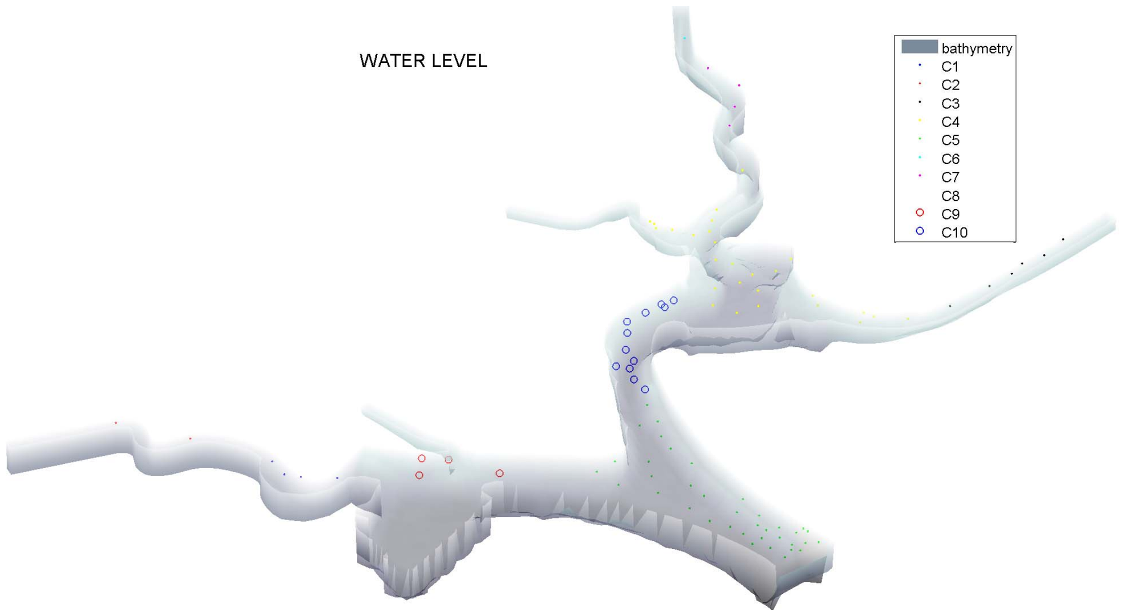

Figure 4.11: Te 10 clusters identified for the water level.

4.3 Variable selection

The reduction problem requires to select the variables $\mathbf{x}_t$, $\mathbf{w}_t$ and $\mathbf{u}_t$ constituting the arguments of the output transformation function $\mathbf{h}_t(\cdot,\cdot,\cdot)$ and the state transition function $\mathbf{f}_t(\cdot,\cdot,\cdot)$. In particular, the Recursive Variable Selection-Iterative Input selection algorithm (RVS-IIS, see Section 1.4.3) proposes to first select the features relevant to the output variable $\mathbf{y}_t$, and to then recursively select all the features relevant to the states $\mathbf{x}_{t+1}$.

In this application, the output is sal_t^{barr}, that represents the salinity concentration in a point close to the barrage (see Section 3.5). As for the underlying model class and ranking procedure, the IIS algorithm is here combined with Extra-Trees (see Castelletti et al. (2012a)), whose parameters are set according to **?** indications and subsequent experiences: the number M of trees in an ensemble is 500 (a good balance between Extra-Trees accuracy and computational requests), the minimum cardinality n_{min} for splitting a node is 2 and the number of alternative cut-directions K (i.e. the number of candidate variables) changes if considering data aggregated with hierarchical clustering rather than data aggregated according to vertical layers. The number p of variables singularly evaluated is 5. The IIS algorithm, whose tolerance ε is posed equal to 0.02, is run only on a part of the whole data-set, in

order to overcome problems connected to loss of time due to the computational requirements of the model structure.
The performance of the emulator being built is evaluated in terms of the coefficient of determination R^2 (in k-fold cross-validation, with $k = 10$) between the values of $\mathbf{Y}_t$ and $\mathbf{y}_t$ predicted by the emulator. The coefficient of determination is defined as follows:

$$R^2 = 1 - \frac{cov(Q_i - \hat{Q}_i)}{cov(Q_i)} \tag{4.1}$$

where Q_i are the observed data and $\hat{Q}_i$ are the measured data.
In this case the number of alternative cut-directions K (i.e. the number of candidate variables) is 59. The vectors to be considered in this phase are $\tilde{\mathbf{X}}_t$, $\tilde{\mathbf{W}}_t$ and $\mathbf{u}_t$, with dimensionality respectively equal to 47, 7 and 3. To these vectors, two more variables were eventually added, i.e. the variable d, which accounts for the system daily periodicity, and the variable H, which accounts for the system hourly periodicity.

4.3.1 Salinity in a point close to the barrage sal_t^{barr}

The first step of the RVS-IIS algorithm requires to identify which variables, among $\tilde{\mathbf{X}}_t$, $\tilde{\mathbf{W}}_t$ and $\mathbf{u}_t$, are relevant to describe the the physically-based model output $\mathbf{Y}_t$: these are the arguments of the emulator output transformation function (see eq. 1.4b) that will be identified in the subsequent step.
The results obtained with *Step 0* of RVS-IIS, which ranks the importance of all the candidate features in explaining sal_t^{barr} behaviour and then singularly evaluates the importance of the first ranked three, are reported in Table 4.6 - *Step 0.* The Table shows that the output behaviour is almost totally explained by only one variable, as confirmed by its score (92.60%, 10% more than in the aggregation by vertical layers), variance reduction and SISO performance: as a matter of fact the average salinity concentration in Cluster 1 sal_t^{C1} provides information about the salinity concentration at the bottom layer in a homogeneous area very close to the barrage.

The IIS algorithm seems to be robust with respect to information redundancy: only salinity concentration in Cluster 1 sal_t^{C1} is selected while salinity concentration in Cluster 4 sal_t^{C4} is discarded, mainly because Cluster 1 is closer to the barrage than Cluster 4. The information content of both the two variables is redundant and it is thus sufficient to employ just one of them in explaining the output sal_t^{barr}. In

Table 4.6: Results obtained using RVS-IIS algorithm to select the most relevant variables to explain sal_t^{barr} for data aggregated with hierarchical clustering.

Step 0

Output variable	sal_t^{barr}
Initial variance	71807.4000

Candidate Feature	Score %	Variance Reduction	Performance SISO (R^2)
sal_t^{C1}	92.6011	66466.7000	0.9894
sal_t^{C4}	5.9314	4257.4100	0.9262
GI_t	0.2811	201.7440	0.1461

Step 1

Output variable	sal_t^{barr} - $\hat{v}_t^0$
Initial variance	767.59

Candidate Feature	Score %	Variance reduction	Performance SISO (R^2)
GI_t	37.2627	279.2710	0.3916
VV^{C3}	9.6575	72.3798	0.1898
u_t^2	4.5759	34.2948	0.0436
WV^{C1}	2.7336	20.4871	0.0757
sal_t^{C5}	2.5936	19.4384	0.0731

this case groundwater inflow GI_t is ranked in position three, with a score equal to 0.2811% and a reduction of variance of 201.7440. At the end of this step, the sal_t^{C1} term is selected, since it is characterized by the highest SISO model performance (0.9894). *Step 1* of RVS-IIS, whose results are reported in Table 4.6 - *Step 1* shows that the feature with highest score (37.2627%) is the groundwater inflow GI_t, with a variance reduction of 279.2710. The horizontal velocity VV^{C3} is ranked in position two; score and variance reduction are definitely low, compared to GI_t ones.

Table 4.7: Selected features and corresponding performance of the MISO models obtained for the case of sal_t^{barr}, for data aggregated with hierarchical clustering. State variables are denoted in bold.

Iteration	Feature selected	Performance MISO (R^2)	ΔR^2
1	$\boldsymbol{sal_t^{C1}}$	0.9893	-
2	GI_t	0.9941	0.0048

This means that also in this case only the groundwater inflow GI_t is relevant in explaining the residual r^0_{t+1} and that the selection of this new feature let the MISO model performance increase, with R^2 passing from 0.9893 to 0.9941 (see Table 4.7). However, the introduction of this new variable into the MISO model lead to an increase of R^2 equal to 0.0048, which is lower than the predefined tolerance (ε is set to 0.02). At this stage the RVS-IIS is stopped and the only selected feature is the salinity concentration in Cluster 1 sal^{C1}_t.

4.3.2 Dynamics of sal^{C1}_{t+1}

In the set $\mathcal{V}^i_{sal^{barr}_t}$ of variables selected at the first call of RVS-IIS algorithm, the salinity concentration in Cluster 1 sal^{C1}_t is a state variable and, as such, its dynamic behaviour must be described through suitable state transition equations. The set $\mathcal{V}^i_{sal^{C1}_t}$ in the subsequent call of the IIS algorithm is still selected among the components of the vectors $\tilde{\mathbf{X}}_t$, $\tilde{\mathbf{W}}_t$ and $\mathbf{u}_t$.

Table 4.8: Selected features and corresponding performance of the MISO models obtained for the case of sal^{C1}_{t+1}. State variables are denoted in bold.

Iteration	Feature selected	Performance MISO (R^2)	ΔR^2
1	$\mathbf{sal}^{C4}_t$	0.7787	-
2	u^2_t	0.9511	0.1724
3	GI_t	0.9771	0.0260
4	u^1_t	0.9806	0.0035

A list of the selected variables is reported in Table 4.8. It can be noticed that sal^{C4}_t, u^2_t, and GI_t, the salinity concentration in Cluster 4, the release from the pipes and the groundwater inflow, are features relevant to the dynamics of the salinity concentration in Cluster 1 sal^{C1}_{t+1}. In this case also the release from gates appears (u^1_t) in the selected features, but it is not selected as the MISO model performance increases only of 0.0035.

4.3.3 Dynamics of sal^{C4}_{t+1}

Among the variables selected, the salinity concentration in Cluster 4 sal^{C4}_t is again state variable, thus requiring a dynamic description too. The results of the RVS-IIS

Table 4.9: Selected features and corresponding performance of the MISO models obtained for the case of sal_{t+1}^{C4}. State variables are denoted in bold.

Iteration	Feature selected	Performance MISO (R^2)	ΔR^2
1	$\mathbf{sal}_t^{C4}$	0.8628	-
2	u_t^2	0.9754	0.1126
3	GI_t	0.9850	0.0096

algorithm application to sal_{t+1}^{C4} is reported in Table 4.9. At this stage the recursive variable selection is over, since no further state variables are selected. The process took three calls of the RVS algorithm, to single out the most suitable subset $\mathcal{V}^i_{sal_t^{barr}}$ of input variables to explain the system output. In particular, the emulator is characterized by a state vector $\mathbf{x}_t$ with 2 components (salinity concentration in Cluster 1 sal_{t+1}^{C1}, and salinity concentration in Cluster 4 sal_{t+1}^{C4}), one component of the exogenous driver vector (i.e. groundwater inflow GI_t), and one component of the original control vector (i.e. pipe inflow u_t^2).
The network of the causal relationships between the selected state variables is sketched in Figure 4.12.
The reduction phase shows that the emulation model output variable sal_t^{barr} can be explained as a function of one exogenous driver (the groundwater inflow GI_t), and one component of the control vector (the pipe inflow u_t^2): even though, the control u_t^2 does not appear to be strongly relevant as its score, variance reduction and Performance SISO have always low values compared to other variables. Also the significance of exogenous drivers is rather limited. Furthermore, the state variables involved are two (the salinity concentration in Cluster 1 sal_t^{C1} and the salinity concentration in Cluster 4 sal_t^{C4}).

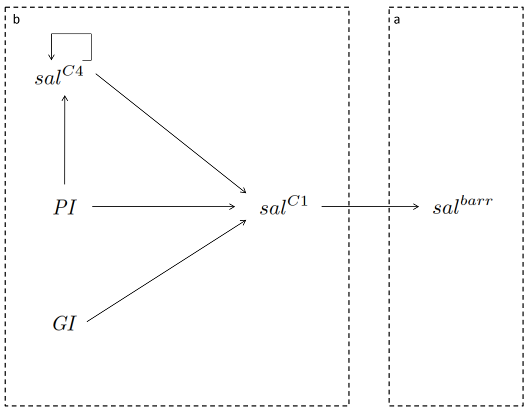

Figure 4.12: Graph representation of the variables interactions involved in the emulator output transformation function (a) and state transition equation (b), for data aggregated with hierarchical clustering.

4.4 Identification of the emulation model

The outcome of the variable selection (Step 3) are the variables characterizing the emulator, as well as the nature of the relationship between these variables and the output $\mathbf{y}_t$. This information can be exploited in Step 4 of the DEMo general procedure (see Figure 1.1), where the structure of the emulator state transition equation $\mathbf{f}_t(\cdot)$ and output transformation function $\mathbf{h}_t(\cdot)$ is selected and the associated parameters estimated.

This step simply requires to select an appropriate structure (class of functions) for the emulator, which can then be calibrated and validated. Considering the good performances provided by Extra-Trees as underlying model in the variable selection process, they are adopted with the same setting also in this step.

Table 4.10: Structure and performances (R^2 and RMSE in k-fold cross validation) of the MISO models composing sal_t^{barr} (salinity concentration in the point close to the barrage) emulation model, for data aggregated with hierarchical clustering.

Output variable	Input variables	R^2	RMSE
sal_t^{barr}	sal_t^{C1}	0.9838	0.3203 (ppt)
sal_t^{C1}	sal_{t-6}^{C4}, PI_{t-6}, GI_{t-6}	0.9437	0.5862 (ppt)
sal_t^{C4}	sal_{t-6}^{C4}, PI_{t-6}	0.9541	0.4501 (ppt)

The final structure of the emulator is thus a cascade of models that is calibrated[2] and validated with a k-fold cross-validation (with $k = 10$) on the data-set generated with the DOE, to check its accuracy and reliability. As for Extra-Trees parameters, the number M of trees in the ensemble and the minimum cardinality n_{min} were chosen equal to 50 and 15, while K the number of alternative cut-directions evaluated when splitting a node, was set equal to the number of inputs characterizing each model.
Table 4.10 reports the output and input variables characterizing each component of the salinity emulation model obtained from the aggregation with hierarchical clustering and the corresponding performances, in terms of R^2 and Root Mean Squared Error (RMSE).
Notice that the emulation model performances are almost the same (with respect to the previous phase), as both the adopted model class and the cross-validation method are unchanged. The small differences in terms of R^2 are simply due to the randomized effects characterizing the Extra-Trees building procedure. A comparison between the trajectories computed with Delft3D and the emulation model for the variable sal_t^{barr} and the corresponding scatterplot is given in Figures 4.13 and 4.14.

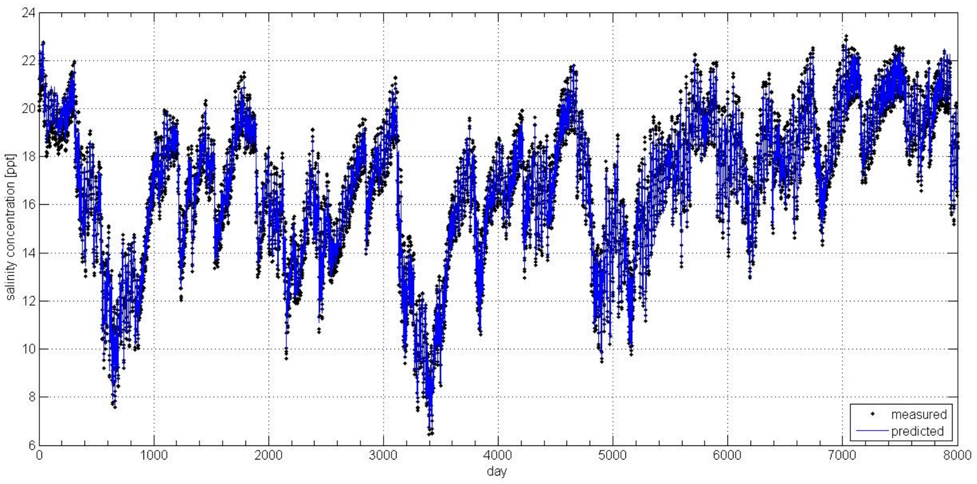

Figure 4.13: Trajectory of the average salinity concentration in the point close to the barrage chosen as output simulated by Delft3D (dotted line) and predicted by the emulation model (solid line), for data aggregated with hierarchical clustering.

[2]As non-parametric model, Extra-Trees (and any other tree-based methods) do not have parameters to be estimated in the traditional meaning of the term. Calibration is replaced by the tree construction algorithm that is run for some pre-selected values of few hyper-parameters

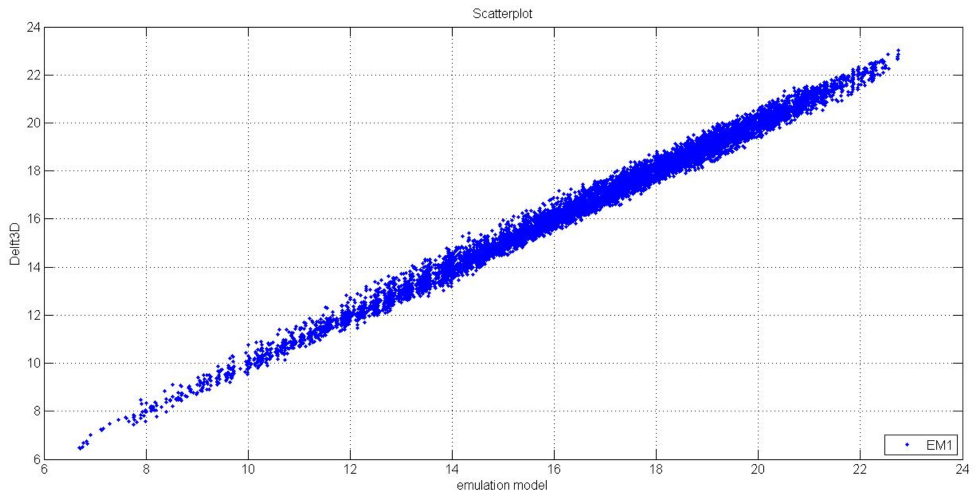

Figure 4.14: Scatterplot between the trajectory of the average salinity concentration in the point close to the barrage simulated by Delft3D (y-axis) and predicted by the emulation model (x-axis), for data aggregated with hierarchical clustering.

Comments

In the previous sections, the procedural, data-driven approach to dynamic emulation modelling combined with hierarchical clustering was applied for the reduction of Delft3D, a physically-based, hydrodynamic-ecological model describing the dynamics of Marina Reservoir (Singapore). The purpose is to achieve a simplified, but effective, description of salinity concentration dynamics in the deepest layer of an area very close to the barrage and to solve an optimal control problem concerning both quantity and quality targets. The reduction part is made by means of hierarchical clustering: the clusters obtained turn out to be a compact and informative representation of the initial larger amount of data available via simulation of the model itself. The complexity reduction with respect to Delft3D is remarkable, i.e. from nearly 10^4 to only 48 variables. The emulation model performances are quite satisfactory as, despite its simple structure, the emulation model provides good performances.

In particular, the potential of hierarchical clustering performed in this work is that, despite being an automatic technique, all the selected variables can be given a physical interpretation: *i*) the state variables selected provide information about the salinity concentration in a homogeneous area very close to the barrage; *ii*) the groundwater flow represents the main source of the salinity intrusion, while *iii*) the pipes, located at the bottom of the barrage, have an obvious key role in releasing water with higher salinity concentrations.

4.5 Choice of a different aggregation method

This section describes the application of DEMo procedure to data grouped with a different aggregation method: the rationale behind this choice is to show how the results can vary according to the particular type of aggregation method chosen. This aggregation method is different from clustering: with the purpose of simply preserving the physical interpretation of the natural system, in this part of the work time-series data (referred to each state variable in each simulation) are divided into groups by assuming that each vertical layer (introduced to take into account the stratification in Marina Reservoir) can be a sufficiently compact and relevant cluster well representing a homogeneous area in the high-dimensional data sets produced via Delft3D simulation runs.

4.5.1 DOE, simulation runs and variable aggregation

The final scope of DOE is to explore, via simulation of the physically-based model, the largest possible area within the $\mathcal{L}_{\mathbf{Y}_t} \times \mathcal{L}_{\mathbf{W}_t} \times \mathcal{L}_{\mathbf{u}_t}$ and $\mathcal{L}_{\mathbf{X}_t} \times \mathcal{L}_{\mathbf{W}_t} \times \mathcal{L}_{\mathbf{u}_t}$ spaces (where, in particular, $\mathcal{L}_{\mathbf{W}_t}$ is the space of drivers, $\mathcal{L}_{\mathbf{u}_t}$ is the space of controls, $\mathcal{L}_{\mathbf{Y}_t}$ is the space of the output to be explained, and $\mathcal{L}_{\mathbf{X}_t}$ is the space of the states). For each simulation run, it is thus necessary to specify a trajectory over the whole simulation horizon H for all the physically-based model input variables, namely the exogenous driver $\mathbf{W}_t$ and the control $\mathbf{u}_t$: these vector are unchanged with respect to the case of data aggregated with hierarchical clustering (see Section 4.1).
As said, in this part of the work time-series data (referred to each state variable in each simulation) are divided into 12 groups according to the number of vertical layer. In Table 4.11 the depth of each layer is reported. In such a way 12 groups within the data are created, in correspondence of the vertical layers. The assumption made is that data contained in the same layer show a similar behaviour. For the upper layer (layer 12) data are not always present for each location point at each time step (for instance, during dry periods), so only the first eleven layers are taken into account in the subsequent computations. Moreover, the number of points belonging to each group is not the same because of the bathymetry of the reservoir: for instance, layer 1 contains only 8 points (the points with greater depth), layer 6 contains 80 points,

Table 4.11: Depth of each vertical layer in Delft3D stratification.

Layer	Depth [m]
Layer 12	0.354 - 1.062
Layer 11	1.062 - 1.753
Layer 10	1.753 - 2.415
Layer 9	2.415 - 3.047
Layer 8	3.047 - 3.653
Layer 7	3.653 - 4.233
Layer 6	4.233 - 4.787
Layer 5	4.787 - 5.318
Layer 4	5.318 - 5.826
Layer 3	5.826 - 6.312
Layer 2	6.312 - 7.050
Layer 1	$>$ 7.050

and layer 11 is made up of 111 points. This difference will affect the next steps of the procedure, as the average trajectories of each state variable calculated for layers with a lower number of points are more similar to the trajectories of each singular point belonging to the layer itself (in this case the cluster well represents the behaviour of the points that belong to the cluster itself).
Notice that this is only one of the possible aggregations for the time-series data concerning Marina Reservoir. This approach can preserve physical interpretability, but it requires a number of a-priori assumptions (i.e. the hypothesis that the values of the state variable measured at the same depth show the same behaviour. In case of non horizontal homogeneity, vertical stratification cannot be adopted as clustering criterion) hardly formalizable in a procedural process.
Carry on through DEMo procedure with this approach, the vectors to be considered in the next phase are $\tilde{\mathbf{X}}_t$, $\tilde{\mathbf{W}}_t$, and $\mathbf{u}_t$, with dimensionality $\mathcal{M}_x$, n_w and n_u respectively equal to 77 (7 state variables for each cluster), 7 and 3. To these vectors, three more variables were eventually added, i.e. the reservoir level h_t, the variable d, which accounts for the system daily periodicity by taking value in the range [1, 365], and the variable H, which accounts for the system hourly periodicity by taking value in the range [1, 24]. This gives a total of 90 candidate variables for the variable selection problem.

4.5.2 Variable selection

The reduction problem requires to select the variables $\mathbf{x}_t$, $\mathbf{w}_t$ and $\mathbf{u}_t$ constituting the arguments of the output transformation function $\mathbf{h}_t(\cdot,\cdot,\cdot)$ and the state transition function $\mathbf{f}_t(\cdot,\cdot,\cdot)$. The output is the same: sal_t^{barr}, that represents the salinity concentration in a point close to the barrage. The only difference is that in the case of data aggregated using vertical layers as aggregation principle, the number of alternative cut-directions K (i.e. the number of candidate variables) is 90 instead of 59.

Salinity in a point close to the barrage sal_t^{barr}

The first step of the RVS-IIS algorithm requires to identify which variables, among $\tilde{\mathbf{X}}_t$, $\tilde{\mathbf{W}}_t$ and $\mathbf{u}_t$, are relevant to describe the the physically-based model output $\mathbf{Y}_t$: these are the arguments of the emulator output transformation function (see eq. 1.4b) that will be identified in the subsequent step.
The results obtained with *Step 0* of RVS-IIS, which rank the importance of all the candidate variables in explaining sal_t^{barr} behaviour and then singularly evaluates the importance of the first ranked, are reported in Table 4.12 - *Step 0.* The Table shows that the output behaviour is almost totally explained by only one variable, as confirmed by its score (84.17%), variance reduction and SISO performance: as a matter of fact the average salinity concentration in layer 1 sal_t^{L1} provides information about the salinity concentration at the bottom layer.

Table 4.12: Results obtained using RVS-IIS algorithm to select the most relevant variables to explain sal_t^{barr}, for data aggregated in vertical layers.

Step 0

Output variable	sal_t^{barr}
Initial variance	71807.4

Candidate Feature	Score %	Variance Reduction	Performance SISO (R^2)
sal_t^{L1}	84.1711	60431.1	0.9930
sal_t^{L2}	14.2826	10254.3	0.9644
GI_t	0.2397	172.067	0.1465

The IIS algorithm seems also to be robust with respect to information redundancy: the selected variables should be characterized by different information contents, and the selection of redundant arguments is avoided. An example is provided by the

Step 1

Output variable	sal_t^{barr} - $\hat{v}_t^0$
Initial variance	497.831

Candidate Feature	Score %	Variance reduction	Performance SISO (R^2)
GI_t	37.6413	185.398	0.4289
UV^{L1}	4.6626	22.9650	0.1630
UV^{L2}	4.4916	22.1229	0.1673
h_t	4.3730	21.5385	0.1285
VV^{L4}	4.2241	20.8050	0.1500

discard of salinity concentration in layer 2 sal_t^{L2}: as Layer 1 and Layer 2 differ only of a small depth (0.70 m), they are characterized by very similar salinity concentrations. The information content of the two variables is redundant and it is thus sufficient to employ just one of them in explaining sal_t^{barr}. Groundwater inflow GI_t is ranked in position three, but with low score (0.2397%) and variance reduction (172.067): probably this is not because its dynamic is not relevant with respect to salinity concentration (as groundwater inflow is the main source of salinity intrusion in the reservoir), but only because the increase in the model performance is really small. At the end of this step, the sal_t^{L1} term is selected, since it is characterized by the highest SISO model performance (0.9930). *Step 1* of RVS-IIS, whose results are reported in Table 4.12 - *Step 1* shows that the hypothesis was the right one, as salinity concentration in Layer 2 sal_t^{L2} is not part of the candidate variables, and the groundwater inflow GI_t is ranked in the first position with high score and variance reduction with respect to the other variables. This means that also GI_t is relevant in explaining the residual r_{t+1}^0. The remaining part of *Step 1* shows that

Table 4.13: Selected features and corresponding performance of the MISO models obtained for the case of sal_t^{barr}, for data aggregated in vertical layers. State variables are denoted in bold.

Iteration	Feature selected	Performance MISO (R^2)	ΔR^2
1	$\boldsymbol{sal_t^{L1}}$	0.9930	-
2	GI_t	0.9964	0.0034

also some components of horizontal velocities in the lower layers seems to affect the behaviour of sal_t^{barr}, but not enough to be chosen by the algorithm: the best feature is definitely GI_t and the selection of this new feature let the MISO model performance increase, with R^2 passing from 0.9930 to 0.9964 (see Table 4.13). However, the introduction of this new variable into the MISO model lead to an increase of R^2 equal to 0.0034, which is lower than the predefined tolerance (ε is set to 0.02). At this stage the RVS-IIS is stopped and the only selected feature is sal_t^{L1}.

Dynamics of sal_{t+1}^{L1}

In the set $\mathcal{V}^i_{sal_t^{barr}}$ of variables selected at the first call of RVS-IIS algorithm, salinity concentration in Layer 1 sal_t^{L1} is a state variable and, as such, its dynamic behaviour must be described through suitable state transition equations. The set $\mathcal{V}^i_{sal_t^{L1}}$ is selected in the subsequent call of the IIS algorithm among the components of the vectors $\tilde{\mathbf{X}}_t$, $\tilde{\mathbf{W}}_t$ and $\mathbf{u}_t$.

Table 4.14: Selected features and corresponding performance of the MISO models obtained for the case of sal_{t+1}^{L1}. State variables are denoted in bold.

Iteration	Feature selected	Performance MISO (R^2)	ΔR^2
1	$\boldsymbol{sal_t^{L2}}$	0.7615	-
2	u_t^2	0.9327	0.1712
3	GI_t	0.9652	0.0325
4	$\boldsymbol{UV^{L2}}$	0.9805	0.0153

A list of the selected variables is reported in Table 4.14. It can be noticed that sal_t^{L2}, u_t^2, and GI_t, the salinity concentration in Layer 2, the release from the pipes and the groundwater inflow, are features relevant to the dynamics of the salinity concentration in Layer 1 sal_{t+1}^{L1}. In particular pipes are relevant because they are located at the bottom of the barrage and have an obvious key role in releasing water with higher salinity concentrations, while the groundwater inflow is the only source of salinity intrusion in the reservoir.

Dynamics of sal_{t+1}^{L2}

Among these features, salinity concentration in Layer 2 sal_t^{L2} is again state variable, thus requiring a dynamic description too. The results of the RVS-IIS algorithm application to sal_{t+1}^{L2} is reported in Table 4.15.

Table 4.15: Selected features and corresponding performance of the MISO models obtained for the case of sal_{t+1}^{L2}. State variables are denoted in bold.

Iteration	Feature selected	Performance MISO (R^2)	ΔR^2
1	$\boldsymbol{sal_t^{L3}}$	0.8276	-
2	u_t^2	0.9387	0.1111
3	$\boldsymbol{temp_t^{L2}}$	0.9639	0.0252
4	GI_t	0.9723	0.0084

Dynamics of $\mathbf{sal}_{t+1}^{L3}$ and $\mathbf{temp}_{t+1}^{L2}$

Also at this iteration two among the selected variables are state variables (salinity concentration in Layer 3 sal_t^{L3} and temperature in Layer 2 $temp_t^{L2}$), and require to be given a dynamic description. Table 4.16 - 4.17 show the results. sal_{t+1}^{L3} reveals to be strongly dependent on its auto-regressive term while $temp_{t+1}^{L2}$ seems to be linked to daily periodicity d_t. The effect of the release from the pipes is rather negligible.

Table 4.16: Selected features and corresponding performance of the MISO models obtained for the case of sal_{t+1}^{L3}. State variables are denoted in bold.

Iteration	Feature selected	Performance MISO (R^2)	ΔR^2
1	$\boldsymbol{sal_t^{L3}}$	0.9818	-
2	u_t^2	0.9953	0.0135

Table 4.17: Selected features and corresponding performance of the MISO models obtained for the case of $temp_{t+1}^{L2}$. State variables are denoted in bold.

Iteration	Feature selected	Performance MISO (R^2)	ΔR^2
1	d_t	0.9404	-
2	u_t^2	0.9724	0.0320
3	$\boldsymbol{temp_t^{L2}}$	0.9804	0.0080

At this stage the recursive variable selection is over, since no further state variables are selected. The process took five calls of the RVS algorithm, to single out the most suitable subset $\mathcal{V}^i_{sal_t^{barr}}$ of input variables to explain the system output. In particular, the emulator is characterized by a state vector $\mathbf{x}_t$ with 4 components (salinity

concentration in Layer 1 sal_t^{L1}, salinity concentration in Layer 2 sal_t^{L2}, salinity concentration in Layer 3 sal_t^{L3}, and temperature in Layer 2 $temp_t^{L2}$) one exogenous driver (i.e. groundwater inflow GI_t), only one component of the original control vector (i.e. pipe inflow u_t^2) and the variable that accounts for daily periodicity of the system (i.e. d).
The network of the causal relationships between the selected state variables is sketched in Figure 4.15.

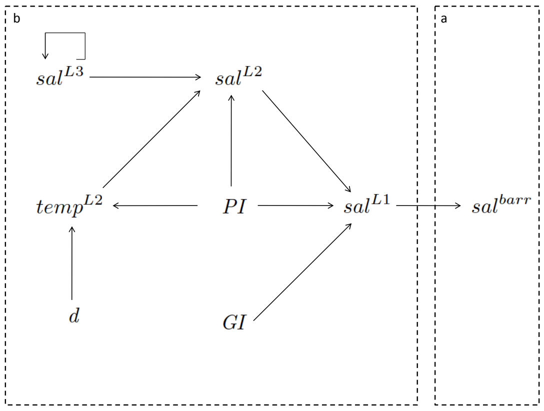

Figure 4.15: Graph representation of the variables interactions involved in the emulator output transformation function (a) and state transition equation (b), for data aggregated in vertical layers.

Identification of the emulation model

The outcome of the variable selection (Step 3) are the variables characterizing the emulator, as well as the nature of the relationship between these variables and the output $\mathbf{y}_t$. This step simply requires to select an appropriate structure (class of functions) for the emulator, which can then be calibrated and validated. Considering the good performances provided by Extra-Trees as underlying model in the variable selection process, they are adopted with the same setting also in this step.
The final structure of the emulator is thus a cascade of models that is calibrated and validated with a k-fold cross-validation (with $k = 10$) on the data-set generated with the DOE, to check its accuracy and reliability. As for Extra-Trees parameters, the number M of trees in the ensemble and the minimum cardinality n_{min} were chosen equal to 50 and 15, while K the number of alternative cut-directions evaluated when splitting a node, was set equal to the number of inputs characterizing each model.
Table 4.18 reports the output and input variables characterizing each component of the salinity emulation model obtained from the aggregation in vertical layers and the

corresponding performances, in terms of R^2 and Root Mean Squared Error (RMSE).

Table 4.18: Structure and performances (R^2 and RMSE in k-fold crossvalidation) of the MISO models composing sal_t^{barr} (salinity concentration in the point close to the barrage) emulation model, for data aggregated in vertical layers.

Output variable	Input variables	R^2	RMSE
sal_t^{barr}	sal_t^{L1}	0.9888	0.2563 (ppt)
sal_t^{L1}	sal_{t-6}^{L2}, PI_{t-6}, GI_{t-6}	0.9210	0.6938 (ppt)
sal_t^{L2}	sal_{t-6}^{L3}, PI_{t-6}, temp_{t-6}^{L2}	0.8333	0.8540 (ppt)
$temp_t^{L2}$	d_{t-6}, PI_{t-6}	0.1743	0.2493 °C
sal_t^{L3}	sal_{t-6}^{L3}	0.9273	0.3762 (ppt)

Also in this case the emulation model performances are almost the same to the ones obtained in the previous phase, as both the adopted model class and the cross-validation method are unchanged. The small differences in terms of R^2 are simply due to the randomized effects characterizing the Extra-Trees building procedure. A comparison between the trajectories computed with Delft3D and the emulation model for the variable sal_t^{barr} and the corresponding scatterplot is given in Figures 4.16 and 4.17.

Comments

The procedural, data-driven approach to dynamic emulation modelling was applied for the reduction of the same 3D model, i.e. Delft3D, to achieve a simplified, but effective, description of salinity concentration dynamics in the deepest layer of an area very close to the barrage and to solve an optimal control problem concerning both quantity and quality targets. The difference stands in the aggregation method: in this case data are aggregated in 11 vertical layers. The clusters obtained are more than in the case of data aggregated with hierarchical clustering: 11 clusters for each state variables (except water level, for which only one cluster is identified) gives a total of 78 state variables (instead of only 47 in case of data aggregated through hierarchical clustering). The complexity reduction with respect to Delft3D is from nearly 10^4 to 90 variables. The emulation model performances are still quite satisfactory, even if the number of the selected state variables (and thus the complexity

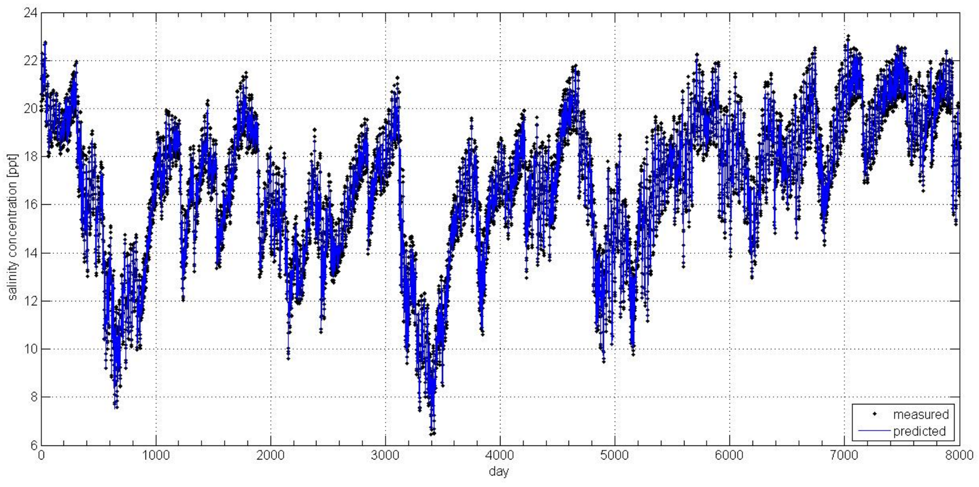

Figure 4.16: Trajectory of the average salinity concentration in the point close to the barrage chosen as output simulated by Delft3D (dotted line) and predicted by the emulation model (solid line), for data aggregated in vertical layers.

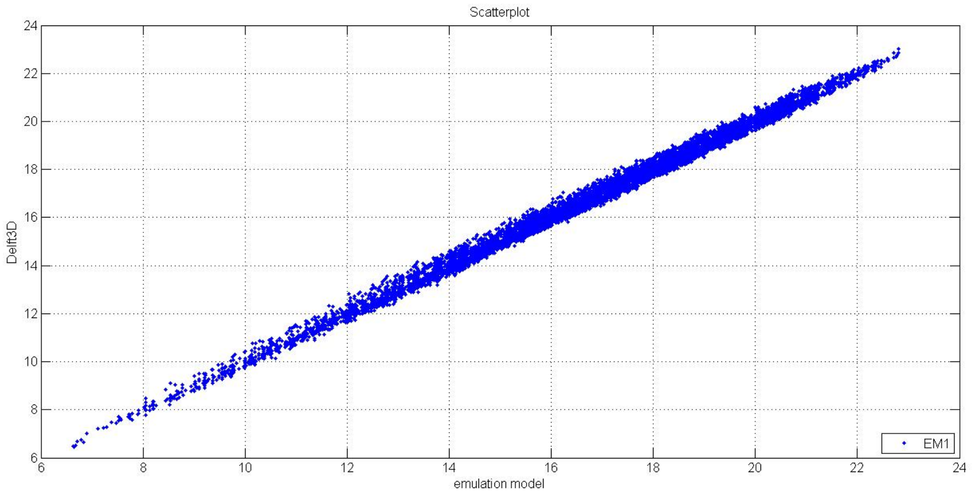

Figure 4.17: Scatterplot between the trajectory of the average salinity concentration in the point close to the barrage simulated by Delft3D (y-axis) and predicted by the emulation model (x-axis), for data aggregated in vertical layers.

of the resulting emulation model) increases from 2 to 4, exogenous drivers and controls being equal. This is due to the fact that aggregation in vertical layers seems to be less efficient in organizing data into homogeneous groups than a fully automatic and system-independent tool (i.e. hierarchical clustering): the introduction of more variables, in fact, does not increase so much the emulator performances.

Concluding remarks

This work describes a hybrid clustering-variable selection approach to automatically discover compact and relevant representations of high-dimension data sets generated by computationally-intensive physically-based models. The approach, which relies on a time-series hierarchical agglomerative clustering method, is demonstrated on the emulation of a large, 3D model (Delft3D) used to simulate the salt intrusion dynamics in Marina Reservoir (Singapore).
As said, advances in scientific computation and data collection techniques have in fact increased the level of fundamental understanding that can be built into the kind of physically-based models which are widely used in the modelling of large environmental systems. These models are definitely useful to enhance the scientific knowledge of natural processes, but their structure becomes progressively more complicated as the complexity of the systems being studied. As the resulting increased complexity of the model structures poses strong limitations in terms of practical implementation and computational requirements, the application of model emulation techniques seems to be one viable solution for systems that must handle with problems that require hundreds or thousands of model evaluations. As such, the DEMo approach here proposed is particularly well-suited for optimal management problems, as it combines two desirable features: it is fully data-driven and preserves the state-space representation of the identified emulator. This is very effective as the emulator identified is not only compact but also physically-meaningful. The original data-set $\mathcal{F}$ was made of about $\sim 8 \cdot 10^4$ tuples: the application of hierarchical procedure on the original data-set strongly enhanced the dimensionality reduction process, as after clustering the number of variables decreased to less than 100. Finally, after variable selection less than 10 variables remained.
The comparison of the results obtained from data aggregated with hierarchical clustering and the ones aggregated in vertical layers shows that the latter aggregation technique is less efficient in automatically discovering homogeneous areas in large

data-sets; this is evident looking at the complexity of the final emulators with respect to the improvement of the respective emulators performances: the increase in the number of variables selected does not necessary correspond to the increase of the emulation model performance. The importance of the selected variables is demonstrated by the performance of the identified emulator, which can also be given a physically meaningful interpretation.
Since the clustering algorithm is embedded in a computationally expensive emulation modelling procedure, an unsupervised clustering approach has been here considered, while a supervised approach, which aims at determining the clustering solution that maximizes the emulator performance, is part of the on-going research activities. The main advantage of this second approach would rely in a further increase of the emulator accuracy and reliability.
Future research include the choice of further distance measures, linkage and indexes, and the comparison of different unsupervised clustering methods: a different choice of the clustering algorithm, as well of a different choice of the distance measure and linkage method, may well not give identical classifications when applied to the same data set. Cluster analysis as such is, indeed, not an automatic task, but an iterative process of knowledge discovery or interactive multi-objective optimization that involves trial and failure.
Finally, further improvement will focus on the identification of time-varying clusters and not only space-varying clusters, in order to find compact and relevant representation of the system at each time step.

Appendix A

Taxonomy and algorithms of DEMo procedure

A.1 Summary of the variables involved in the DEMo general procedure

- $\mathcal{M}$, original process-based model.
- $\mathbf{X}_t$, $\mathbf{Y}_t$, $\mathbf{W}_t$, physically-based model state, output and exogenous driver vector.
- $\mathbf{u}_t$, control vector.
- $\mathcal{N}_x$, $\mathcal{N}_y$, $\mathcal{N}_w$, $\mathcal{N}_u$, dimensionality of the vectors.
- $\mathbf{x}_t$, $\mathbf{y}_t$, $\mathbf{w}_t$, $\mathbf{u}_t$ emulator state, output, exogenous driver vector, and control vector.
- $\mathbf{f}_t(\cdot)$, $\mathbf{h}_t(\cdot)$, emulator state transition and output transformation function.
- $\tilde{\mathbf{X}}_t$, $\tilde{\mathbf{W}}_t$, physically-based model state and exogenous driver vector (after spatial aggregation).
- $\mathcal{F}$, data-set of tuples $\{\mathbf{X}_t, \mathbf{W}_t, \mathbf{u}_t, \mathbf{Y}_t, \mathbf{X}_{t+1}\}$ (with $t = 1, \ldots, H$) for the DEMo process.
- $\tilde{\mathcal{F}}$, data-set of tuples $\{\tilde{\mathbf{X}}_t, \tilde{\mathbf{W}}_t, \mathbf{u}_t, \mathbf{Y}_t, \tilde{\mathbf{X}}_{t+1}\}$ (with $t = 1, \ldots, H$) for the DEMo process (after spatial aggregation).
- H, simulation horizon.

A.2 Summary of the variables involved in the RVS-IIS methodology

- $\mathbf{v}_t^i = \{\tilde{\mathbf{X}}_t, \tilde{\mathbf{W}}_t, \mathbf{u}_t\}$, $\mathbf{v}_t^o = \{\tilde{\mathbf{X}}_{t+1}, \mathbf{Y}_t\}$ input and output data employed in the variable selection process.

- v_t^o, i-th component of the vector $\mathbf{Y}_t$.

- $v^i = \{\tilde{\mathbf{X}}, \tilde{\mathbf{W}}, \mathbf{u}\}$, $v^o = \{\tilde{\mathbf{X}}, \mathbf{Y}\}$, set of the candidate input and output variables for the variable selection process.

- v_{tar}^o, subset of the output variables that need to be explained ($v_{tar}^o \subseteq v^o$).

- v_{sel}^i, set of the input variables selected during the i-th iteration of the variable selection process.

- $v_{v^o}^i$, set of the input variables that will appear in the output transformation function for explaining v^o.

- $v_{\tilde{X}}^{new} = v_{v^o}^i \cap \tilde{X}$, set of the output variables to be explained.

- $v_{\mathbf{Y}}^i$, set of the input variables to explain the output $\mathbf{Y}$.

- v^*, most significant variable added to the set $v_{v^o}^i$.

- $\hat{m}(\cdot)$, underlying model to explain v^o.

- $\hat{v}^o$, residuals of $\hat{m}(\cdot)$.

- $D(v^o, \hat{m}(v_{v^o}^i))$, distance metric between the output vo and the model $\hat{m}(\cdot)$ predictions.

A.3 Recursive Variable Selection algorithm

Algorithm 1 RVS($\tilde{\mathcal{F}}$, $\mathcal{V}^o_{tar}$, $\mathcal{V}^i_{sel}$): Recursive Variable Selection

```
Require: The dataset $\tilde{\mathcal{F}}$, the set $\mathcal{V}^o_{tar}$ of variables to be explained and the set $\mathcal{V}^i_{sel}$
    of previously selected variables
Ensure: $\mathcal{V}^i_{\mathcal{V}^o_{tar}}$ : the set of input variables to explain $\mathcal{V}^o_{tar}$
  Initialize: $\mathcal{V}^i_{\mathcal{V}^o_{tar}} \leftarrow \emptyset$
  //For each variable that has to be explained
  for all $v^o \in \mathcal{V}^o_{tar}$ do
    //Select, with a suitable IS algorithm, the most relevant variables to explain $v^o$
    $\mathcal{V}^i_{v^o} \leftarrow \mathrm{IS}(\tilde{\mathcal{F}}, v^o)$
    //Consider the new state variables, i.e. not yet in $\mathcal{V}^i_{sel}$
    $\mathcal{V}^{new}_{\tilde{\mathbf{X}}} \leftarrow \left(\mathcal{V}^i_{v^o} \setminus \mathcal{V}^i_{sel}\right) \cap \tilde{\mathbf{X}}$
    //Add variables obtained by recursively execute RVS
    $\mathcal{V}^i_{v^o} \leftarrow \mathcal{V}^i_{v^o} \cup \mathrm{RVS}(\tilde{\mathcal{F}}, \mathcal{V}^{new}_{\tilde{\mathbf{X}}}, \mathcal{V}^i_{sel} \cup \mathcal{V}^i_{v^o})$
    //Add the selected input variables $\mathcal{V}^i_{v^o}$ to the set of input variables to be returned
    $\mathcal{V}^i_{\mathcal{V}^o_{tar}} \leftarrow \mathcal{V}^i_{\mathcal{V}^o_{tar}} \cup \mathcal{V}^i_{v^o}$
  end for
  return $\mathcal{V}^i_{\mathcal{V}^o_{tar}}$
```

A.4 Iterative Input Selection algorithm

Algorithm 2 IIS($\tilde{\mathcal{F}}$, v^o): Iterative Input Selection

```
Require: The dataset $\tilde{\mathcal{F}}$ and the variable $v^o$ to be explained
Ensure: $\mathcal{V}^i_{v^o}$: the set of variables selected to explain $v^o$
  Initialize: $\mathcal{V}^i_{v^o} \leftarrow \emptyset$, $\hat{v}^o \leftarrow v^o$, $D_{old} \leftarrow 0$
  repeat
    //With an Input Ranking (IR) algorithm, select the most relevant input variable $v^*$ to explain $\hat{v}^o$
    $v^* \leftarrow \mathrm{IR}(\tilde{\mathcal{F}}, \hat{v}^o)$
    //If such variable has been previously selected, then the algorithm stops and returns the set $\mathcal{V}^i_{v^o}$ of the input variables selected up to that point
    if $v^* \in \mathcal{V}^i_{v^o}$ then
      return $\mathcal{V}^i_{v^o}$
    end if
    //Add $v^*$ to the set $\mathcal{V}^i_{v^o}$ of selected variables
    $\mathcal{V}^i_{v^o} \leftarrow \mathcal{V}^i_{v^o} \cup v^*$
    //By using $\tilde{\mathcal{F}}$ estimate a model $\hat{m}(\cdot)$ that explains the variable $v^o$ using $\mathcal{V}^i_{v^o}$ as argument
    $\hat{m}(\cdot) \leftarrow \mathrm{MB}(\tilde{\mathcal{F}}, v^o, \mathcal{V}^i_{v^o})$
    //Compute the residuals
    $\hat{v}^o \leftarrow v^o - \hat{m}(\mathcal{V}^i_{v^o})$
    //Compute the variation of the coefficient of determination
    $\Delta D \leftarrow D(v^o, \hat{m}(\mathcal{V}^i_{v^o})) - D_{old}$
    //Backup D for the next iteration
    $D_{old} \leftarrow D(v^o, \hat{m}(\mathcal{V}^i_{v^o}))$
    //Stop iterating when the improvement is too low
  until $\Delta D < \epsilon$
  return $\mathcal{V}^i_{v^o}$
```

Appendix B

Clustering results

B.1 Plots of DBI and DI indexes

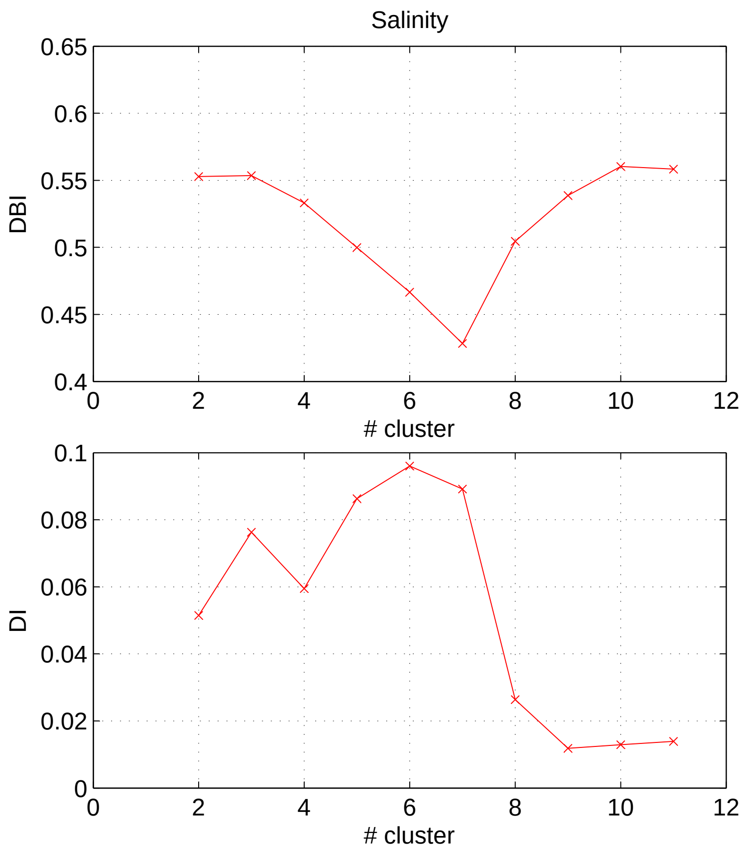

Figure B.1: Average value (over the 10 simulation runs) of the DBI and DI indexes for salinity (sal).

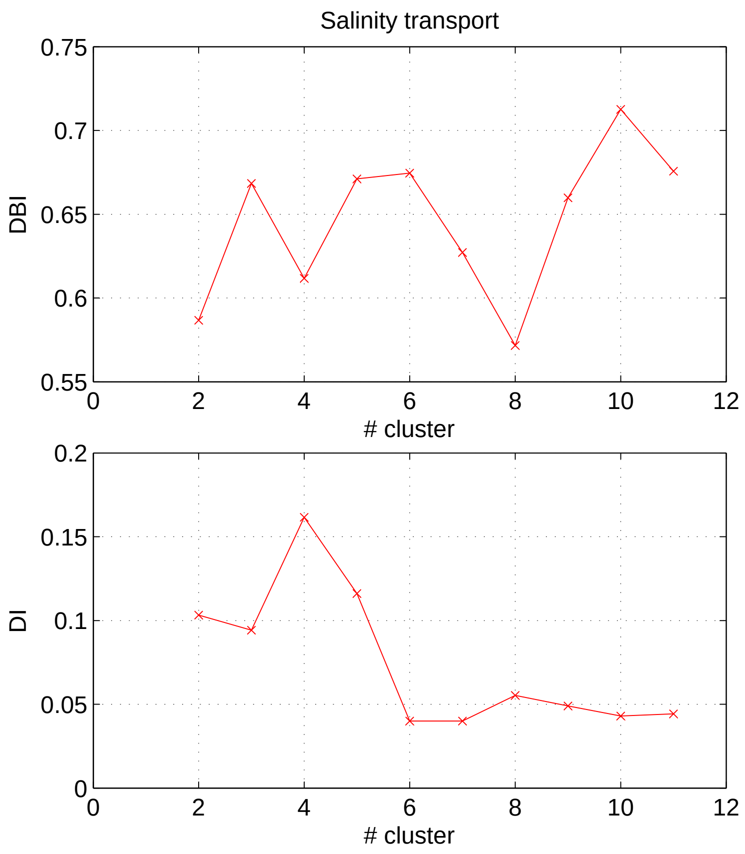

Figure B.2: Average value (over the 10 simulation runs) of the DBI and DI indexes for the salinity transport (ST).

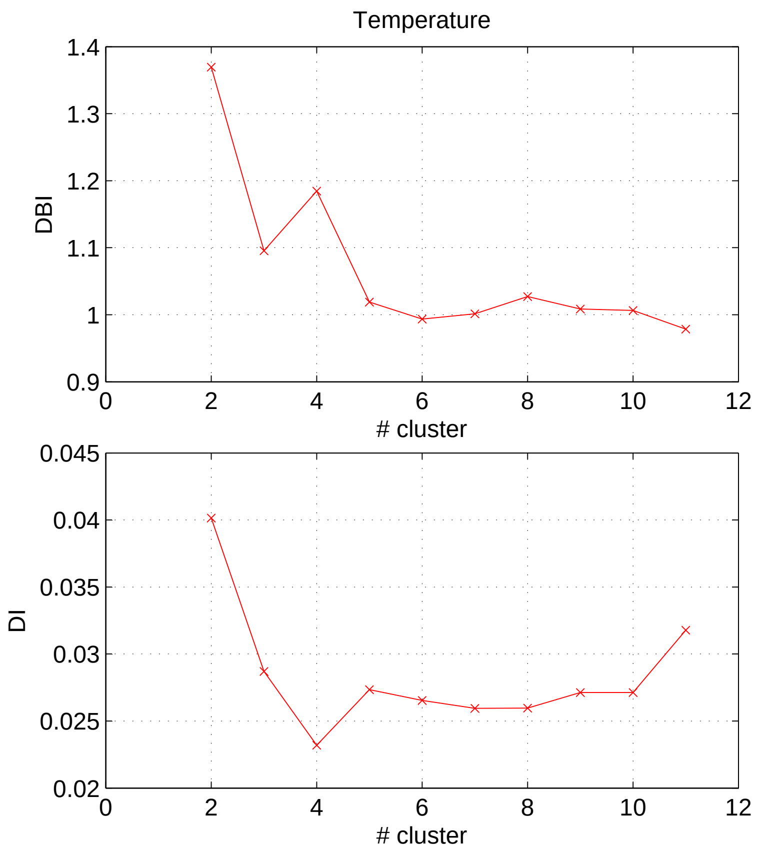

Figure B.3: Average value (over the 10 simulation runs) of the DBI and DI indexes for temperature ($temp$).

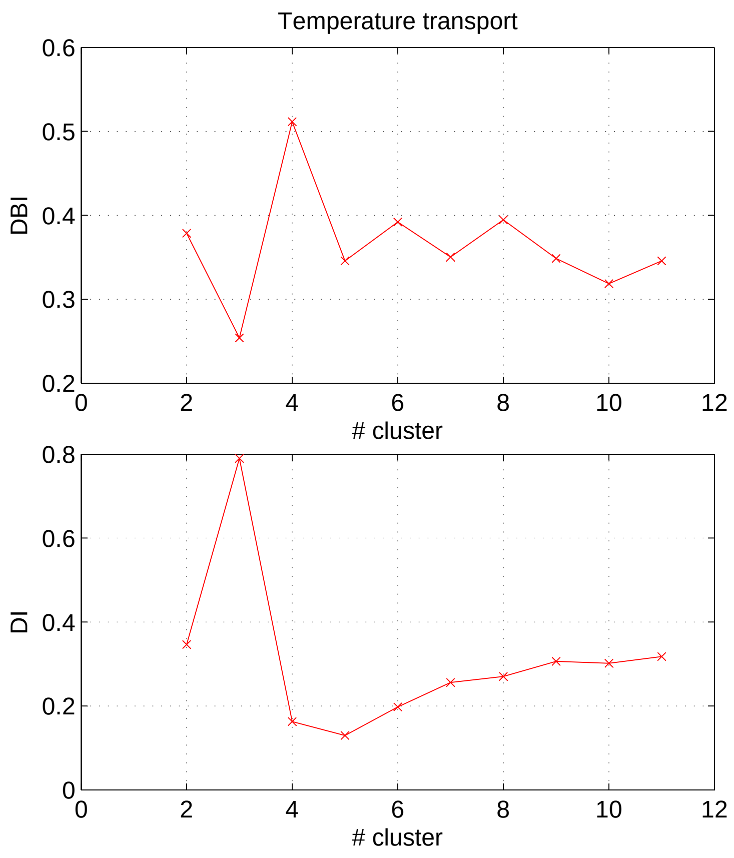

Figure B.4: Average value (over the 10 simulation runs) of the DBI and DI indexes for the temperature transport (TT).

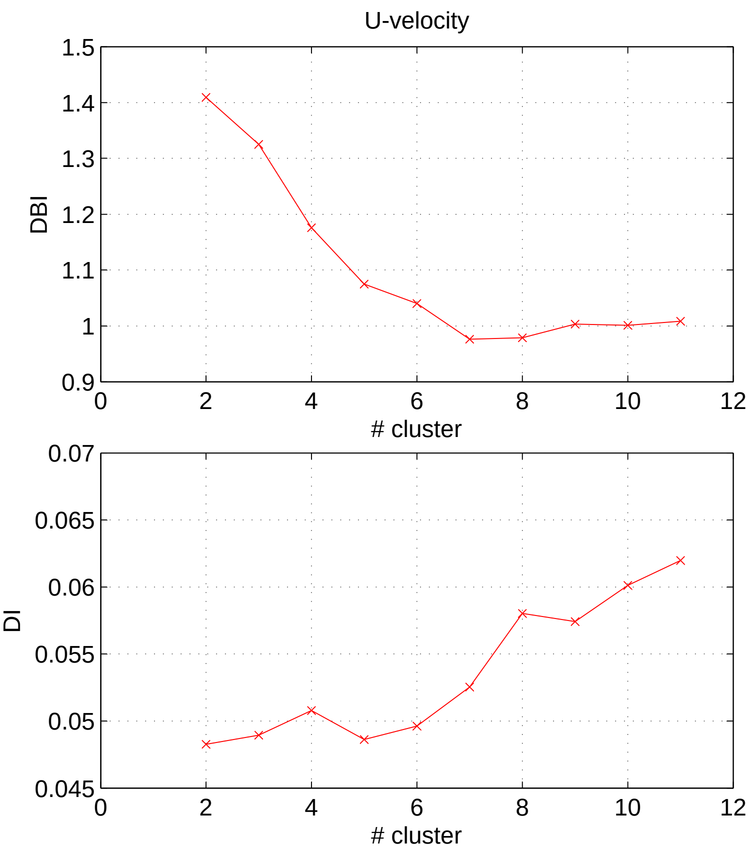

Figure B.5: Average value (over the 10 simulation runs) of the DBI and DI indexes for u-velocity (UV).

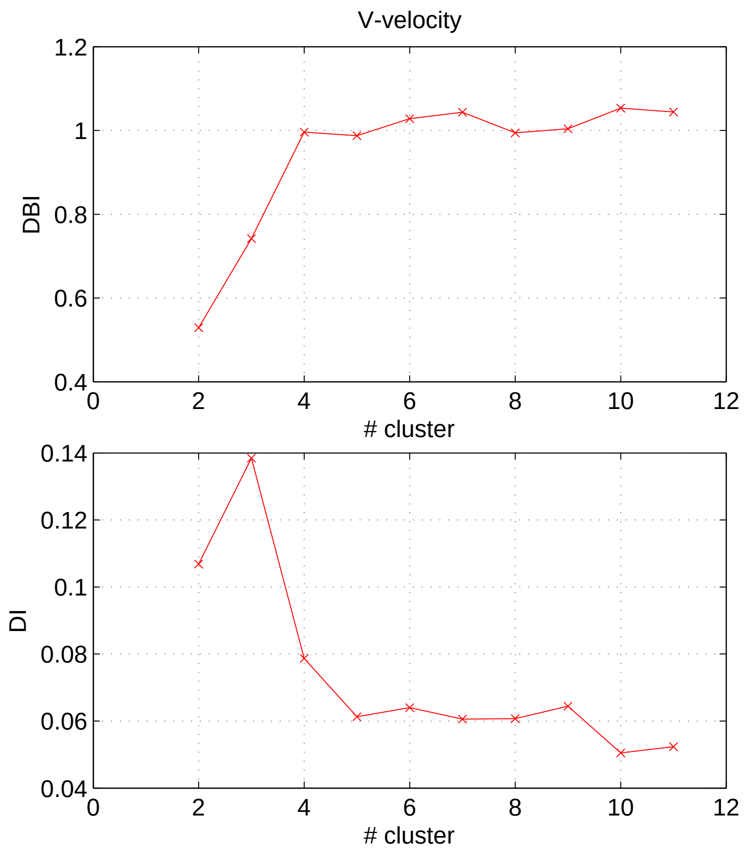

Figure B.6: Average value (over the 10 simulation runs) of the DBI and DI indexes for v-velocity (VV).

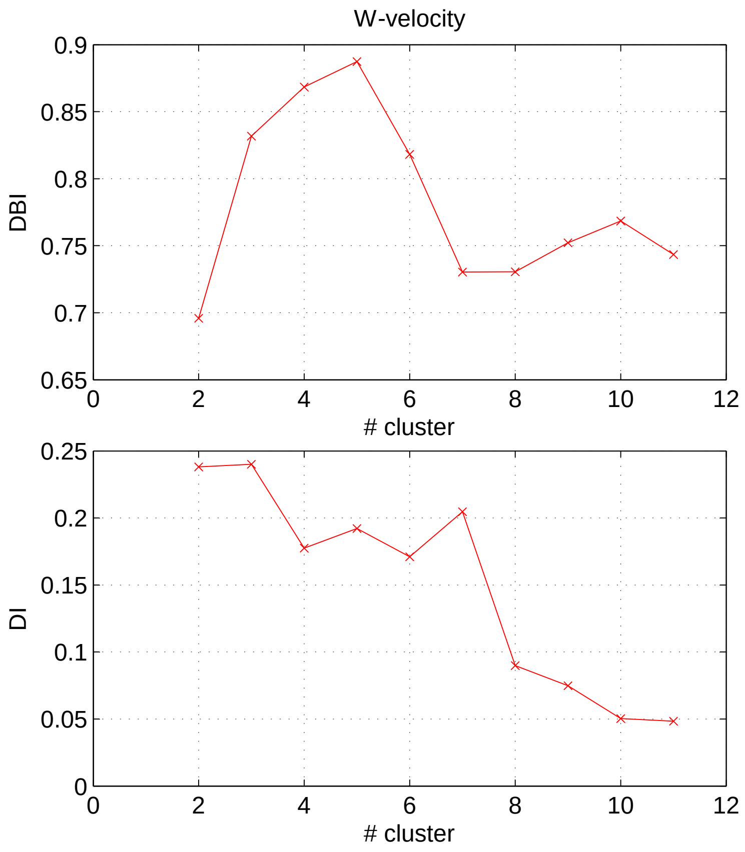

Figure B.7: Average value (over the 10 simulation runs) of the DBI and DI indexes for w-velocity (WV).

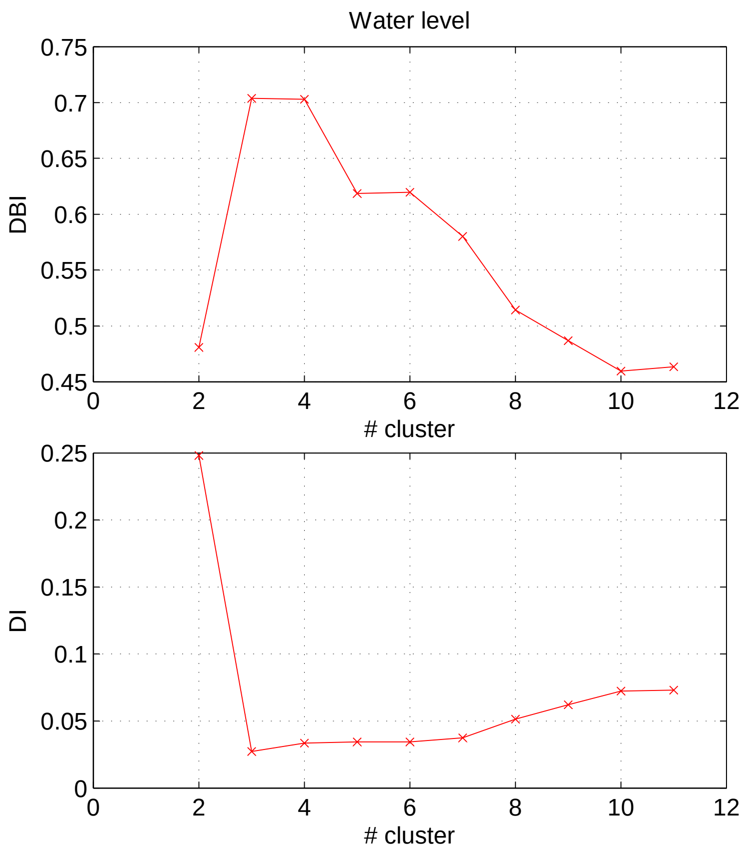

Figure B.8: Average value (over the 10 simulation runs) of the DBI and DI indexes for the water level (h).

B.2 Number of points per layer per cluster

Salinity						
	Cluster 1	Cluster 2	Cluster 3	Cluster 4	Cluster 5	Cluster 6
Layer 1	8	0	0	0	0	0
Layer 2	14	0	0	4	4	0
Layer 3	0	0	0	0	48	0
Layer 4	0	0	0	0	59	0
Layer 5	0	0	5	0	66	0
Layer 6	0	0	79	0	0	1
Layer 7	0	0	81	0	0	4
Layer 8	0	2	0	0	0	96
Layer 9	0	0	0	0	0	108
Layer 10	0	0	0	0	0	111
Layer 11	0	0	0	0	0	111

Table B.1: Number of points per layer per cluster for salinity (sal).

Salinity transport				
	Cluster 1	Cluster 2	Cluster 3	Cluster 4
Layer 1	0	0	0	8
Layer 2	0	0	0	22
Layer 3	0	0	0	48
Layer 4	0	0	0	59
Layer 5	0	0	0	71
Layer 6	0	4	0	76
Layer 7	1	5	0	79
Layer 8	4	5	0	89
Layer 9	4	7	0	97
Layer 10	3	8	1	99
Layer 11	2	8	1	100

Table B.2: Number of points per layer per cluster for salinity transport (ST).

Temperature						
	Cluster 1	Cluster 2	Cluster 3	Cluster 4	Cluster 5	Cluster 6
Layer 1	0	0	0	0	0	8
Layer 2	0	0	0	0	1	21
Layer 3	0	0	0	0	12	36
Layer 4	0	0	0	0	16	43
Layer 5	0	0	6	0	0	65
Layer 6	0	3	35	12	0	30
Layer 7	0	9	13	8	0	55
Layer 8	2	0	0	7	0	89
Layer 9	0	0	0	80	0	28
Layer 10	0	0	0	88	0	23
Layer 11	0	0	0	87	0	24

Table B.3: Number of points per layer per cluster for temperature (*temp*).

Temperature transport			
	Cluster 1	Cluster 2	Cluster 3
Layer 1	0	0	8
Layer 2	0	0	22
Layer 3	0	0	48
Layer 4	0	0	59
Layer 5	0	0	71
Layer 6	0	1	79
Layer 7	0	1	84
Layer 8	1	2	95
Layer 9	0	0	108
Layer 10	0	1	110
Layer 11	0	0	111

Table B.4: Number of points per layer per cluster for temperature transport (TT).

U-velocity				
	Cluster 1	Cluster 2	Cluster 3	Cluster 4
Layer 1	0	0	8	0
Layer 2	0	5	12	5
Layer 3	0	0	30	18
Layer 4	0	0	41	18
Layer 5	6	0	48	17
Layer 6	6	0	70	4
Layer 7	6	0	68	11
Layer 8	7	3	44	44
Layer 9	7	0	0	101
Layer 10	7	0	0	104
Layer 11	3	0	4	104

Table B.5: Number of points per layer per cluster for u-velocity (UV).

V-velocity						
	Cluster 1	Cluster 2	Cluster 3	Cluster 4	Cluster 5	Cluster 6
Layer 1	0	0	5	0	0	3
Layer 2	0	0	5	0	0	17
Layer 3	0	0	6	0	0	42
Layer 4	0	5	6	0	0	48
Layer 5	0	5	5	0	0	61
Layer 6	0	8	1	1	0	70
Layer 7	0	8	0	3	0	74
Layer 8	0	9	0	6	0	83
Layer 9	0	4	0	8	0	96
Layer 10	2	0	0	4	7	98
Layer 11	0	0	0	0	20	91

Table B.6: Number of points per layer per cluster for v-velocity (VV).

W-velocity								
	Cluster 1	Cluster 2	Cluster 3	Cluster 4	Cluster 5	Cluster 6	Cluster 7	Cluster 8
Layer 1	0	0	1	7	0	0	0	0
Layer 2	0	0	0	9	0	13	0	0
Layer 3	0	0	0	0	0	48	0	0
Layer 4	0	0	0	0	0	59	0	0
Layer 5	0	0	0	0	0	69	1	1
Layer 6	0	0	0	0	0	78	1	1
Layer 7	1	0	0	0	2	81	0	1
Layer 8	0	0	0	0	2	94	1	1
Layer 9	0	0	0	0	3	103	1	1
Layer 10	0	1	0	0	3	106	0	1
Layer 11	0	1	0	9	5	96	0	0

Table B.7: Number of points per layer per cluster for w-velocity (WV).

Water level									
Cluster 1	Cluster 2	Cluster 3	Cluster 4	Cluster 5	Cluster 6	Cluster 7	Cluster 8	Cluster 9	Cluster 10
4	2	6	27	37	2	4	13	4	12

Table B.8: Number of points per layer per cluster for water level (h).

Appendix C

Variable selection results

C.1 Aggregation by hierarchical clustering

C.1.1 Salinity near the barrage sal_t^{barr}

Table C.1: Results obtained using IIS-RVS algorithm to select the most relevant variables to explain sal_t^{barr}.

Step 0

Output variable	sal_t^{barr}
Initial variance	71807.4000

Candidate Feature	Score %	Variance Reduction	Performance SISO (R^2)
sal_t^{C1}	92.6011	66466.7000	0.9894
sal_t^{C4}	5.9314	4257.4100	0.9262
GI_t	0.2811	201.7440	0.1461

Step 1

Output variable	sal_t^{barr} - $\hat{v}_t^0$
Initial variance	767.59

Candidate Feature	Score %	Variance reduction	Performance SISO (R^2)
GI_t	37.2627	279.2710	0.3916
VV_t^{C3}	9.6575	72.3798	0.1898
u_t^2	4.5759	34.2948	0.0436
WV_t^{C1}	2.7336	20.4871	0.0757
sal_t^{C5}	2.5936	19.4384	0.0731

C.1.2 Dynamics of salinity in cluster 1 sal_{t+1}^{C1}

Table C.2: Results obtained using IIS-RVS algorithm to select the most relevant variables to explain sal_{t+1}^{C1}.

Step 0

Output variable	sal_{t+1}^{C1}
Initial variance	116.4780

Candidate Feature	Score %	Variance Reduction	Performance SISO (R^2)
sal_t^{C4}	46.4205	53.9914	0.7787
sal_t^{C1}	16.6586	19.3755	0.7380
u_t^2	10.4154	12.1141	0.2027
sal_t^{C5}	9.5679	11.1284	0.7360
GI_t	5.5935	6.5058	0.1015

Step 1

Output variable	sal_{t+1}^{C1} - $\hat{v}_{t+1}^0$
Initial variance	25.6537

Candidate Feature	Score %	Variance reduction	Performance SISO (R^2)
u_t^2	56.1475	14.3125	0.7387
GI_t	24.2330	6.1772	0.6234
u_t^3	1.6724	0.4263	0.1906
UV_t^{C2}	0.8070	0.2057	0.1005

Step 1.1

Output variable	sal_{t+1}^{C1} - $\hat{v}_{t+1}^1$
Initial variance	5.6695

Candidate Feature	Score %	Variance reduction	Performance SISO (R^2)
GI_t	33.6883	1.8630	0.3321
UV_t^{C2}	6.2316	0.3446	0.0285
WV_t^{C3}	2.8864	0.1596	0.0121
u_t^1	2.6062	0.1441	0.0372
$temp_t^{C5}$	2.4781	0.1370	0.1037

Step 1.2

Output variable	sal_{t+1}^{C1} - $\hat{v}_{t+1}^{2}$
Initial variance	2.6577

Candidate Feature	Score %	Variance reduction	Performance SISO (R^2)
u_t^1	9.0774	0.2321	0.1180
UV_t^{C2}	7.1100	0.1818	0.1177
WV_t^{C3}	2.9675	0.0759	0.0348
WV_t^{C4}	2.4358	0.0623	0.0379
$temp_t^{C5}$	2.2503	0.0576	0.0863

C.1.3 Dynamics of salinity in cluster 4 sal_{t+1}^{C4}

Table C.3: Results obtained using IIS-RVS algorithm to select the most relevant variables to explain sal_{t+1}^{C4}.

Step 0

Output variable	sal_{t+1}^{C4}
Initial variance	98.6165

Candidate Feature	Score %	Variance Reduction	Performance SISO (R^2)
sal_t^{C4}	53.8712	53.0850	0.8629
sal_t^{C1}	15.4741	15.2483	0.8206
sal_t^{C5}	12.1302	11.9532	0.8185
u_t^2	7.1364	7.0323	0.1297
sal_t^{C3}	4.5926	4.5256	0.7364

Step 1

Output variable	sal_{t+1}^{C4} - $\hat{v}_{t+1}^{0}$
Initial variance	13.4640

Candidate Feature	Score %	Variance reduction	Performance SISO (R^2)
u_t^2	48.9985	6.5488	0.7484
GI_t	15.7999	2.1117	0.5652
u_t^1	5.8067	0.7761	0.1819
UV_t^{C2}	2.8651	0.3829	0.1517
WV_t^{C3}	2.8269	0.3778	0.1425

Step 1.1

Output variable	sal_{t+1}^{C4} - $\hat{v}_{t+1}^{1}$
Initial variance	2.4163

Candidate Feature	Score %	Variance reduction	Performance SISO (R^2)
GI_t	18.2733	0.4266	0.2549
VV_t^{C3}	6.5482	0.1529	0.1316
UV_t^{C2}	4.0532	0.0946	0.0867
u_t^1	3.2215	0.0752	0.0438
I_t	2.9322	0.0685	0.0619

C.2 Aggregation in vertical layers

C.2.1 Salinity near the barrage sal_t^{barr}

Table C.4: Results obtained using IIS-RVS algorithm to select the most relevant variables to explain sal_t^{barr}.

Step 0

Output variable	sal_t^{barr}
Initial variance	71807.4

Candidate Feature	Score %	Variance Reduction	Performance SISO (R^2)
sal_t^{L1}	84.1711	60431.1	0.9930
sal_t^{L2}	14.2826	10254.3	0.9644
GI_t	0.2397	172.067	0.1465

Step 1

Output variable	sal_t^{barr} - $\hat{v}_t^{0}$
Initial variance	497.831

Candidate Feature	Score %	Variance reduction	Performance SISO (R^2)
GI_t	37.6413	185.398	0.4289
UV_t^{L1}	4.6626	22.9650	0.1630
UV_t^{L2}	4.4916	22.1229	0.1673
h_t	4.3730	21.5385	0.1285
VV_t^{L4}	4.2241	20.8050	0.1500

C.2.2 Dynamics of salinity in layer 1 sal_{t+1}^{L1}

Table C.5: Results obtained using IIS-RVS algorithm to select the most relevant variables to explain sal_{t+1}^{L1}.

Step 0

Output variable	sal_{t+1}^{L1}
Initial variance	120.106

Candidate Feature	Score %	Variance Reduction	Performance SISO (R^2)
sal_t^{L2}	34.1195	40.9388	0.7613
sal_t^{L1}	14.9457	17.9329	0.7282
sal_t^{L3}	11.4312	13.7159	0.7428
u_t^2	8.98024	10.7751	0.1994
sal_t^{L6}	6.48655	7.78298	0.7017

Step 1

Output variable	sal_{t+1}^{L1} - $\hat{v}_{t+1}^0$
Initial variance	28.5366

Candidate Feature	Score %	Variance reduction	Performance SISO (R^2)
u_t^2	50.3218	14.3131	0.6855
GI_t	27.187	7.7329	0.5918
u_t^1	1.9080	0.5427	0.2169
h_t	1.5384	0.4376	0.1732

Step 1.1

Output variable	sal_{t+1}^{L1} - $\hat{v}_{t+1}^1$
Initial variance	8.0409

Candidate Feature	Score %	Variance reduction	Performance SISO (R^2)
GI_t	35.72	2.8419	0.300597
UV_t^{L2}	6.04684	0.481088	0.0928751
u_t^1	5.08762	0.404773	0.0615848
UV_t^{L3}	3.41868	0.271991	0.0680266
h_t	2.85791	0.227377	0.0516562

C.2.3 Dynamics of salinity in layer 2 sal_{t+1}^{L2}

Table C.6: Results obtained using IIS-RVS algorithm to select the most relevant variables to explain sal_{t+1}^{L2}.

Step 0

Output variable	sal_{t+1}^{L2}
Initial variance	97.6546

Candidate Feature	Score %	Variance Reduction	Performance SISO (R^2)
sal_t^{L2}	31.1665	30.4163	0.8227
sal_t^{L3}	24.6635	24.0698	0.8276
sal_t^{L5}	8.7907	8.57907	0.7921
u_t^2	7.4692	7.2894	0.1565
sal_t^{L6}	7.1822	7.00933	0.7412

Step 1

Output variable	sal_{t+1}^{L2} - $\hat{v}_{t+1}^0$
Initial variance	16.7514

Candidate Feature	Score %	Variance reduction	Performance SISO (R^2)
u_t^2	45.2788	7.5452	0.6048
GI_t	10.1806	1.6965	0.4164
u_t^1	5.2352	0.8724	0.1927
$temp_t^{L2}$	4.0496	0.6748	0.0581
$temp_t^{L1}$	2.4065	0.4010	0.0481

Step 1.1

Output variable	sal_{t+1}^{L2} - $\hat{v}_{t+1}^1$
Initial variance	5.96178

Candidate Feature	Score %	Variance reduction	Performance SISO (R^2)
$temp_t^{L2}$	9.1683	0.5394	0.1916
GI_t	7.4504	0.4383	0.1122
$temp_t^{L1}$	6.4878	0.3817	0.1670
u_t^1	3.7934	0.2232	0.0467
$temp_t^{L3}$	3.5910	0.2113	0.1613

Step 1.2

Output variable	sal_{t+1}^{L2} - $\hat{v}_{t+1}^{2}$
Initial variance	3.50768

Candidate Feature	Score %	Variance reduction	Performance SISO (R^2)
GI_t	10.8073	0.3712	0.1379
u_t^1	5.17201	0.1777	0.0640
$temp_t^{L10}$	3.7840	0.1300	0.1070
$temp_t^{L11}$	3.5369	0.1215	0.1029
$temp_t^{L9}$	3.1879	0.1095	0.1037

C.2.4 Dynamics of salinity in layer 3 sal_{t+1}^{L3}

Table C.7: Results obtained using IIS-RVS algorithm to select the most relevant variables to explain sal_{t+1}^{L3}.

Step 0

Output variable	sal_{t+1}^{L3}
Initial variance	63.5384

Candidate Feature	Score %	Variance Reduction	Performance SISO (R^2)
sal_t^{L3}	37.1280	23.5887	0.9818
sal_t^{L4}	23.8781	15.1706	0.9683
sal_t^{L5}	13.3729	8.49625	0.9134
sal_t^{L11}	4.7563	3.02186	0.5721
sal_t^{L10}	4.3524	2.76522	0.5733

Step 1

Output variable	sal_{t+1}^{L3} - $\hat{v}_{t+1}^{0}$
Initial variance	1.14446

Candidate Feature	Score %	Variance reduction	Performance SISO (R^2)
u_t^2	28.9517	0.3302	0.6725
u_t^1	15.1117	0.1724	0.3010
GI_t	7.6087	0.0868	0.4714
h_t	4.9324	0.0563	0.2123
I_t	4.7457	0.0541	0.4544

C.2.5 Dynamics of temperature in layer 2 $temp_{t+1}^{L2}$

Table C.8: Results obtained using IIS-RVS algorithm to select the most relevant variables to explain $temp_{t+1}^{L2}$.

Step 0

Output variable	$temp_{t+1}^{L2}$
Initial variance	61.2627

Candidate Feature	Score %	Variance Reduction	Performance SISO (R^2)
$temp_t^{L3}$	26.2025	16.0475	0.9194
$temp_t^{L4}$	21.6484	13.2584	0.8683
$temp_t^{L1}$	21.0337	12.8819	0.8644
$temp_t^{L2}$	18.5094	11.3359	0.9253
d_t	2.7818	1.7037	0.9396

Step 1

Output variable	$temp_{t+1}^{L2}$ - $\hat{v}_{t+1}^0$
Initial variance	3.64568

Candidate Feature	Score %	Variance reduction	Performance SISO (R^2)
u_t^2	20.3046	0.7342	0.3787
GI_t	8.5625	0.3096	0.3227
$temp_t^{L2}$	8.3002	0.3001	0.2019
u_t^1	5.8765	0.2125	0.1181
$temp_t^{L1}$	5.8327	0.2109	0.1563

Step 1.1

Output variable	$temp_{t+1}^{L2}$ - $\hat{v}_{t+1}^1$
Initial variance	1.6907

Candidate Feature	Score %	Variance reduction	Performance SISO (R^2)
$temp_t^{L1}$	11.1909	0.1868	0.2674
$temp_t^{L2}$	10.5893	0.1767	0.2883
GI_t	5.1110	0.0853	0.0812
$temp_t^{L3}$	2.3815	0.0398	0.1617
u_t^1	2.0444	0.0341	0.0268

Bibliography

M.S. Aldenderfer and R.K. Blachfield. *Cluster Analysis.* Sage, Beverly Hills, 1984.

M. Amann. Integrated assessment tools. the greenhouse and air pollution interactions and synergies (gains) model. *Pollution Atmospherique*, pages 73–76, 2009.

M.R. Anderberg. *Cluster analysis for applications.* Academic Press, New York and London, 1973.

M. Ankerst, M. Breunig, H.P. Kriegel, and J. Sander. Optics: ordering points to identify the clustering structure. In *Proceedings of the 1999 ACM-SIGMOD International Conference on Management of Data, Philadelphia, PA*, pages 49–60, 1999.

J.P. Antenucci, K.M. Tan, H.S. Eikaas, and Imberger J. The importance of transport processes and spatial gradients on in-situ estimates of lake metabolism. *Hydrobiologia*, pages 1–13, 2012.

C.A. Aumann. Constructing model credibility in the context of policy appraisal. *Environmental Modelling & Software*, 26(3):258–265, 2011.

V. Babovic. Introducing knowledge into learning based on genetic programming. *Journal of Hydroinformatics*, 11(3-4):181–193, 2009.

The World Bank. Dealing with water scarcity in singapore: Institutions, strategies and enforcement. Technical report, The World Bank, 2006.

R.R. Barton. Simulation metamodels. In *Proceedings of the Winter Simulation Conference*, pages 167–174, 1998.

A. Bennett. *Inverse modeling of the ocean and atmosphere.* Cambridge University Press, Cambridge, U.K., 2002.

J. Beran and G. Mazzola. Visualizing the relationship between time series by hierarchical smoothing models. *Journal of Computational and Graphical Statistics*, 8 (2):213–238, 1999.

J.C. Bezdek. *Pattern Recognition with Fuzzy Objective Function Algorithms.* Plenum Press, New York and London, 1987.

R.W. Blanning. The construction and implementation of metamodels. *Simulation*, 24(6):177–184, 1975.

Public Utilities Board. Four taps provide water for all. Technical report, Public Utilities Board, Singapore, 2005.

G.J. Bowden, G.C. Dandy, and H.R. Maier. Input determination for neural network models in water resources applications. *Journal of Hydrology*, 301(1-4):75–92, 2005.

G.E.P. Box and K.B. Wilson. On the experimental attainment of optimum conditions (with discussion). *Journal of the Royal Statistical Society Series B*, 13(1): 1–45, 1951.

G.A. Carpenter and S. Grossberg. A massively parallel architecture for a self-organizing neural pattern recognition machine. *Computer Vision, Graphics and Image Process*, 37:54–115, 1987.

A. Castelletti and R. Soncini-Sessa. A procedural approach to strengthening integration and participation in water resource planning. *Environmental Modelling & Software*, 21(10):1455–1470, 2006.

A. Castelletti and R. Soncini-Sessa. Bayesian networks and participatory modelling in water resource management. *Environmental Modelling & Software*, 22(8):1075–1088, 2007.

A. Castelletti, S. Galelli, A. Salvetti, and A. Ventimiglia. Extremely Randomized Trees and Feature Ranking for daily streamflow prediction. In *Proceedings of the 9th International Conference on Hydroinformatics. Tianjin, RC.*, 2010a.

A. Castelletti, S. Galelli, and R. Soncini-Sessa. A tree-based feature ranking approach to enhance emulation modelling of 3D hydrodynamic-ecological models.

In *Proceedings of the International Congress on Environmental Modelling and Software*. (eds) IEMSS2010, 2010b.

A. Castelletti, F. Pianosi, R. Soncini-Sessa, and J.P. Antenucci. A multi-objective response surface approach for improved water quality planning in lakes and reservoirs. *Water Resources Research*, 46(W06502), 2010f. doi: 10.1029/2009WR008389.

A. Castelletti, S. Galelli, M. Restelli, and R. Soncini-Sessa. Tree-based feature selection for dimensionality reduction of large-scale control systems. In *Proceedings of the IEEE Symposium on Adaptive Dynamic Programming and Reinforcement Learning. Paris, F.*, 2011.

A. Castelletti, S. Galelli, M. Restelli, and R Soncini-Sessa. Data-driven dynamic emulation modelling for the optimal management of environmental systems. *Environmental Modelling & Software*, pages –, 2012a. doi: 10.1016/j.envsoft.2011.09.003.

A. Castelletti, S. Galelli, M. Ratto, R Soncini-Sessa, and P. Young. A general framework for dynamic emulation modelling in environmental problems. *Environmental Modelling & Software*, pages –, 2012b. doi: 10.1016/j.envsoft.2012.01.002.

P. Cheeseman and J. Stutz. *Advances in Knowledge Discovery and Data Mining.*, chapter Bayesian classification (AutoClass): theory and results, pages 153–180. 1996.

L. Chen and V. Ozsu, M.T.and Oria. Robust and fast similarity search for moving object trajectories. In *SIGMOD*, 2005.

M.A. Chen, Y. andNascimento, B.C. Ooi, and A.K.H. Tung. Spade: On shape-based pattern detection in streaming time series. In *ICDE*, 2007.

V.C.P. Chen, K.L. Tsui, R.R. Barton, and M. Meckesheimer. A review on design, modeling and applications of computer experiments. *Transactions*, 38:273–291, 2006.

D.L. Davies and D.W. Bouldin. A cluster separation measure. *IEEE Transactions on Pattern Analysis and Machine Intelligence*, 1(2):224–227, 1979.

Deltares. *Delft3D-FLOW, Simulation of multi-dimensional hydrodynamic flows and transport phenomena, including sediments.*, 2010.

H. Ding, G. Trajcevski, P. Scheuermann, X. Wang, and E. Keogh. Querying and mining of time series data: experimental comparison of representations and distance measures. In *Proceeding of VLDB, Endow.*, volume 1, pages 1542–1552. VLDB Endowment, August 2008.

J.C. Dunn. A fuzzy relative of the isodata process and its use in detecting compact well-separated clusters. *Journal of Cybernetics*, 3(3):32–57, 1973.

M. Ester, H.P. Kriegel, J. Sander, and X. Xu. A density-based algorithm for discovering clusters in large spatial databases. In *Proceedings of the 1996 International Conference on Knowledge Discovery and Data Mining (KDD'96), Portland, OR*, 1996.

B. Everitt. *Cluster Analysis.* Halsted, New York, 1980.

E. Frentzos, K. Gratsias, and Y. Theodoridis. Index-based most similar trajectory sear. In *ICDE*, 2007.

S. Galelli, C. Gandolfi, R. Soncini-Sessa, and D. Agostani. Building a metamodel of an irrigation district distributed-parameter model. *Agricultural Water Management*, 97(2):187–200, 2010.

P. Geurts and D. Ernst. Extremely randomized trees. *Machine Learning*, 63(1): 3–42, 2006.

R. Givan, T. Dean, and M. Greig. Equivalence notions and model minimization in Markov decision processes. *Artificial Intelligence*, 147(1-2):163–223, 2003.

G.C. Goodwin and R.L. Payne. *Dynamic System Identification: Experiment Design and Data Analysis.* Academic Press, New York, N.Y., 1977.

S. Guha, R. Rastogi, and K. Shim. Cure: an efficient clustering algorithm for large databases. In *Proceedings of the 1998 ACMSIGMOD International Conference on Management of Data, Seattle, WA*, pages 73–84, 1998.

I. Guyon and A. Elisseeff. An introduction to variable and feature selection. *Journal of Machine Learning Research*, 3:1157–1182, 2003.

I. Guyon, S. Gunn, M. Nikravesh, and L. Zadeh. *Feature Extraction, Foundations and Applications (Series Studies in Fuzziness and Soft Computing).* Physica-Verlag, Springer, Berlin, D., 2006.

J. Hartigan. *Clustering Algorithms.* Wiley, New York, 1975.

J.A. Hartigan. Consistency of single linkage for high-density clusters. *Journal of the American Statistical Association*, 76(374):388–394, 1981.

J.A. Hartigan and M.A. Wong. Algorithm as 136: A k-means clustering algorithm. *Journal of the Royal Statistical Society. Series C (Applied Statistics)*, 28(1):100–108, 1979.

M.I. Hejazi and X. Cai. Input variable selection for water resources systems using a modified minimum redundancy maximum relevance (mMRMR) algorithm. *Advances in Water Resources*, 32(4):582–593, 2009.

A.K. Jain and R.C. Dubes. *Algorithms for Clustering Data.* Prentice Hall, Englewood Cliffs, New Jersey, 1988.

A.K. Jain, M.N. Murty, and P.J. Flynn. Data clustering: a review. *ACM Computing Surveys*, 31(3):264–323, 1999a.

Anil K. Jain, M. Narasimha Murty, and Patrick J. Flynn. Data clustering: a review. *ACM Computing Surveys - CSUR*, 31(3):264–323, 1999b.

A. Janssen and H. Ogink. Singapore marina reservoir study.hydrological and hydraulic model report. Technical report, Delft, The Netherlands, Deltares, 2007.

N. Jardine and R. Sibson. *Mathematical Taxonomy.* Wiley, London, 1971.

I.T. Jollife. *Principal Component Analysis.* Springer, New York, NY., 1986.

K. Jong, J. Mary, A. Cornuéjols, E. Marchiori, and M. Sebag. *Ensemble feature ranking.* Springer, Verlag, 2004.

E. Kalnay. *Atmospheric Modeling, Data Assimilation, and Predictability.* Cambridge University Press, Cambridge, U.K., 2002.

G. Karypis, E.H. Han, and V. Kumar. Chameleon: hierarchical clustering using dynamic modeling. *Computer*, pages 68–75, 1999.

L. Kaufman and P.J. Rousseeuw. *Finding Groups in Data: An Introduction to Cluster Analysis.* Wiley, New York, 1990.

E.J. Keogh and C.A. Ratanamahatana. Exact indexing of dynamic time warping. *Data Mining and Knowledge Discovery*, 3(3):263–286, 2005.

J.P.C. Kleijnen. Response surface methodology for constrained simulation optimization: An overview. *Simulation Modelling Practice and Theory*, 16(1):50–64, 2008.

T. Kohonen. The self-organizing map. In *Proceedings of the IEEE*, 1990.

K. Košmelj and V. Batagelj. Cross-sectional approach for clustering time varying data. *Journal of Classification*, pages 99–109, 1990.

R. Krishnapuram, A. Joshi, O. Nasraoui, and L. Yi. Low complexity fuzzy relational clustering algorithms for web mining. *IEEE Trans. Fuzzy Systems*, 9(4):595–607, 2001.

J.A. Lee and M. Verleysen. *Nonlinear Dimensionality Reduction.* Springer, New York, NY., 2007.

T.W. Liao. Clustering of time series data - a survey. *Pattern Recognition*, 38(11): 1857–1874, 2005.

S.C. Liew, S.Y. Liong, and M.T. Vu. A study of urban stormwater modeling approach in singapore catchment. *Advances in Geosciences, Hydrological Science (HS)*, 23:89–101, 2001.

M. Lorr. *Cluster analysis for social scientists.* Jossey-Bass (San Francisco), 1983.

J. MacQueen. Some methods for classification and analysis of multivariate observations. In L.M. LeCam and J. Neyman, editors, *Proceedings of the Fifth Berkeley Symposium on Mathematical Statistics and Probability*, volume 1, pages 281–297, 1967.

P. Magni, F. Ferrazzi, L. Sacchi, and R. Bellazzi. Timeclust: a clustering tool for gene expression time series. *Bioinformatics Application Note*, 24(3):430–432, 2008.

R.J. May, H.R. Maier, G.C. Dandy, and T. Fernando. Non-linear variable selection for artificial neural networks using partial mutual information. *Environmental Modelling and Software*, 23(10-11):1312–1326, 2008a.

R.J. May, G.C. Dandy, H.R. Maier, and J.B. Nixon. Application of partial mutual information variable selection to ANN forecasting of water quality in water distribution systems. *Environmental Modelling and Software*, 23(10-11):1289–1299, 2008b.

M. Nayak and S. Dash. Gpac-apso clustering using modified s-transform for data mining. *International Journal of Engineering Science and Advanced Technology*, 2(1):38–48, 2012.

H. Peng, F. Long, and C. Ding. Feature selection based on mutual information: criteria of max-dependency, max-relevance, and minimum redundancy. *IEEE Transactions on Pattern Analysis and Machine Intelligence*, 27(8):1226–1238, 2005.

N.V. Queipo, R.T. Haftka, W. Shyy, T. Goel, R. Vaidyanathan, and P.K. Tucker. Surrogate-based analysis and optimization. *Progress in Aerospace Sciences*, 41 (1):1–28, 2005.

E. Rendon, I. Abundez, A. Arizmendi, and E.M. Quiroz. Internal versus external cluster validation indexes. *International Journal of Computers and Communication*, 5(1):27–34, 2011.

H.C. Romesburg. *Cluster Analysis for Researchers.* Lifetime Learning, California, 1984.

J. Sacks, W.J. Welch, T.J. Mitchell, and H.P. Wynn. Design and analysis of computer experiments. *Statistical Science*, 4(4):409–435, 1989.

N. Sadegh. Minimal realization of nonlinear systems described by input-output difference equations. *IEEE Transactions on Automatic Control*, 46(5):698–710, 2001.

A. Saltelli, K. Chan, and M. Scott. *Sensitivity Analysis.* Wiley, New York, NY., 2000.

A. Saltelli, S. Tarantola, F. Campolongo, and M. Ratto. *Sensitivity analysis in practice. A guide to assessing scientific models.* John Wiley & Sons, Ltd, Hoboken, NJ., 2004.

A. Saltelli, M. Ratto, T. Andres, F. Campolongo, J. Cariboni, D. Gatelli, M. Saisana, and S. Tarantola. *Global Sensitivity Analysis. The Primer.* John Wiley & Sons, Ltd, Hoboken, NJ., 2008.

L.M. See, A. Jain, C.W. Dawson, and R.J. Abrahart. *Visualisation of hidden neuron behaviour in a neural network rainfall-runoff model. In: Practical Hydroinformatics.* Water Science and Technology Library, 2008.

S. Selvalingam, S.Y. Liong, and P.C. Manoharan. Use of RORB and SWMM models to an urban catchment in Singapore. *Advances in Water Resources*, 10(2):78–86, 1987.

C. Shaw and G.P. King. Using cluster analysis to classify time series. *Physica D: Nonlinear phenomena*, 58:288–298, 1992.

T.W. Simpson, J.D. Peplinski, P.N. Koch, and J.K. Allen. Metamodels for computer based engineering design: survey and recommendations. *Engineering with Computers*, 17(2):129–150, 2001.

J. Smits and Beek J.V. Marina reservoir study: Water quality mitigation scenario analysis. Technical report, Delft, The Netherlands, Deltares, 2007a.

J. Smits and Beek J.V. Marina reservoir study. water quality modelling. Technical report, Delft, The Netherlands, Deltares, 2007b.

R.R. Sokal and C.D. Michener. *A Statistical Method for Evaluating Systematic Relationships.*, volume 28. University of Kansas Scientific Bulletin, 1958.

T. Sorensen. *A Method of Establishing Groups of Equal Amplitude in Plant Sociology Based on Similarity of Species Content and Its Application to Analyses of the Vegetation on Danish Commons.*, volume 5. Biologiske Skrifter, 1948.

D. Twigt and D. Burger. Water quality operational management system (wq oms), functional and technical design. Technical report, Delft, The Netherlands, Deltares, 2010.

J.J. Van Wijk and E.R. Van Selow. Cluster and calendar based visualization of time series data. In *Proceedings of IEEE Symposium on Information Visualization, San Francisco, CA*, October 25-26 1999.

M. Vlachos, D. Gunopulos, and G. Kollios. Discovering similar multidimensional trajectories. In *ICDE*, 2002.

A. Voinov and F. Bousquet. Modelling with stakeholders. *Environmental Modelling & Software*, 25(11):1268–1281, 2010.

W. Wang, J. Yang, and R. Muntz. Sting: a statistical information grid approach to spatial data mining. In *Proceedings of the 1997 International Conference on Very Large Data Base (VLDB'97), Athens, Greek*, pages 186–195, 1997.

L. Wehenkel. *Automatic Learning Techniques in Power Systems.* Kluwer Academic, Boston, MA., 1998.

H.S. Wheater, A.J. Jakeman, and K.J. Beven. *Modelling Change in Environmental Systems.* IWA Publishing, Wiley, Chichester, U.K., 1993.

K. Willcox and J. Peraire. Balanced model reduction via the proper orthogonal decomposition. *AIAA Journal*, 40(11):2323–2330, 2002.

Y. Xiong and D.Y. Yeung. Mixtures of arma models for model-based time series clustering. In *Proceedings of the IEEE International Conference on Data Mining, Maebaghi City, Japan*, December 9-12 2002.

B.-K. Yi and C. Faloutsos. Fast time sequence indexing for arbitrary l_p norms. In *VLDB*, 2000.

P. C. Young and M. Ratto. A unified approach to environmental systems modeling. *Stochastic Environmental Research and Risk Assessment*, 23:1037–1057, 2009.

P. C. Young and M. Ratto. Statistical emulation of large linear dynamic models. *Technometrics*, 53(1):29–43, 2011.

P.C. Young. Data-based mechanistic modeling of environmental, ecological, economic and engineering systems. *Environmental Modelling & Software*, 13(2):105–122, 1998.

T. Zhang, R. Ramakrishnan, and M. Livny. Birch: an efficient data clustering method for very large databases. In *Proceedings of the 1996 ACM-SIGMOD International Conference on Management of Data, Montreal, Canada*, pages 103–114, 1996.

W. Zhang and B. Michaelis. Shape control with karhunen-love decomposition: Theory and experimental results. *Journal of Intelligent Material Systems and Structures*, 14(7):415–422, 2003.

F. Zijl and D. Twigt. Singapore marina reservoir study. hydrodynamic modelling. Research Report Z.4265.10/20/30, Deltares, 2007.